A STUDY OF CHARACTERISTIC ENERGY LOSSES FROM CERTAIN METALS

A thesis presented for the degree of Doctor of Philosophy at the University of Keele by

R.M.Allen, B.A.

SERL
Baldock
HERTFORDSHIRE

May 1969

SYNOPSIS

The characteristic energy loss spectra of five metals have been measured under clean, ultra-high vacuum conditions. Primary electron beams with energies of several hundred eV were used and the 'reflected' secondary electrons were analysed by 127° electrostatic analysers.

The five metals studied were nickel, silver, tantalum, tungsten and platinum. High purity polycrystalline strips of each metal were thoroughly cleaned and mounted in a stainless steel vacuum chamber. Getter-ion and sorption pumps were used to produce UHV conditions, and the targets were outgassed by resistive heating.

The beam of primary electrons was usually incident at 45° to the target normal and those electrons scattered through 90° were focussed into the analyser entrance aperture. The final 127° analyser had a FWHM resolution of less than 0·9%.

The characteristic energy losses observed in each spectrum have been correlated with the losses predicted by the theories of plasma oscillation, interband transition and subshell ionisation.

In addition to a number of new losses, the present work has found most of the losses reported by previous authors. Evidence of contamination was seen in some spectra, even with the target in a vacuum of below 10^{-8} torr. The residual gases in the vacuum were analysed by a quadrupole mass filter. It is suggested that the disagreements between previous workers have been due to the presence of contaminating layers.

ACKNOWLEDGMENTS

The author wishes to express his gratitude to

Professor D.J.E.Ingram for the use of his laboratory and research facilities,

Professor D.E.Davies and Dr. E.B.Pattinson for their excellent supervision and helpful suggestions,

Dr. R.G.C.Leckey, Dr. S.Thomas and colleagues in the Physics department, Keele, for their useful discussions,

Mr. F.Rowerth and Mr. H. Wardell and their technical staff for their assistance in constructional work:

The Ministry of Defence for the provision of a research assistantship, research funds [CVD contracts RU 20-2 and RU 20-4], and for permission to use the facilities at SERL for the production of this thesis,

and to his wife, family and colleagues at SERL for their constant encouragement.

CONTENTS

page

CHAPTER 1

Introduction and review of previous experimental work

page

CHAPTER 2

Discussion on the theoretical position

CHAPTER 3 page

Present experimental apparatus and techniques

CHAPTER 4

page

Instrumentation

APPENDIX A

page

The 127° electrostatic analyser

APPENDIX B

The quadrupole residual gas analyser

CHAPTER I

INTRODUCTION AND REVIEW OF PREVIOUS EXPERIMENTAL WORK

1.1 *Introduction and basic definitions.*

It was over sixty five years ago that AUSTIN and STARKE[1] discovered the phenomenon of secondary electron emission, when they observed that a metal target was able to emit more cathode rays than it received. They attached the terms 'primary' and 'secondary' to the entrant and emitted rays respectively. For the next twenty years however there was surprisingly little research done to uncover further details of the process. The abundance of other tempting projects in gas discharges and the relative scarcity of vacuum systems probably account for this. However the newly born valve industry of the 1910-1920 era stimulated interest in the interaction of electrons with metal surfaces, and the production of the Gaede diffusion pump in 1915 made the attainment of high vacuum feasible and relatively cheap.

Of the parameters descriptive of the emission the one of immediate practical interest was the yield, or the average number of secondary electrons produced for each incident primary. Experimentally this is rather straightforward to measure since the magnitudes of only two currents are needed: the total current of electrons being emitted from the target, $-i_s$, and the net current to the target, $i_s - i_p$, where i_p is the total primary current. The yield is then given by:

$$\delta = i_s / i_p$$

The variation of the yield with primary energy, called the yield curve, most early workers found to be dependent on target material, but their results rarely correlated one with another. This basic problem of reproducibility of results is one which remains with us today, and is in part justification of further work on secondary electron emission.

To put discussion of this problem into suitable perspective it is convenient to outline the history of the broad field of secondary electron emission from metals.

1.2 *The work of Farnsworth*

One of the earliest investigators was FARNSWORTH who published his first results on secondary emission between 1922 and 1928[2-7]. It is a most illuminating set of papers, and he introduces the first one:

"Studies of the secondary electrons produced by electronic bombardment of metal surfaces have previously been made by various experimenters[8,9]. However the fact that most of the results were obtained previous to the development of modern high vacuum technique combined with the failure of the small amount of recent work to agree with these older results, leaves the important questions of this problem quite unanswered. It is well known that the number of secondary electrons depends upon the velocity of the incident or primary beam, that more electrons leave the surface than strike it if the primary velocity is great enough, but the following characteristics of various metals are still not definitely determined: (1) the magnitude of the secondary electron current as a function of the primary velocity, (2) the velocity

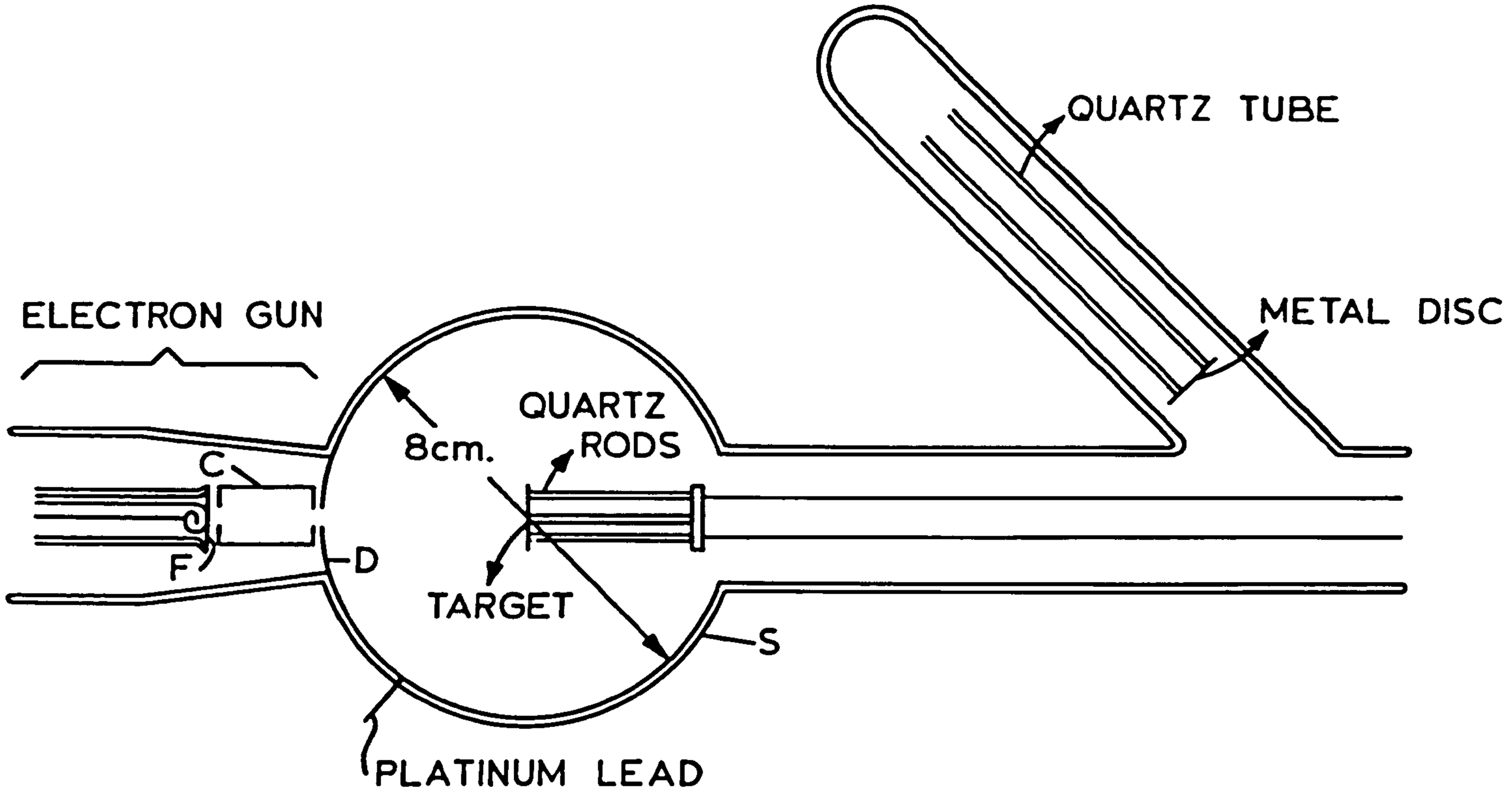

FIGURE 1.1 Apparatus of FARNSWORTH[3]

distribution of the secondary electrons for any given primary velocity."

In fact the 'modern high vacuum technique', combined with his rigorous measures to obtain clean target surfaces put him on the threshold of several important discoveries.

He had a spherical glass vacuum system, one side arm containing an electron gun which pointed at a target supported in the centre of the sphere from an opposing side arm, as shown in Figure 1.1. This second arm communicated with the pumping chain via a liquid air trap, the intention of which was to condense any oil or mercury vapour escaping from the pumps. The primary electrons were accelerated up to earth potential from a negative oxide cathode and collimated by two small holes. By adjusting the potential of these last electrodes slightly away from earth he exercised a certain amount of focussing control. The secondaries escaping from the earthed target were collected on the inner surface of the glass sphere which was coated with a sputtered film of platinum. By taking individual measurements of the target and collector currents he was able to calculate the yield at any primary voltage.

He is distinguished from the earlier experimenters in the number of inherent sources of error which he recognised and against which he took precautions. One potential danger is the possibility of tertiary electrons, or those electrons which, having been ejected from the target, eject further secondaries from the collector which it then may not re-collect. He estimated that the effect of this phenomenon was negligible, because when he repeated the experiment with a cylindrical

collector he obtained virtually identical results, whereas the change of geometry would surely have introduced a marked difference in the probability of the tertiaries being re-collected. Of deeper importance, however, he recognised the need to have absolutely clean target surfaces and of keeping them clean by maintaining them in as high a vacuum as possible. The fact that some previous workers had been unable to distinguish the yield curves of different metals implied, he thought, that their surfaces were covered with layers of contaminating gas, and today we readily endorse his view.

As previous workers had done he thoroughly cleaned the target outside the system with solvents and acids to remove gross contamination, and he tried the effect of physical methods such as using emery cloth to leave a rough surface and polishing with jeweller's rouge. Once the target was inside the system he employed two further methods to obtain clean surfaces: he heated the target by high frequency induction to various temperatures and for varying periods of time, and under the high vacuum the gases evolved from the hot surface were pumped away or adsorbed on the cool walls of the system. An alternative to this procedure was to deposit a film of fresh metal onto a substrate by evaporation from an adjacent filament.

Following these precautions FARNSWORTH proceeded with the investigation of fine structure in the yield curve which had been reported by experimenters such as CAMPBELL and HULL[8,9] in the primary energy region 0 - 250 eV. It had been discovered that the yield curve exhibited a broad maximum in the region of several hundred

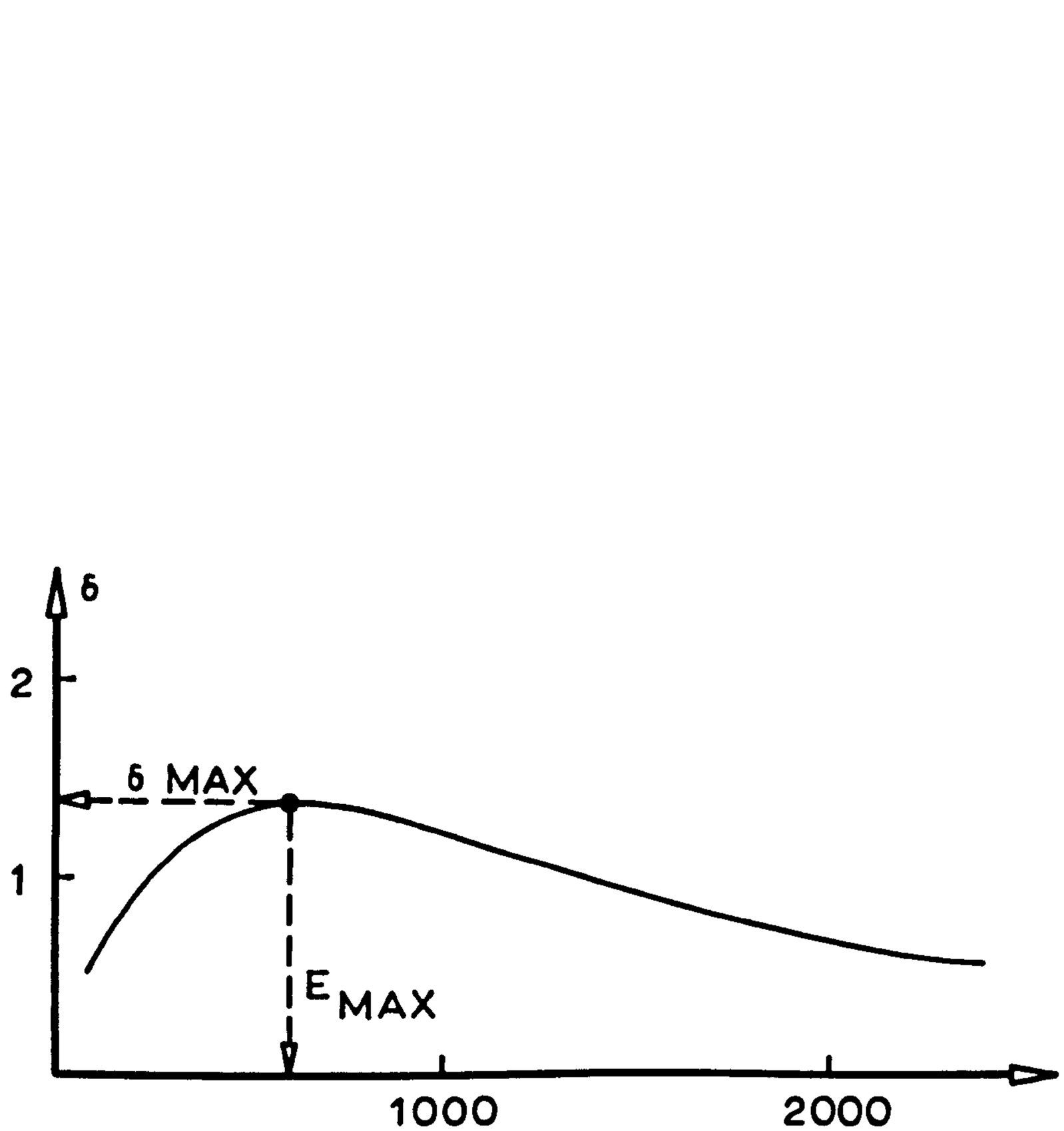

FIGURE 1.2 General shape of the yield curve.

primary volts for all metals, as is shown in Figure 1.2. FARNSWORTH found a number of small maxima occurring at primary energies below 30 eV. Theoretically he tried to correlate these peaks with 'critical potentials' within the metal structure, and sought confirmation of them in the results he obtained in the energy distribution of the secondaries. He was not very successful in this, and subsequent workers such as RICHARDSON and RAO[10-12] in 1930, pursuing the subsidiary maxima in the yield curve, attempted to link them with inflections in the intensity of soft X-rays excited by electrons of varying energy. However later experiments revealed that most of the fine structure disappeared following a really thorough outgassing of the target, and it is now believed to have arisen from the excitation or ionisation of still remaining gas atoms on the surface.

Second in FARNSWORTH'S investigation came the energy distribution of the emitted electrons. Using the apparatus as in Figure 1.1, he kept the final anode of the electron gun and the target at earth, and applied retarding potentials to the surrounding sphere. Secondaries coming from the target were collected on the sphere only if they had energy equal to or greater than the retarding potential, and as this was varied, so the collector current gave the integral of the energy distribution. In other words, if the energy distribution is represented by $f(E)$, a function extending from zero energy $E = 0$ up to primary energy $E = p$, then at some intermediate energy $E = i$, the current reaching the collector is given by $I = \int_i^p f(E)\, dE$. To obtain the true distribution $f(E)$ FARNSWORTH had to find the slope at many points of the

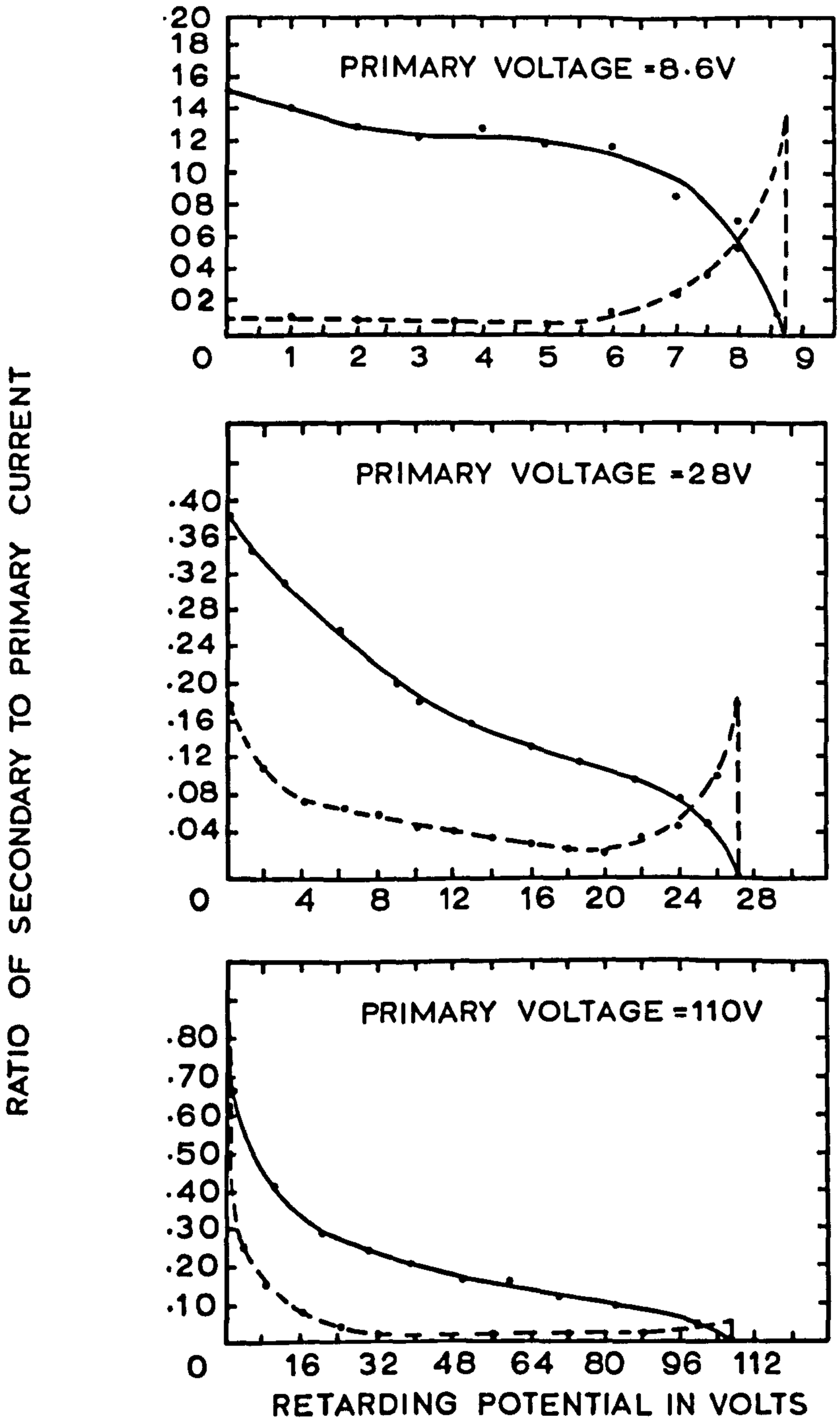

FIGURE 1·3 Energy distribution of secondary electrons emitted from nickel as obtained by FARNSWORTH[2] (Solid line is the integral curve and the dashed its approximate differential.)

curve *I/E* graphically, a tedious and inaccurate task at best and with which he did not usually bother.

His results were sufficient however to confirm the existence of two principal parts to the energy distribution curve. Typical diagrams of his are reproduced in Figure 1.3. In general there was a broad peak in the slow region corresponding to 'true secondaries', and a sharper peak just below primary energy, corresponding to primaries reflected with little or no loss of energy. He further observed that for primary voltages below a certain limiting value (about 10 V) most of the secondaries had energies approximately equal to the primary energy. Above this limiting value the two groups began to separate, the importance of the reflected electrons diminishing with increase of primary energy (see Figure 1.3).

The accumulation of this sort of evidence illustrated the severe limitation of the yield curve as a tool for studying the inner structure of metals, for measurement of simple numbers of electrons disregarding their fundamentally different energies, inevitably obscures any information each particular group may carry concerning its distinct origin. The energy distribution was potentially a far more valuable source of knowledge, but the crude retarding system of FARNSWORTH needed much improvement in resolution before this could be realised.

1.3 Early work on characteristic energy losses

The existence of fine structure in the energy distribution curve seems to have been suggested first by BECKER[13] who in 1924 was studying the energy distribution of photo-electrons excited by soft X-rays. In

FIGURE 1.4 CEL spectrum of platinum ^{199} as observed by RUDBERG. Primary energy was 355·6eV.

one part of the experiment he allowed electrons as well as X-rays to strike the target, and a spectrum he shows of the secondary electrons, analysed by a 180° magnetic field, reveals the presence of a subsidiary maximum just below the primary energy. FARNSWORTH published a paper in 1925[3] showing energy distribution curves of electrons emitted from copper in which "slight kinks indicating inelastic collisions" are apparent. In later experiments[4] however he was unable to repeat this result so considered the earlier evidence to be spurious. Thus it was left to RUDBERG[14-16] in 1929 to announce the discovery of new maxima in the energy distribution which he called 'characteristic energy losses' (CEL).

RUDBERG had found a series of small peaks a few eV below the primary energy which he observed were probably 'reflected primaries' which had lost discrete amounts of energy by some scattering process within the target (Figure 1.4). The amount of energy lost did not depend upon the primary energy but was characteristic of the target material. He used a 180° magnetic deflection spectrometer with a nominal resolution of 0.6% and took care to outgas the targets (Cu, Ag, Au, Pt and various oxides) well. He typically baked the operating tube to 400°C and kept the target incandescent over the period of days during which he made his measurements. In his 1936 paper he reported on targets of Cu, Ag, Au, Ba and Ca which had been evaporated in a vacuum of about 10^{-7} torr, and established the existence of their individual 'loss spectra' for primary energies ranging from below 100 eV to 900 eV. He was able to show that with polycrystalline targets the

TABLE 1.1

REFERENCE	AUTHOR	DATE	RESOLUTION	PRIMARY ENERGY	METHODS OF OBSERVATION	METHODS OF ANALYSIS
14-16	RUDBERG	1930-36	1.2 %	50-400 eV	reflection	magnetic
54	HAWORTH	1935-36	0.6 %	20-150 eV	reflection	magnetic
58	TURNBALL & FARNSWORTH	1938	2.7 %	3-120 eV	reflection	magnetic
17	RUTHEMANN	1941-48	1 eV ?	2k-8keV	transmission	magnetic
59	LANG	1948	1 eV ?	7.6 keV	transmission	magnetic
29	REICHERTZ & FARNSWORTH	1949	2.7 %	50-130 eV	reflection	127^{o} Elect.
60-67	MARTON et al.	1953-63	0.6 eV	20k-30 keV	transmission	Mollenstedt
68	KLEIN	1954	1 eV	35 keV	reflection	Mollenstedt
69-72	WATANABE	1954-61	1 eV	22 keV	transmission	Mollenstedt
73-74	GAUTHE	1954-59	1 eV	18k-30 keV	transmission	Mollenstedt
24	HABERSTROH	1956	?	45 keV	transmission	Retarding
30-31	HARROWER	1956	1 %	100-2 keV	reflection	127^{o} Elect.
32-39	POWELL et al.	1958-62	0.2 %	700-2keV	reflection	127^{o} Elect.
75-77	BOERSCH et al.	1962-68	0.4 eV	20k-50keV	transmission	filter
18,47,78	KLEMPERER & SHEPHERD	1963	2.2 eV	10 keV	transmission	magnetic
79,80	SCHEIBNER & THARP	1967	3 %	30-350 eV	reflection	RPSA (LEED)

the positions of the CEL were virtually independent of parameters such as the angles of incidence and observation and thickness of the target.

Much of recent work on the upper end of the energy distribution shows no advance over RUDBERG, except perhaps in use of instruments with marginally better resolution and often, as in the case of POWELL et al. (1958-1962), the vacuum conditions have been poorer. In fact many of the procedures prominent in secondary emission today were conceived by RUDBERG: for instance, his technique of evaporating films of varying thickness of one metal onto another and observing the transition between the two loss spectra, which allows the depth of electron penetration and escape to be deduced. He also observed the effects of progressive contamination and oxidation of the target. His prediction of ultra-violet radiation from the target at frequencies connected with the loss peaks was repeated by FERRELL in 1958 and realised in 1960.

Immediately following RUDBERG's investigations a number of other research workers announced confirmation of his results and extended them to include other metals. Some details of the most noteworthy studies are recorded in Table 1.1

1.4 *Techniques of energy analysis.*

At this point it is advantageous to digress a little from the historical sequence and include a section on the several different techniques that have been developed to observe CEL. There are two basically different approaches :

(a) Reflection experiments

(b) Transmission experiments

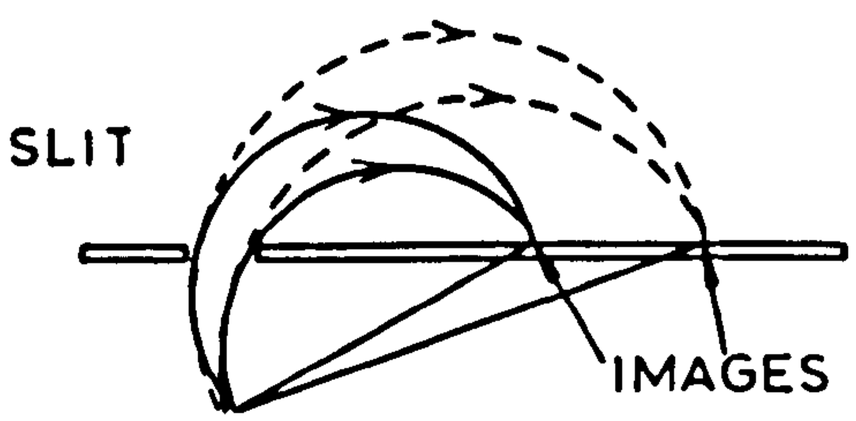

FIGURE 1.5

Analysis by 180 magnetic field.[200] Field is normal to diagram.

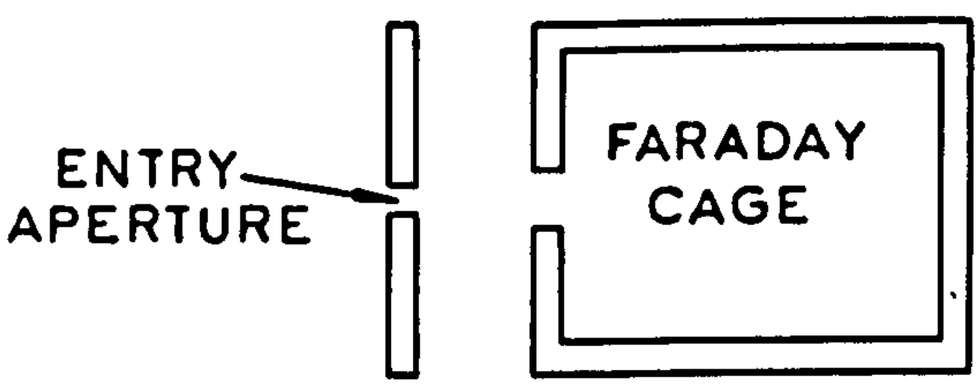

FIGURE 1.6

Schematic of a simple retarding field analyser. There is a retarding potential between the aperture and Faraday cage.

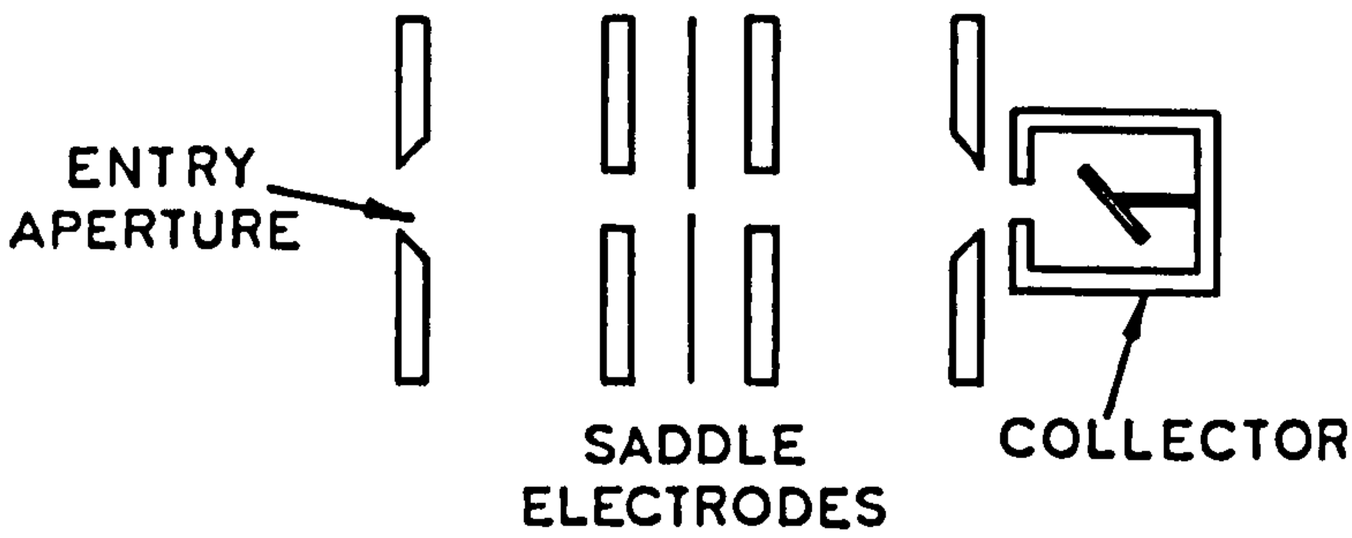

FIGURE 1.7

Five electrode filter lens[25] The saddle electrodes are at the same negative potential.

The secondary electrons are then resolved into a spectrum of energies, usually by one of the following types of analyser:

(1) Magnetic Deflection
(2) Spherical Retarding Potential
(3) Retarding Field
(4) 127° Cylindrical Condenser

} Electrostatic

The primary electrons are usually in a well defined beam focussed onto one face of the target. Secondaries may then be found which have been scattered back through the same face, this process being called 'reflection'. Generally the primaries used in this sort of experiment are of fairly low energy (less than 1000 eV) because the yield of secondaries decreases with increasing primary voltage.

Alternatively if the target is sufficiently thin (about 100 Å), and the primary energy sufficiently high (about 10 keV) then secondaries may be found being emitted from the further side of the target, this process being called 'transmission'.

A brief consideration of some electron energy analysers is now presented, a fuller treatment of the 127° analyser being given in Appendix A.

1.4.1

Analysis by means of deflection in a magnetic field is extremely common. The earliest ones all employed 180° deflection in a homogeneous field (Figure 1.5). The well known relation

$$B\ e\ v = \frac{m\ v^2}{r}$$

describes the motion of the electron and gives a circular orbit of

radius $r = mv/Be$.

Using the equality $eV = \frac{1}{2}mv^2$,

it can be seen that the radius of the electron orbit is given by

$$r = \sqrt{[2mV/eB^2]}$$

depending on the square root of the electron voltage V.

The spectrum of CEL can be scanned either by varying the magnetic field strength or, more simply, by varying an accelerating potential drawing the secondary electrons into the analyser. Alternatively if the width of the spectrum to be scanned is very much less than the primary voltage then the latter can be swept, thus raising each portion of the upper end of the spectrum successively through the fixed pass voltage of the analyser.

The resolving power of simple semicircular analysers is rather poor owing to their inherent spherical aberration, but this can be corrected by modifying the homogeneous field with specially shaped pole pieces or with correcting current coils. Using the latter method RUTHEMANN[17] was able to locate CEL in transmission spectra of 2 to 8 keV electrons with an accuracy of 0.1 eV.

Methods using prior deceleration of very fast transmitted electrons, and magnetic field sectors as focussing prisms have succeeded in reaching the ultimate where the resolution is limited by the spread in energy of the primary electrons[18,19].

1.4.2

The retarding potential spherical analyser [RPSA] of FARNSWORTH has

already been described. Ideally in this arrangement all secondaries with energy sufficient to overcome the retarding potential are collected, whatever their angle of emission. Practice falls short of this ideal unless the target is spherical and at the exact centre of the collector, these conditions being necessary to ensure radial field lines. Any aperture in the collector, such as is necessary to admit the primary beam, and any support, such as is necessary to hold the target, will also distort the field lines from radial symmetry. These practical limitations tend to degrade the possible resolution of the RPSA well below the ideal

$$\frac{\delta E}{E} = (a/b)^2$$

where $\underline{a}$ and $\underline{b}$ are the radii of the target and collector respectively[20].

The simple design of FARNSWORTH can be improved upon with the introduction of a retarding spherical grid just within the spherical collecting shell. This avoids substantial emission of tertiaries from the collecting surface.

The distribution curve can be readily obtained by modulating the retarding voltage with a small (about 0.1 V) a.c. component. The a.c. current reaching the collector will then be proportional to the gradient of the integral distribution curve and may be suitably measured with phase sensitive detection equipment[21,22].

1.4.3.

The simplest retarding field analyser is that based on a parallel plate geometry. Electrons entering normally through an aperture in one

plate have to overcome a retarding electrostatic field to reach the other plate, the collector. As in the case of theRPSA the collector current represents the integral of the energy distribution curve.

To suppress the escape of tertiaries the flat collector plate can be changed into a Faraday cage [figure 1.6] so that electrons have to make many reflections before they can possibly emerge. The electron beam must be sufficiently small however to enter the cage aperture completely, for tertiaries produced by electrons striking the outside of the cage would not be suppressed. Therefore a second aperture which collimates the beam is usually placed in front of the Faraday cage. An analyser of this sort was constructed by BOERSCH[23] in 1954 and it had a very acceptable resolution.

Improvement is possible with the introduction either of a third parallel plate, or a tubular retarding section which permits the beam to be focussed into the cage. Such a retarding field analyser was used to investigate CEL of transmitted electrons by HABERSTROH[24].

"Filter lenses" are the next logical step in the progress of development: electrons have to surmount a saddle field in free space in order to be collected. This arrangement embodies many advantages the most important of which is that the field is naturally converging and that the electrons may be collected at high energy by a collector at ground potential. SIMPSON & MARTON[25,26] have described the construction of a filter lens containing five electrodes, which essentially form two short focus immersion lenses placed back to back, and this arrangement is shown in figure 1.7 .

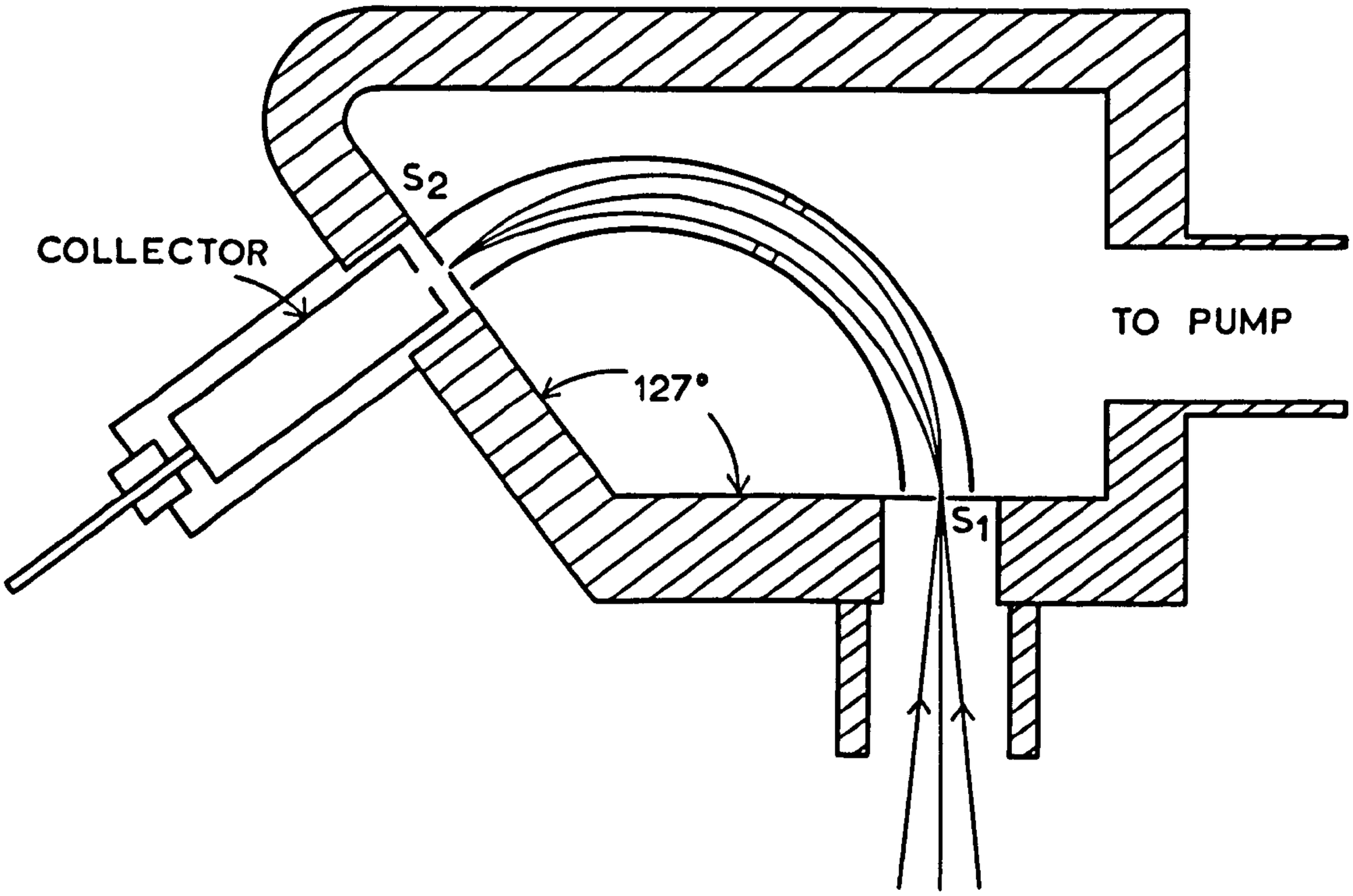

FIGURE 1.8 THE 127° ELECTROSTATIC ANALYSER AS USED BY HUGHES & McMILLEN.[27] S_1= 0·3mm, S_2= 1·0mm, ARC RADII 50mm AND 60mm.

1.4.4

The 127° electrostatic analyser was first described in 1929 by HUGHES and McMILLEN[27] with the theory developed by HUGHES and ROJANSKY[28]. The angle $\frac{\pi}{\sqrt{2}}$ radians (127°17') is the angle subtended at the centre by a pair of cylindrical arcs as shown in Figure 1.8. An electron incident on the front slit may travel through the radial electrostatic field in a circular orbit and emerge through the exit slit, provided it lies within a narrow energy range defined by the arc voltages and slit widths, As is shown in Appendix A, the angle $\frac{\pi}{\sqrt{2}}$ radians is that necessary for maximum resolution and best refocussing of an electron beam focussed on the front slit.

Many investgators of the energy spectra of secondary electrons have used the 127° analyser: for example REICHERTZ and FARNSWORTH in 1949[29] and HARROWER in 1956[30,31], who obtained resolutions of 2.7% and 1% respectively. In more recent years a group in Western Australia have obtained extensive results using a 127° analyser, and their work is considered in the next section.

1.5 *Recent Work on CEL: Powell et alia*

Up to the present date it has been a most difficult task to draw up a definitive table comparing the various CEL of metals. This situation has arisen because the measurements of different workers often reveal striking disagreement, in spite of the fact that each one may have claimed an accuracy of about 0.1 eV in the location of their peaks. Table 1.2 showing the CEL of Aluminium as obtained by a number of workers illustrates this point.

REFERENCE	AUTHOR	ENERGY LOSSES (eV)											
17	RUTHEMANN	(7)	14.7			29.6		44.3		59.3	73.8		
59	LANG		14.5			29.4		44.2		58.6	75.2	90.4	
23	BOERSCH	8.7	14.9			29.8							
68	KLEINN	6.8	14.9	21.9		30.0		44.6					
81	GAUTHE		16.5										
60	MARTON & LEDER	6.2	13.9	19.2		27.8	35.0						
69	WATANABE	6.5	14.8	23.0		29.5		45					
82	BLACKSTOCK et al.		14.8			30.0		44.2		59.8			
24	HABERSTROH	(7)	15.2			30.6							
83	JULL	7	14.6	20.5		29.2		43.8		58.4	73.0		
62	LEDER	7	14.6	22.0		29.2	38.0	44.5					
84	FERT & PRADAL	7.8	15.8	23.5		31.6	39.0	47.4	54.6	63.2	79	100	116
85	LEDER & SIMPSON	7.5	15.0	22.0		30.0							
64	MARTON et al.	6.3	15.3										
33	POWELL & SWAN	10.3	15.3	20.5	25.6	30.5	41.1	46.1	56.0	61.4	77	91.8	108.6
18	KLEMPERER & SHEPHERD	(7)	15.4	(23)		30.9	(39)	46.1					

TABLE 1.2 CEL in Aluminium as measured by various workers

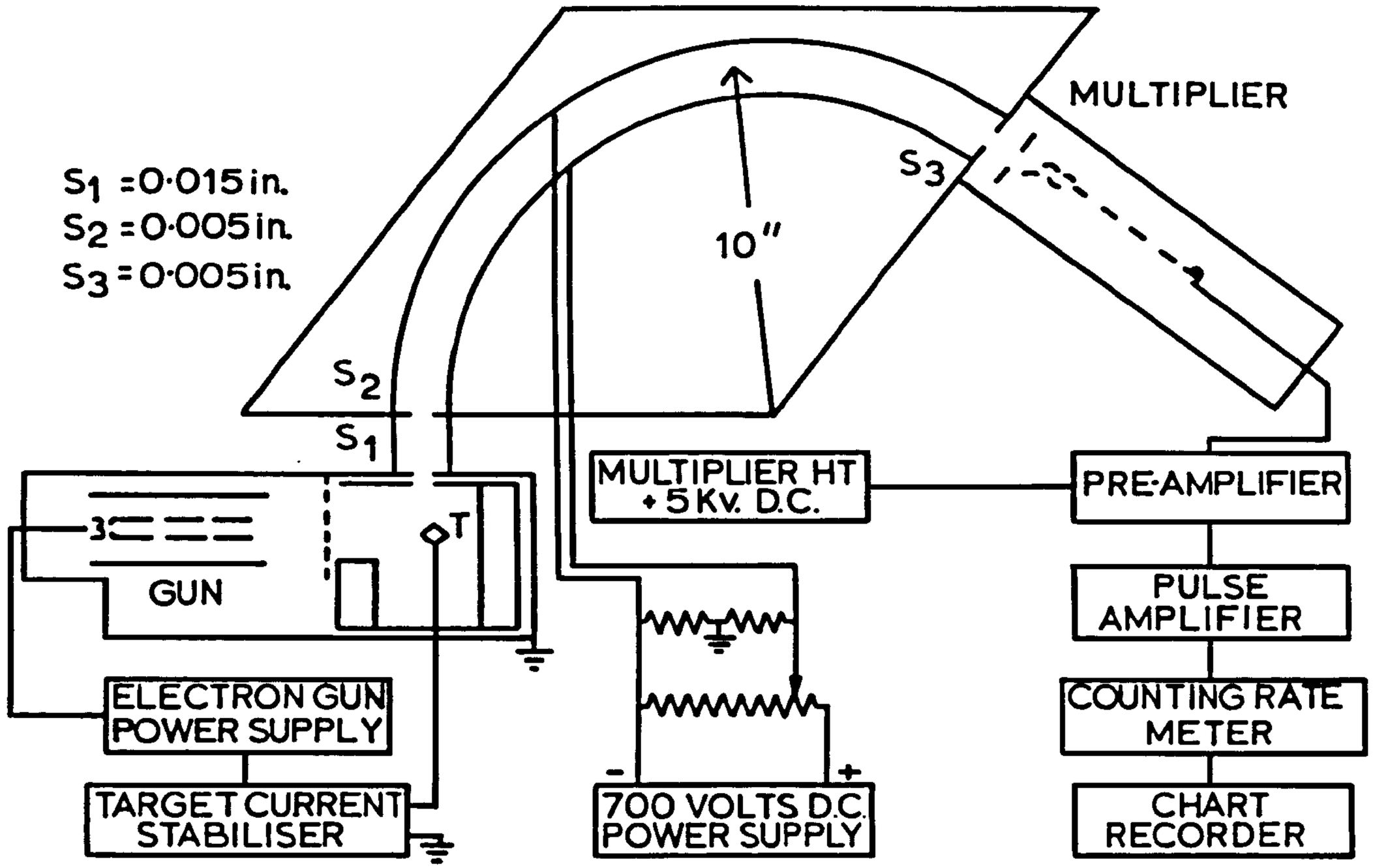

FIGURE 1.9 Apparatus of POWELL et al.

The techniques used by each worker in preparing his targets, obtaining his vacuum and measuring his spectra seem to critically affect the outcome. To rationalise this state of affairs somewhat, and to make comparison from metal to metal possible over a wider range, the group in Australia has made many measurements on a long sequence of metals under more or less identical conditions. Members of this group, POWELL, ROBINS, SWAN and LEST have published their results[32-39] through the years 1958-1962.

A schematic diagram of their apparatus is given in Figure 1.9. They measured the CEL spectra of secondary electrons from freshly evaporated metals which had been reflected through 90°. They evacuated their apparatus with oil diffusion pumps, obtaining pressures of 3×10^{-5} torr (with no liquid air trap) and 2×10^{-6} torr (with a liquid air trap). A table summarising their results and interpretations is given in reference[47].

1.6 *Target preparation and vacua*

As was intimated in the last section different experimental conditions often lead to different loss values for apparently the same metal. The disagreement undoubtedly arises through variation of one or more of the following parameters - which may all affect the degree of contamination of the target.

(1) Target preparation

(2) The vacua employed and the nature of the pumping system.

These will be considered in the following sub-sections.

1.6.1.

Generally the purest metals obtainable have been used, the reflection studies usually employing methods of

(a) Freshly evaporated layers,

(b) Thermal desorption, either by resistance heating or electron bombardment, or

(c) Sputtering.

The transmission experiments usually prepare thin films by one of the standard methods ex vacuo, which will be considered below in (d).

Evaluation of the cleanliness or otherwise of a metal surface may be carried out using a variety of surface sensitive phenomena, including incidently study of the CEL. Some of these methods involve measurement of work function, Auger emission of electrons, secondary electron yield, pressure changes during flash heating, and low energy electron diffraction (LEED). Of these the use of LEED apparatus is the most powerful, and a considerable volume of work has appeared in recent years regarding the surface conditions of the various faces of single crystals[40-42]. A complete review of these techniques, however, lies somewhat outside the compass of this thesis, although some of their results will be drawn upon later.

1.6.1.(a)

The intention of freshly evaporating a target material is to obtain a layer free from bulk contamination, and without oxide or other surface layers. A great deal of this precaution is pointless unless the vacua used are extremely good (less than 10^{-8} torr), and as free as possible

from hydrocarbons and other contaminants which may be admitted from the pumping system, even though several liquid air traps intervene[43-46]. As HARROWER[30] noted, a simple calculation shows that the number of gas atoms striking a surface can produce a monolayer of contamination in about 1 second at a pressure of 10^{-6} torr, assuming a sticking coefficient of unity. Since most experiments have involved a spectrum scanning time of the order of one minute, then even if one assumes that the surface is initially clean, the spectrum obtained cannot be representative of the pure metal, unless the vacuum is very much below 10^{-6} torr.

Moreover during the evaporation of a metal the pressure inevitably rises, often well above 10^{-6} torr. POWELL and SWAN[35] reveal that during evaporation their pressure rose to about 5×10^{-5} torr. KLEIPERER and SHEPHERD[47] note that, at an average rate of evaporation (500 Å/min.), 5×10^{15} metal atoms/cm^{2}sec strike the substrate surface. Besides the residual gas atoms entrained in the metallic vapour stream at a pressure of 5×10^{-5} torr the substrate is subject to the bombardment of about 2×10^{16} gas atoms/cm^2.sec. This means that the metal will be deposited in compound form if the vacuum includes reactive gases, or at best the metal will contain considerable quantities of occluded gas.

1.6.1.(b)

For a range of metals thermal desorption is the simplest method of producing a clean surface. It may be accomplished either by electron bombardment or resistance heating of the target itself or its support.

SYSTEM	δH (kcal/mole)	T_h (^oK)	T_s (^oK)
O_2 on W	155	3100	
N_2 on W	95	1900	
H_2 on W	45	900	3653
C_2H_4 on W	102	2040	
N_2 on Ta	140	2800	
H_2 on Ta	45	900	3303
C_2H_4 on Ta	138	2760	
O_2 on Fe	75	1500	
N_2 on Fe	40	800	
H_2 on Fe	32	640	1808
C_2H_4 on Fe	68	1360	
CO on Fe	32	640	
O_2 on Ni	130	2600	
H_2 on Ni	31	620	
C_2H_4 on Ni	58	1160	1726
CO on Ni	35	700	

TABLE 1.3 List of temperatures T_h necessary to outgas metal surfaces covered with different gases. The temperature T_s is the melting point of the metal.

When a metal is heated under vacuum physically and chemically absorbed foreign molecules may be desorbed if the temperature is sufficient to overcome their binding energy. Using the generous guide $T = 20\ \delta U$ (where δU is the binding energy in kcal/mole), KAMINSKY[48] presents a table showing what temperatures (T) are necessary to break various gas-metal bonds. The contents of Table 1.3 are drawn from this source. Apparently W, Ta and Fe may be readily cleaned by this means, but the Ni - O_2 bond is too strong, so that the metal melts before it is broken. KAMINSKY's information is only "rule of thumb" really and some empirical sources[49-53] show that in practice somewhat different temperatures are sufficient. For instance, it is generally accepted that flash heating tungsten to only 2200°K cleans it of all surface contaminants, although authorities differ as to the removal of bulk carbon which may diffuse to the surface[51].

In the past thermal desorption has been very popular: RUDBERG and HAWORTH[54] used the method, and kept some of their targets incandescent whilst they took measurements to avoid adsorption of residual gases from their vacua. Prior to this procedure HAWORTH typically not only baked his system to 500°C but also degassed his targets over periods as lengthy as 3500 hours (22 weeks). HARROWER with his better vacua (base pressure about 10^{-10}torr) could afford to use cold targets and outgassed them for more reasonable periods of about 12 hours.

1.6.1.(c)

Clean surfaces can also be prepared by the process of sputtering[55-57]:

energetic ions on hitting the metal can tear away layers of metal atoms, together with any surface contaminants. Usually the bombarding ion is of a rare gas, such as argon, which will not chemically react with the surface. After the sputtering any argon left on the surface may be removed by heating the target, much of the damage caused by the sputtering being annealed away in the same step. Sputtering however requires rare gas pressures of about 10^{-3} torr which means that diffusion pumps are normally employed.

1.6.1.(d)

Transmission specimens are thin .foils of thickness ranging from 30 Å to several hundred Angstroms, and may be prepared by a large number of methods, depending on the material involved. A common one is to evaporate the metal in vacuum onto a substrate which may subsequently be dissolved away. Under these circumstances surface contamination is unavoidable. A better technique has been developed in which a special plastic substrate can be sublimed away, the evaporated film remaining in the vacuum all the while. This prevents atmospheric or solvent contamination, but it seems quite likely that traces of hydrocarbon will be left on one surface.

1.6.2

In the early part of section 1.6.1.(a) reasons were advanced for working under ultra-high vacuum (UHV) conditions (i.e. pressure less than 10^{-8} torr), and in a system where oil and mercury contaminants are absent. As mentioned much recent work still employs diffusion pumps, separated from the experimental chamber by a series of liquid air traps. With good baking techniques extremely good vacua

have been obtained but there is no doubt that despite these precautions some degree of contamination still occurs.

It seems a far better procedure never to introduce contaminants in the first place. This can be realised if fluid-free pumps are used in conjunction with bakeable stainless steel systems, which form closed units free from oils and grease etc. There are three principal designs of fluid-free pump: the ion pump (also known as the sputter or getter ion pump), the titanium sublimation pump, and the orbitron pump (also known as the orb-ion pump). The relative operational advantages and disadvantages of these pumps and the merits of stainless steel vacuum systems will be discussed in Chapter 3.

Having obtained a good vacuum with fluid-free pumps one parameter which may yet cause differences between workers is the constituency of the residual gas background. Only with a complete knowledge of the total target environment will consistency become possible. Thus a thorough modern investigation of secondary electron emission requires some sort of mass spectrometer as an essential adjunct to the apparatus.

CHAPTER 2

DISCUSSION ON THE THEORETICAL POSITION

2.1 *Introduction*

When an electron is fired into a polycrystalline metal it has to move through a sea of conduction electrons, the 'electron glue'[86] which holds the individual atoms together. For the purpose of a simple theory it is assumed that the crystallites are large enough to present a continuous lattice to most electrons, and yet small enough so that gross diffraction effects average out. In its progress through the lattice the electron suffers interaction with its environment: because of its charge it interacts with any other electron or ionic charge, and because of its momentum it may be diffracted at lattice planes. Any one interaction, however, involves not merely two bodies but all of the particles within a large volume. This is because the electronic field extends, in principle, to infinity. Analysis of the collisions therefore falls into the category of 'many body problems', approximate solutions of which can only be obtained by making simplifying assumptions. In one approach the simplifying assumption is to divide the forces involved into long and short range terms, each of which is treated in isolation. The final picture is constructed by summation of the different interactions and then is checked against experiment.

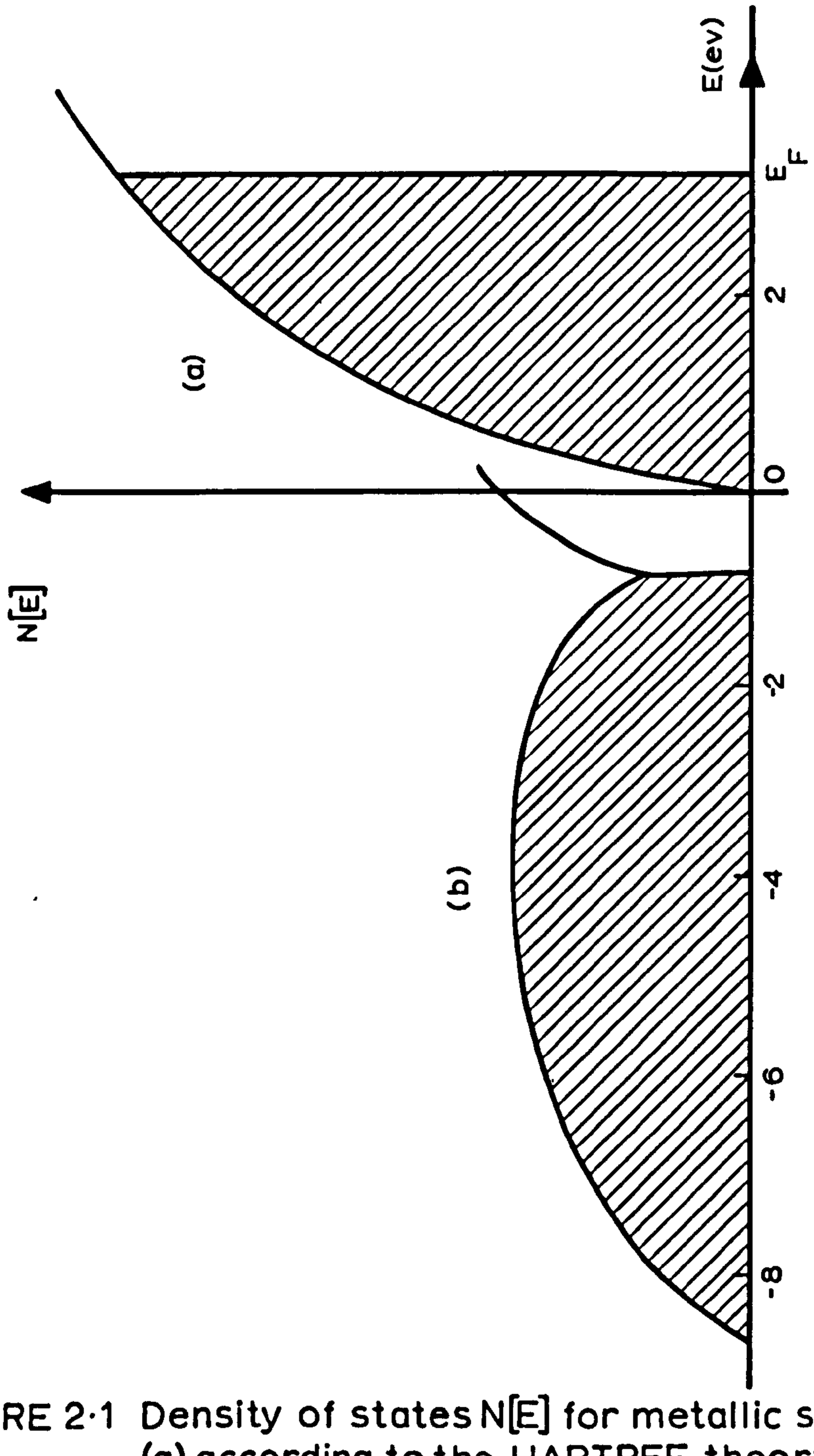

FIGURE 2·1 Density of states N[E] for metallic sodium:
(a) according to the HARTREE theory and
(b) according to the HARTREE-FOCK theory.
Both curves are referred to the same zero of energy, and the shaded regions are occupied at O°K.

In metals the conduction electrons are very densely packed: about 10^{29} m^{-3} . The interaction between them would seem likely to be at the root of the macroscopic qualities of a metal. However the simple HARTREE model, which treats the conduction electrons as if they did not interact, is remarkably successful in 'explaining' many metallic properties; such as electronic specific heat, paramagnetic susceptibility, and the emission spectrum of soft x-rays. All of these rely upon the shape of the N[E] curve, the density of states, as a function of energy [see figure 2.1]. It fails however when applied to the calculation of cohesive energy: that is the energy required to dissociate a unit mass of metal at $0^{o}K$ into free atoms. The HARTREE model predicts this to be negative, which is clearly unacceptable.

The HARTREE-FOCK model admits some degree of interaction by including the Pauli principle: there is zero probability of finding two electrons with parallel spin in the same place, and only a small probability of finding two such electrons close together. It is as if during its motion each electron were surrounded by a hole in the distribution of electronc with parallel spins. The effect of this 'exchange hole' is to screen the field of these electrons. This correlation [i.e. restriction on motion] between electrons of parallel spin does give a positive cohesive energy, although it is much too small[87] . The N[E] curve as shown in figure 2.1 is very different from that predicted by the HARTREE model, with the result that those metallic properties

TABLE 2.1

EXCITATION	DEFINITION	THEORETICAL MODEL	CORRELATIONS
Plasma Oscillations	1. Collective oscillation of free electrons over volumes 1000 Å across 2. Collective oscillation of free electrons close to the surface	Long range Coulomb interaction: incoming electron disturbs the free electron density distribution	1. Reflectivity of light 2. Emission of light at characteristic frequency
Band Transitions	1. Intraband: excitation of conduction electrons to unoccupied levels in same band. 2. Interband: excitation of outer electrons to unoccupied levels in higher bands	Maxima in the density of states at the unoccupied levels.	Fine structure in the x-ray absorption spectrum
Atomic Transitions	Excitation of core electrons to conduction band. [Also called 'ionisation of shells']	Atomic energy levels	Edges in the x-ray absorption spectrum

which depend on its shape are less well explained.

An improved model would be one where there was correlation between all the electrons, including those with anti-parallel spin. The result of taking into account all the Coulomb correlations is discussed in the next section on the theory of plasma oscillations.

First of all, though, the relevance of these considerations to an understanding of CEL must be made clear. The CEL peaks observed in the backscattered spectrum represent primary electrons which have lost discrete amounts of energy in one or more interactions, and are returned to the vacuum after one or more elastic collisions at lattice points. The interactions which may give rise to discrete energy losses are listed in table 2.1 which gives simple definitions and shows some of the theoretical models which have been built to describe each interaction. Also listed are some other experimental fields which yield corroborative evidence to be compared with the CEL measurements.

It is proposed to deal with the three types of interaction in turn, enlarging on each of the theoretical models. Finally the predictions of all the models will be summarised with particular reference to the metals studied in this investigation.

2.2 *Plasma Oscillations (a) the plasmon*

The long range Coulomb interaction can be described as a long range correlation of electron movements. In other words the 'free' electrons may oscillate collectively over a large volume compared with the inter-electron spacing. Each participating electron may only move a very small distance, however, giving rise to longitudinal density variations which can be directly compared to the propogation of sound. The analogy should not be pressed very far however since there are very important differences[88,89].

The classical theory, which is developed below, conceives the sea of conduction electrons against a background of ionic charge to be a plasma, and hence the density oscillations are called plasma oscillations. The excitation of a plasma oscillation requires a quantum of energy $\hbar\omega_p$, where ω_p is the fundamental frequency of oscillation derived from the density of free electrons. This energy is in excess of the kinetic energy available at the Fermi level, and so normally the excitation is in the ground state. In the terms of the quantum theory the zero point energy of the plasma oscillator is $\hbar\omega_p/2$, the energy of the oscillator always having the value $(N + \frac{1}{2})\hbar\omega_p$, where N is a positive integer or zero. PINES[90] has given the name 'plasmon' to this quantised plasma oscillator.

The plasma theory thus describes the long range Coulomb interaction as giving rise to collective behaviour among the conduction electrons which cannot be observed unless excited by the passage of energetic particles. Under normal circumstances then, the long range Coulomb interaction may be ignored. Similarly the remaining short range interaction turns out to have such a very short range that individual electron interactions may reasonably be ignored. This means that for calculations on the density of states the electrons can be treated as non-interacting particles, which is the basis of the HARTREE approximation. The interaction, however, is vitally important in working out the cohesive energy: the total energy of the system is made up of the sum of the kinetic energy of all the particles, the exchange energy due to the short range interaction, the zero point energy of the plasmons and the potential energy of the conduction electron cloud. Making a few reasonable assumptions[87] one finds a lower total energy than in the HARTREE-FOCK theory, and one obtains excellent agreement with observed cohesive energies.

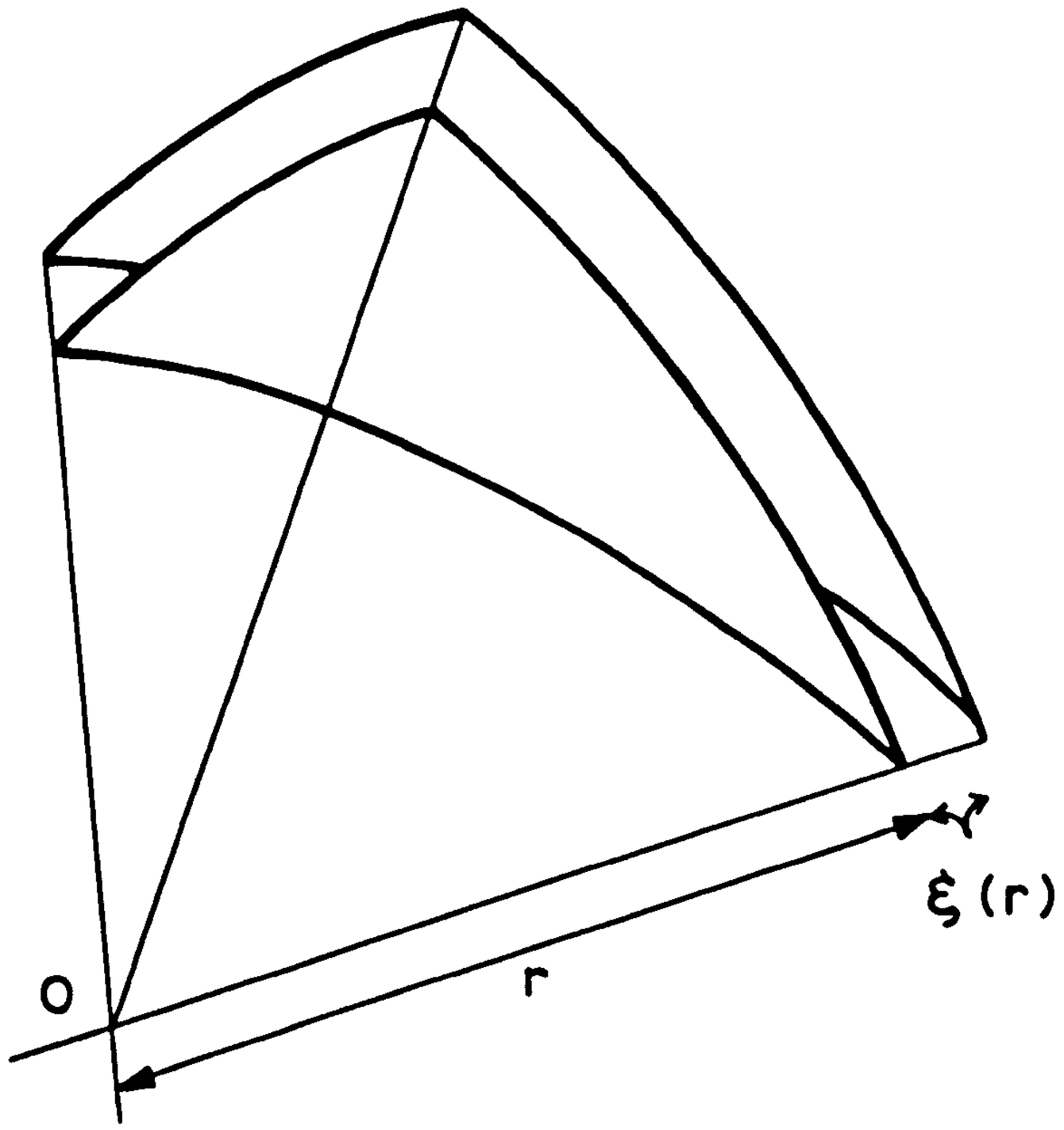

MEAN ELECTRON DENSITY $n.m^{-3}$

DISPLACEMENT $\xi(r) << r$

$\dot{\xi}(r) << 1$

FIGURE 2.2 Diagram for classical derivation of plasma frequency.

2.2 (b) *Classical theory*

The simple theory of plasma oscillations was developed in the years about 1930[91-94] to account for the energy spread acquired by an electron beam in passing through a gas discharge plasma. More recently BOHM & GROSS[88,89] published a graphic description of plasma oscillations using a classical framework, and many of their conclusions may be extended to metallic plasmas. In the case of a low pressure discharge there are about 10^{16} m^{-3} electrons and ω_p is found to be 6×10^9 sec^{-1}. Maxwell-Boltzman statistics can be applied validly to the behaviour of such a low density electron gas, but the notion of a high density electron gas, as found in metals, should be treated by Fermi-Dirac statistics. Nevertheless classical mechanics do give reasonable quantitative results for electrons in metals, for the same reason that the HARTREE theory is successful, and this is the approach adopted here.

If one takes a metal containing n free electrons per unit volume, then the model assumes a uniform background distribution of positive charge en. Ignoring the thermal motion of the electrons one then supposes a localised disturbance takes place in the electron density. In the notation of figure 2.2 a number of electrons leave a sphere of radius r, centre O. If the displacement $\xi(r)$ and its derivative are small then the number of electrons leaving the sphere is roughly $4\pi r^2 n\xi(r)$,

the number of electrons contained in a thin shell of thickness $\xi(r)$. This outwards motion of electrons leaves the sphere with an excess positive charge equal to $4\pi r^2 ne\xi(r)$. At the surface of the sphere this charge creates a field

$$\frac{4\pi r^2 ne}{4\pi r^2 \varepsilon_o} \cdot \xi(r) = \frac{ne}{\varepsilon_o} \cdot \xi(r) ,$$

directed radially outwards, so that adjacent electrons experience a restoring force $-\frac{ne^2}{\varepsilon_o}\xi(r)$ in the same direction. By Newton's second law one obtains:

$$\ddot{\xi} + \left(\frac{e^2 n}{m\varepsilon_o}\right)\xi = 0 \qquad (1)$$

which is the equation of simple harmonic motion.

Thus the electron density oscillates with angular frequency:

$$\omega_p = \left(\frac{e^2 n}{m\varepsilon_o}\right)^{\frac{1}{2}} \qquad (2)$$

If the valence electrons are assumed to be the only ones free to participate in plasma oscillation, then one calculates the free electron density to be:

$$n = 6 \times 10^{26} \times \frac{dZ}{A} \ m^{-3} \qquad (3)$$

where A is the atomic weight, d the density in $kg.m^{-3}$ and Z is the valency. One then finds:

$$\hbar\omega_p = \frac{6.62 \times 10^{-34}}{2\pi} \times \frac{6.12.\sqrt{(15\pi)}.10^{23}}{9.545} \times \left(\frac{dZ}{A}\right)^{\frac{1}{2}} \text{ joule}$$

or

$$\hbar\omega_p = 28.8 \times \left(\frac{dZ}{A}\right)^{\frac{1}{2}} \text{ eV} \qquad (4)$$

where d is now in $gm.cm^{-3}$.

For aluminium equation 4 gives the plasmon energy:

$$\hbar\omega_p = 15.8 \text{ eV}$$

The HARTREE theory predicts the kinetic energy of an electron at the Fermi level to be:

$$E_F = \frac{\hbar^2}{2m} \cdot (3\pi^2 n)^{2/3}$$

Putting in the constants and using equation 3 this gives:

$$E_F = 26.5 \times \left(\frac{dZ}{A}\right)^{2/3} \text{eV} \qquad (5)$$

In the case of aluminium one finds E_F is 11·9 eV which is in close accord with the 11·8 eV conduction band width as measured by soft x-ray emission. Thus the most energetic conduction electrons have insufficient energy to stimulate plasma oscillation; this justifies the statement made above that the plasmon remains in the ground state until excited by the passage of a more energetic particle.

The actual process of plasmon excitation can be described as the effect of a wake set up in the electron density by the fast particle. This has been treated in a semiclassical way[95-97] by methods analogous to those used to explain the Cerenkov effect. A quantum mechanical approach along the same lines has been made [98] and NOZIERES & PINES[99-103] have developed a theory based on the dielectric formulation of the many body problem. A macroscopic treatment using the effective dielectric constant of the electron gas has also been given[104-106] .

2.2 (c) *Dispersion relation*

It has been shown by BOHM & PINES[96,97] that if the kinetic energy of the conduction electrons is taken into account then equation 1 is modified by the inclusion of a second term linear in ξ. The solution then shows that the electron density oscillates with a frequency ω given by:

$$\omega^2 = \omega^2_p + k^2\overline{v^2} = \omega^2_p + \frac{3}{5}k^2v_o^2 \qquad (6)$$

where $k=2\pi/\lambda$ is the wavenumber of the plasma wave, $\overline{v^2}$ is the mean square velocity of the electrons and v_o is the velocity at the Fermi level. This equation is called the dispersion relation. In effect it means that oscillations of small wavenumber occur at frequencies close to ω_p, but for wavenumbers close to k_c given by:

$$k_c = \frac{5}{3}.\ \omega^2_p/v_o^2 \qquad (7)$$

collective oscillation becomes impossible. If aluminium is chosen:

$$k_c = \frac{2.4 \times 10^{16}}{2.04 \times 10^6} \times \sqrt{1.67} = 1.52 \times 10^{-10}\ m^{-1}$$

so

$$\lambda_c = 2\pi k_c^{-1} = 4.1\ \text{Å}$$

The corresponding wavelength λ_c is the minimum beyond which thermal motion upsets the interelectron correlation and, reasonably, this is comparable to the interelectron spacing.

The theory of plasma oscillations identifies λ_c with the electron screening length beyond which electron interactions may be described on a collective basis, but within which each electron maintains a modified Coulomb potential.

A more detailed consideration of k_c has been given by FERRELL [107] in which he estimated that the practical k_c corresponds to the momentum which is just sufficient to cause one electron at the surface of the Fermi sea to make a band transition, absorbing the plasmon energy. In general he found the number of excited electrons per plasmon to be approximately $\frac{1}{2}\omega_p/v_o k$ Thus for the long wavelength oscillation a very large number of electrons may be participating simultaneously, while for wavelengths close to λ_c only one electron may be excited at any one instance. The collective nature of the oscillation, he pointed out, is due to the number of electrons which are free to participate.

2.2 (d) *Plasmon production*

The mean free path of a primary electron between plasmon interactions has been given by FERRELL[108] and PINES[90] and may be written:

$$\Lambda = \frac{1.06.E}{\hbar\omega_p} \times \frac{1}{\ln\left(\frac{1}{v_o}\left[\frac{10E}{3m}\right]^{\frac{1}{2}}\right)} \quad \text{Å} \qquad (8)$$

For a 500 eV primary in aluminium this gives a mean free path between plasmon interactions of about 20 Å . An alternative formulation due to QUINN[109] gives the identical answer. It is very difficult to assess the accuracy of this result experimentally, although work on the transmission of high energy electrons [$\sim 10^5$ eV] through thin foils confirm the formulae in this region[47, 160].

Another parameter which the plasma theory predicts is the maximum scattering angle a primary may suffer in exciting a plasmon. Substantial agreement has been found using thin foil targets: for 10^4 eV primaries in aluminium $\theta_c \simeq 15$ mr. PINES[90] gives the relation as:

$$\theta_c = \frac{\pi\hbar c}{P}$$ where P is the primary momentum.

However the present work concerns low voltage electrons: for 500 eV primaries in aluminium θ_c is about 100 mr. Individual electron interactions with the primary can give much larger scattering angles[108] so in experiments using thin foil targets the barely deflected beam contains most of the plasmon-scattered primaries. At larger angles from the direct beam electron-electron scattering should predominate.

In reflection experiments from polycrystalline targets one expects no such variation with collecting angle: the individual electron interactions have a longer mean free path[90] but a larger scattering angle, and the plasmon interaction shorter Λ but a smaller θ_c. Thus backscattered electrons should represent both types of energy loss over all angles of collection, the proportion depending upon the actual metal.

2.2 (e) The surface plasron

It can be shown by a simple classical argument that if a plasmon type interaction takes place at, or close to, the surface of a metal then the frequency of oscillation which is excited is $\omega_p/\sqrt{2}$. This is called the lowered, or surface, plasma loss. Using the linearised hydrodynamical equations of BLOCH[110] to describe the behaviour of perturbed conduction electrons in thin foils, RITCHIE[111, 112] was the first to show that plasma oscillation could occur at this frequency.

The situation of plasmons at the surface of bulk material is rather different: STERN & FERRELL [113]used the effective dielectric properties of an electron gas to show that a surface plasmon would oscillate with frequency

$$\omega_s = \omega_p/\sqrt{1+\epsilon} \qquad (9)$$

where ϵ is the dielectric constant of the bounding medium.

Thus for a clean metal surface in vacuum, $\epsilon = 1$ and the frequency becomes $\omega_p/\sqrt{2}$. For a contaminated surface $\epsilon > 1$ and so the frequency changes accordingly. Deviation from absolute smoothness would also affect the frequency, although to some degree departure from the ideal would merely broaden the resonance by an averaging effect. JENSON[114] has shown that the resonant frequency of a plasma contained in a layer of small spheres is $\omega_p/\sqrt{3}$ and this may be applicable to thin films and foils where appreciable granulation and agglomeration is present.

2.2 (f) *Plasmon decay*

According to BOHM & PINES[97,98] and NOZIERES & PINES [99], plasma oscillations are damped primarily through a linear plasmon-electron interaction. This process is one in which a single electron, or a small group of them, rather than propogating the electrostatic wave by a slight displacement, suddenly absorbs the whole energy of the wave with a drastic change of its wavefunction. In other words the long range order is destroyed and a small number of electrons undergo band transitions. Electron-electron and electron-phonon interactions are relatively weak sources of damping and are significant only in those metals which have no suitable band transitions[90, 97-99].

As shown by PINES[90] the presence of band transitions with frequency in the neighbourhood of ω_p tend to move the resonance and broaden it. This arises when the metal departs from the ideal of free valence electrons and tightly bound core electrons. Aluminium, for example, is close to this ideal and a plasmon lifetime of the order of $10/\omega_p = 10^{-15}$ sec. is expected. This gives rise to a fairly sharp resonance close to ω_p, as is in fact observed in CEL measurements. A few other metals should be close to ideal, including the alkali metals and, despite the experimental difficulties associated with the latter, CEL spectra seem to conform with the predictions of the plasma theory.

On the other hand, in the transition metals the d-electrons are not all tightly bound as compared with the s-electrons, and it is reasonable to consider the possibility of both bands giving electrons free enough to participate in collective oscillations. As one goes through the mass sequence of transition metals, at first the core charge is small so the d-electrons are fairly free. They have only a low energy transition [$\hbar\omega_b < \hbar\omega_p$] to make to the s-band and, according to PINES, this effectively increases the plasma frequency. Towards the end of each sequence, when the d-band is nearly full, some of the d-electrons are tightly bound by the large core charge. These electrons have fairly high energy transitions [$\hbar\omega_b > \hbar\omega_p$] to make to the s-band, and this acts to suppress the plasma frequency.

PINES argues that when the d-band is roughly half full the high and the low energy transitions should effectively cancel out, giving a plasma frequency close to ω_p . He correlates these observations with CEL measurements and finds qualitative agreement. Furthermore, when the d-band is half full, both the high and low energy transitions act to dampen plasma oscillation, and so it is expected that the resonance width would be greater in this case than when the band is nearly empty or full. This is borne out by the measurements of MARTON & LEDER[67] who found the Cr and Mn CEL peaks to be twice as wide as those of Ti and Co.

The noble metals can be considered as being similar to the transition metals since the plasmon energy, taking just the single s-electron, is larger than the energy required to raise one of the d-electrons to the s-band. Taking all the d and s-electrons as being free is clearly inaccurate, and plasmon energies calculated on this basis are much too high. It can be argued that high frequency band transitions act to lower the plasmon energy or, alternatively, that only a certain number of d-electrons are free enough to participate in oscillations.

There are other theories connecting the shift in plasma frequency and resonance width [67, 115], but they do not appear to correlate with experimental observations.

2.2 (g) Radiative decay

When plasma oscillations are excited in very thin films of a metal [several 100 Å] FERRELL and RITCHIE & ELDRIDGE[116 117] have shown that they may decay by the emission of light at a frequency very close to the frequency of oscillation.

Several workers[118-122] have confirmed the presence of such radiation from a number of metals, and have shown that its intensity follows the predicted dependence on foil thickness and angle of observation. Interesting work has also been done with thin foils of several metals in which plasmons were excited by photons and their radiative decay observed[123].

This mode of decay is impossible however when the plasmons are contained in bulk material: the plasma density fluctuations are longitudinal in nature, so electron motion is in the direction of the plasmon momentum and, therefore, cannot be coupled in general with the transverse waves of an electromagnetic field. The image forces at the surfaces of a foil, however, constrain the electrons to remain inside and this contributes uncertainty to the momentum normal to foil.

Measurement of decay radiation thus affords a very sensitive check on the plasma frequencies deduced from CEL measurements. However the general difficulties associated with the preparation and thickness measurement of very thin foils do not permit the identification to be sufficiently definitive to exclude other possible sources of radiation. Transition, bremsstrahlung and Cerenkov radiation have been proposed and some experiments[47, 117] seem to favour the theory of transition radiation.

2.2 (h) *Optical correlation*

Another connection between plasma oscillations and optical measurements can be made using the phenomenological dielectric model. It can be shown that the way a metal reflects and absorbs light as a function of frequency is described by a varying complex dielectric constant. The Drude theory, based on a free electron gas, gives the real and imaginary parts of the dielectric constant respectively as:

$$\left.\begin{aligned} \varepsilon_1(\omega) &= 1 - \frac{\omega_p^2 \tau^2}{1 + \omega^2\tau^2} \\ \varepsilon_2(\omega) &= \frac{\omega_p^2 \tau}{1 + \omega^2\tau^2} \end{aligned}\right\} \qquad (10)$$

where τ is the relaxation time which corresponds to the interaction of the electrons with their surroundings and amongst themselves. If $\omega\tau \gg 1$, which corresponds to $\omega \sim \omega_p$ and long wavelength oscillation, then equation 10 becomes:

$$\left.\begin{aligned} \varepsilon_1(\omega) &= 1 - \frac{\omega_p^2}{\omega^2} = 1 - \omega_p^2 (2\pi c)^{-2} . \lambda^2 \\ \omega . \varepsilon_2(\omega) &= \frac{\omega_p^2}{\omega^2 \tau} \end{aligned}\right\} \qquad (11)$$

where c is the velocity of light and λ is the wavelength of the light. Now a metal is essentially reflecting when $\varepsilon_1(\omega)$ is negative, and transmitting when positive. The absorption is proportional to $\omega . \varepsilon_2(\omega)$. Values for ω_p and τ can thus be deduced from the optical characteristics of metals as a function of wavelength.

For example, plotting $\varepsilon_1(\omega)$ against λ^2 should give a straight line of gradient $-\omega_p^2(2\pi c)^{-2}$. MENDLOWITZ[125] has plotted data for aluminium in this way and deduced $\hbar\omega_p = 14{\cdot}1$ eV which is equivalent to $2{\cdot}4$ free electrons per atom, and close to the average CEL measurement of $14{\cdot}6$ eV.

The Drude model however is inapplicable to frequencies in the region of interband transitions. In fact if a metal departs from the ideal of the free electron model, both the Drude and the plasma theory give only qualitative explanations of $\hbar\omega_p$. However, as FROHLICH & PELZER[105] have shown, the general condition for the existence of plasma oscillations at a frequency Ω is $\varepsilon(\Omega) = 0$. The solution of this equation gives a complex frequency $\Omega = \omega_p + i\Gamma$, where Γ describes the damping of the plasma oscillation[126]. Thus when the damping is small the condition reduces to $\varepsilon_1(\omega_p) = 0$; however, when the damping is not negligable it is necessary for both ε_1 and ε_2 to be small and the loss function

$$Im\ \varepsilon^{-1} = \frac{\varepsilon_2}{\varepsilon_1^2 + \varepsilon_2^2}$$

to have a maximum. Interband transitions occur when $Im\ \varepsilon^{-1}$ goes through a maximum while ε_1 and ε_2 are not small.

Optical data in the critical regions is still very scarce, however, and so comparison with CEL measurement is very restricted. Of the metals studied in this thesis relevant optical measurements are available only for silver[126-128] and these are discussed below in <u>chapter 5</u> .

2.2 (i) Summary

As discussed in review papers[46, 47] the plasma theory is not unique in its unit of energy loss

$$\hbar\omega_p = \hbar(e^2n/m\epsilon_o)^{\frac{1}{2}}$$

but as a whole it has been remarkably successful in justifying the free electron model and improving upon it in matters such as the cohesive energy[98,129]. The existence of plasmons has received substantial support from other than CEL measurements: FERRELL's predicted radiative decay, the optical stimulation of plasmons, and correlation with light reflection and transmission experiments[124, 130-3] have all confirmed the general principles and properties of such an oscillation. CEL measurements have shown that many features of the theory such as spectral variations with change of state, temperature and scattering angle, to be substantially correct[63,65, 71, 134-136]. Even for non-metallic elements andcompounds the dielectric formulation of the plasma theory has been reasonably successful in explaining CEL measurements[90,137].

However, as far as quantitative accuracy is concerned the plasma theory fails in all but the most ideal elements. The fit with theory is excellent for Be, Mg, Al, Si and Ge, the alkali metals and certain of the transition metals, but on the whole the noble and transition metals have losses at variance with the plasma theory. The discrepancy can be accounted for by invoking band transitions which modify the free electron density, but lack of knowledge of the band structure generally precludes quantitative correction.

That many peaks in CEL spectra may arise from single electron interactions is not denied in the plasmon explanation, although it does require some inhibition of transitions lower in energy than $\hbar\omega_p$. The plasmon explanation simply offers a particularly likely source of discrete energy losses.

2.3 *Band Transitions (a) Introduction*

One of the earliest theories which was proposed to explain the CEL peaks is based on single electron-electron interactions [138]. Electrons in a metal can be split into two main categories: those in the outer orbits of the free atom, which in the solid interact among themselves to form energy bands; and those nearer the nuclei which are so little affected by neighbouring atoms in the solid that their energy levels are discrete as in the free atom.

Electrons in the energy bands can be graded between those which are virtually free and participate in conduction processes, and those which are fairly tighly bound and spend relatively long times in the proximity of given atoms. The disturbance caused by the passage of a fast electron, photon or phonon may cause the transition of one of the free electrons into unoccupied levels of higher energy,or it may promote one of the more tightly bound electrons to the Fermi level. Such transitions may require 10 to 20 eV.

Electrons in the innermost shells have discrete energies and are very tighly bound to the nucleus, but those nearer the outer shells may be raised to the Fermi level by interactions involving energy transfer up to several hundred eV. This 'shell ionisation' can be stimulated by fast electrons or energetic photons; the subsequent neutralisation process in which a conduction electron drops down to the shell may give rise to soft x-ray or Auger electron emission. This is discussed below in section 2.4 .

The division proposed above is somewhat artificial in some cases but in general it provides a rational basis for 'model construction'.

2.3 (b) *Theoretical model*

The band structure of a metal is determined by the lattice: the atomic spacing determines the overlap of electron wavefunctions and hence the width of the energy bands. Changes of state, temperature and pressure may thus influence the band structure.

A theoretical approach is to consider the motion of electron wave packets through the crystal lattice: if the electron is travelling at angle θ to a lattice plane of spacing a and it has a momentum $Pc = 2\pi\hbar/\lambda$ such that

$$p_c . a . \cos\theta = n\pi\hbar \quad \text{where } n \text{ is an integer,}$$

then it suffers Bragg reflection. In quantum mechanical terms there is no solution to the Schrödinger equation for such momenta. There are solutions for momenta either side of p_c, but it is found that there is an energy gap between the solutions on either side. In other words, for each p_c there is a range of energies for which there is no solution to the Schrödinger equation which represents a travelling wave.

In three dimensional space the lattice unit cell may have different atomic spacing in the principal directions and so the energy discontinuities occur at different absolute energies. In momentum-space a surface can be drawn through the planes of constant p_c and the polyhedron so obtained is called a Brillouin zone. Since p_c varies as $1/a$ the zones can be drawn equivalently in reciprocal lattice space, the shape of the Brillouin zones being identical for metals with the same lattice structure.

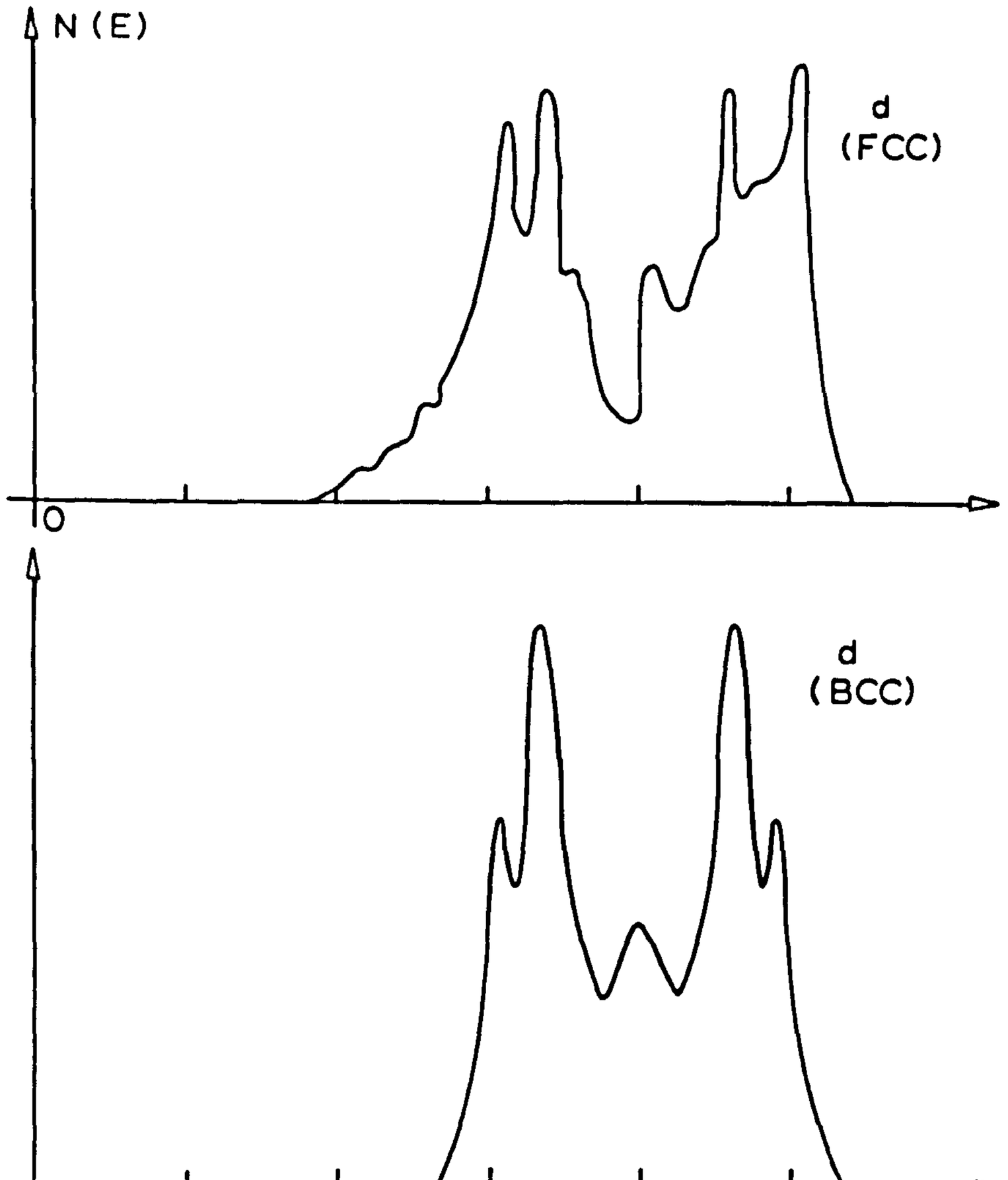

FIGURE 2.3 Density of states N(E) for transition metals, with d-band structure corresponding to FCC and BCC lattices.[140]

Since each orbital state can accommodate two electrons with opposite spins, a Brillouin zone can hold a number of electrons equal to twice the number of unit cells in the crystal[87] . All the metals considered in this thesis are of a simple cubic structure, so can be drawn as simple Bravais lattices, with one atom per unit cell. Thus a Brillouin zone in such metals can accommodate two electrons per atom.

In the case of the d-electrons in the transition and noble metals there is sufficient overlap between orbitals in various directions to make the Brillouin zones overlap in energy. Thus any of the electrons in a d-orbital has a range of permitted energies in the crystal, the width of which defines the d-band. However the probability of finding an electron at any one energy within the band varies with energy. This is because, although the zones do overlap, the probability of finding an electron at some energy within each zone is a peaked function. Thus the summed probabilities covering all the overlapping zones is a complicated series of peaks [five principal ones arise from the ten d-electrons] and this is known as the density of states in the band, referred to above as N[E].

Metals which are close in atomic number and form the same crystal structure are therefore likely to have very similar density of states curves. Figure 2.3 shows the curves which are thought applicable to the metals in the first transition series which form bcc and fcc structures. There are several

theoretical ways to calculate the N[E] curve [139-142], but none give very accurate results. For the transition metals in general a significant feature of the d and s-bands is that they overlap in energy and are incompletely full. These facts help to explain several of the distinctive properties of the transition metals, such as their high electrical resistance.

However the immediate purpose of this argument is to postulate the existence of unfilled levels and bands at energies higher than the Fermi level. Although these are unoccupied under normal conditions, a curve representing the density of potential states can be derived from the successive Brillouin zones in the various lattice directions. An electron which is raised from near the Fermi level to one of these unoccupied levels will do so with a transition probability depending on the N[E] curves in its original and excited states. Thus fairly discrete CEL are possible, given sufficiently sharp N[E] curves.

RUDBERG & SLATER[138] were the first to carry out detailed calculations regarding band transitions and relate them to CEL spectra. They took copper as their model, considering the d-electron wavefunctions to be approximately atomic, and the s-electron wavefunctions to be those of the free electron. They evaluated the transition integrals for the excitation of electrons from the d-band to the top of the s and p-bands. [In copper the 4p-band, although empty, overlaps the 4s-band]. The discreteness of the loss spectrum then arose because of

the double humped character of the N[E] curve for the filled d-band, as shown in figure 2.3 for the fcc structure.

Another approach has been that of VIATSKIN [143,144] who considered transitions from the Fermi level to the various Brillouin zones, which he called *n* transitions. He found the average energy transferred in one of these transitions to be:

$$E_n = \frac{\hbar^2}{2m} \cdot n^2 = \frac{150\, n^2}{a^2} \text{ eV} \qquad (12)$$

for the cubic lattice, where $n^2 = n_1^2 + n_2^2 + n_3^2$, the square of the reciprocal lattice vector, and a is the lattice constant in Angstroms. He deduced the values of E_n for twenty metals in the major crystallographic directions, and formulae for the angular dispersion and primary mean free path.

Many of those CEL which are apparently well explained by the plasmon model can also be explained on the basis of VIATSKIN's transitions, although the principal loss in aluminium is a notable exception. VIATSKIN noted only two areas where a test might be made between the two theories: in the different angular dependence of the inelastic scattering differential cross-section for small θ; and in the fact that his model predicted the existence of Auger electrons, with energies close to $\bar{E}_n$, in the spectrum of true secondary electrons.

2.3 (c) *Experimental correlations*

As noted by VIATSKIN, when an electron decays from its excited state it may give its energy to another electron near the Fermi level; this may then be emitted as an Auger electron. Alternatively it may decay emitting a characteristic photon. The spectrum of soft x-rays has been used to determine the higher band structure [10], but since the initial electron state in such x-ray emission is necessarily an excited one, it is difficult to relate to processes leading to CEL [47].

A sharper experimental tool is the study of x-ray absorption spectra. With increasing wavelength the amount of x-ray absorption goes through a succession of sharp 'edges': these correspond to the energy required to excite core electrons to the Fermi level, and so they are called the K-edge, L-edge etc. Taking any one edge the initial electron state is closely defined because it is so tightly bound, and the sharp edge arises when the x-ray wavelength just equals the binding energy, and the electron makes its transition to the Fermi level. If it is given energy in excess of its binding energy the electron may reach the unoccupied levels above the Fermi level. The transition probability will be governed by the shape of the N[E] curve in this region, and this is the interpretation of the train of small peaks which are observed experimentally in the tail of each edge. A maximum in absorption is taken to reflect a maximum in the N[E] curve.

Thus, following HAWORTH[54], WATANABE[69,70] and GAUTHE[73], one can measure the energy difference between the edge and its fine structure and compare it with known CEL. In making the comparison the primary is visualised as exciting an electron at the Fermi level [or sometimes at the maximum in the N[E] curve immediately below] to make the transition to the unoccupied level. This has been done by the above authors and by LEDER et al.[145] with reasonable success for a range of metals and alkali halides.

However, as PINES[90] has pointed out, this interpretation of the fine structure in the x-ray absorption spectra may not be entirely valid. The correlation between the valence electrons which gives rise to plasmon excitation may be just such as to enhance the density of states of the system at a distance $\hbar\omega_p$ above the ground state of the valence electron assembly; the transition of a core electron to such a state would be definitely favoured, and this would give rise to fine structure in the x-ray absorption spectrum.

Many workers[36, 39, 73, 80, 90, 108 146] prefer to explain CEL results using band transition and plasmon theory as complementary possibilities. Some[37-39] have also found evidence of a third type of loss mechanism which is discussed in the next section.

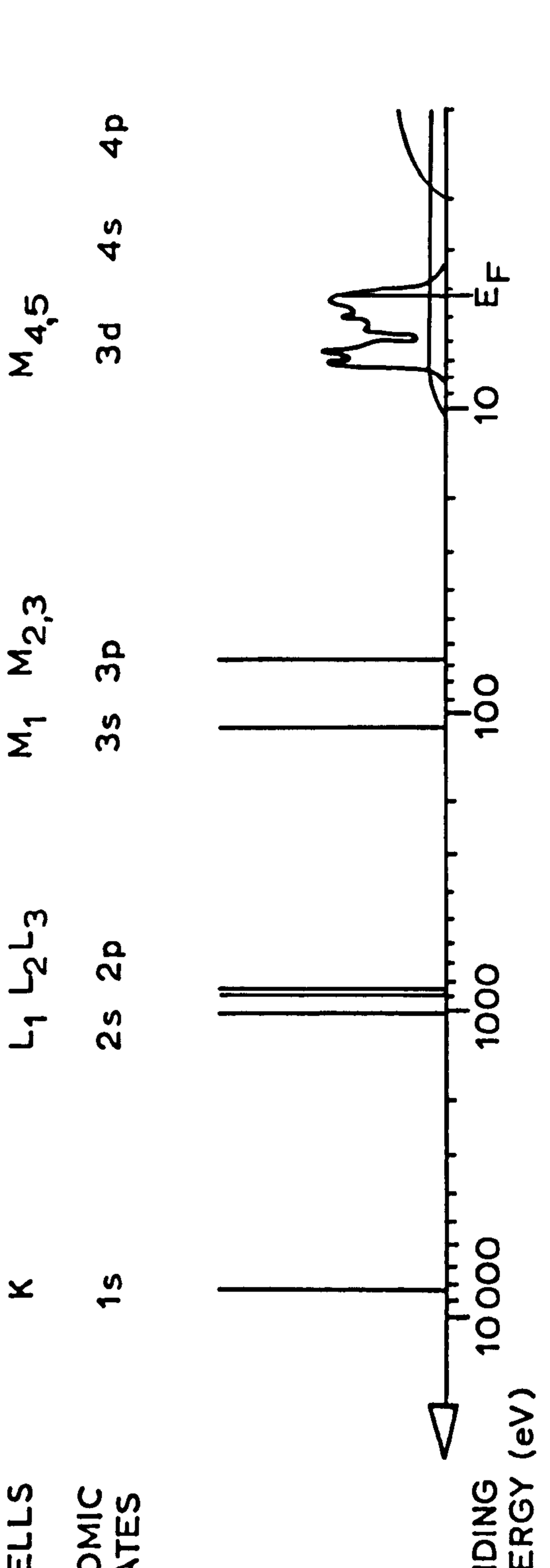

FIGURE 2.4 Electronic energy levels of Nickel [87, 139, 147].

2.4 *Atomic transitions*

The nature of an atomic transition has already been discussed in the introduction to the theory of band transitions. It has been described as the ionisation of an electronic subshell. In this process an electron in some subshell is excited to the Fermi level, and so can be compared directly with the x-ray absorption edges. The energy level scheme which has been built up as a result of x-ray measurements on nickel[147] is given in figure 2.4 . Clearly the K and L shells could not be ionised by a low energy [400 eV say] primary, even if it transferred all its momentum. Electrons in the M shell, however, are much less tightly bound: those subshells which correspond to the 3s and 3p atomic states appear to be fairly discrete in energy and give rise to edges M_1 = 111 eV and $M_{2,3}$ = 66·9 eV.

As pointed out by ROBINS & SWAN [37] CEL assigned to atomic transitions should not be peaked about the transition energy: rather, as the spectrum is scanned in the direction of increasing energy loss, there should be a sharp rise in the background emission at the critical energy. This would correspond to reflected primaries having given kinetic energy greater than E_F to the excited electron, and perhaps enough for it to escape from the metal. Presumably, however, the shape of the CEL immediately above the sharp rise should resemble the shape of

the N[E] curve above the Fermi level, and if this were sharply peaked then the loss would also be peaked. ROBINS & SWAN attribute some of their losses to atomic transitions, and explain that they are peak shaped only because they occur on top of a sloping background.

The $M_{4,5}$ subshell is distinct from the other M subshells in that it is far from discrete. Its contribution to CEL is thus counted as involving band transitions.

In their CEL analyses ROBINS, SWAN and POWELL [see [47]] have attributed many of their peaks to subshell ionisation, but consider in addition peaks due to plasma oscillations and band transitions. This would seem to be a rational approach for no single theory is sufficiently comprehensive to explain all of the losses which have been observed.

In particular the atomic transition theory as proposed by STERNGLASS[148] would appear to have some difficulties. STERNGLASS attempted to show that even the low CEL could be explained by single and multiple low energy ionisations. Arguing on the basis of the BOHR-BETHE theory[149] he found close correlation with loss spectra from gold and aluminium. However the crucial test which he proposed to check the validity of his interpretation, has not generally borne out his expectations. Since his case rested on the ionisation

of the outer occupied shells, changes of state of the metal should affect the CEL spectra little. For the same reason metallic compounds and alloys should give CEL spectra which contain features of the individual elementary spectra. LEDER [63] has measured the spectra of nine metallic vapours and found little evidence for the ionisation process: in general his spectral losses differed greatly from the prominent CEL as measured with the same apparatus on <u>solid</u> metals. Other work has not given such a conclusive result however [76, 150]. Work on intermetallic compounds and alloys [74, 78, 151] has found that the principle CEL in these materials are intermediate to those of the component metals, and this does not favour the STERNGLASS theory.

In view of these considerations the next section only includes the higher energy atomic transitions: these are still quite probable according to the BOHR-BETHE theory, although not so much as band transitions or plasmon excitations.

		NICKEL	SILVER	TANTALUM	TUNGSTEN	PLATINUM
Atomic wt.		58.7	107.9	180.9	183.9	195.1
Subshell	d	9.46	10	3	4	9
structure	s	0.54	1	2	2	1
Lattice structure		fcc 3.51 Å	fcc 4.08 Å	bcc 3.30 Å	bcc 3.16 Å	fcc 3.92 Å
Plasmon energy [eV]		P3=19.4 P4=22.5	P1=9.0	P5=19.5	P6=22.8	P4=19.1
TRANSITIONS [eV]	Viatskin theory [100]	[12.2]	[8.9]	[13.8]	[15.0]	[9.7]
	[110]	[24.4]	[17.8]	27.5	30.0	[19.4]
	[111]		26.7	[41.3]	[45.0]	29.1
	[200]	48.8	35.6	55.1	60.0	
	[210]	[61.0]	[44.5]			[48.5]
	[211]					[58.2]
INTERBAND		2.4	17.0			3.3
	X-ray fine structure	7.7	24.0			20.3
		15.7	33.0			33.3
		27.2	44.0			53.3
		45.7				
ATOMIC TRANSITIONS [X-ray absorption edges]	M_1	111				
	$M_{2,3}$	67				
	N_1	95				
	N_2	64				
	N_3	57				
	N_6		20	31		68
	N_7		18	28		62
	O_1		65	73		94
	O_2		39	43		58
	O_3		28	34		45

TABLE 2.2

2.5 Summary

All of the metals considered in this thesis lie in one of the first three sequences of transition metals. Nickel in the first, silver in the second, and tantalum, tungsten and platinum in the third. Silver is perhaps an exception in that it is the only one with a full d-band, but it still possesses some characteristics in common with the others. The particular properties which are interesting from the point of view of CEL spectra are:

[a] the 'free'electron density, and the associated plasmon energy,

[b] the lattice structure and the associated energy band scheme,

[c] the atomic energy levels.

Table 2.2 summarises this data for the five metals. The plasmon energies are referred to as 'P3' etc., where the 3 indicates the numberof electron per atom which are assumed to be free. The band transition energies are quoted from VIATSKIN [144] for all the metals except tantalum. Those for tantalum were calculated using equation 12 . The transitions in parentheses are 'forbidden' by a structural factor, and VIATSKIN predicts relatively low intensity CEL peaks at these values. The x-ray fine structure information is drawn from LEDER et al.[145], and the atomic transition data from SANDSTROM [147].

Any of the theoretical models considered above can be used to explain a CEL spectrum, although with not equal justification for all metals. Following PINES [90] one expects plasmon production

to dominate band transitions for momentum transfer less than k_c. Thus those transition metals with only a very few electrons in the d-band should have well defined and dominant losses due to plasmon interaction, since the d-electrons are loosely bound. As argued above, however, PINES says that as the low energy transitions are inhibited so is the plasmon energy raised above $\hbar\omega_p$, where the number of free electrons per atom is taken to include all the d and s-electrons. None of the metals which are considered here seems to fit in this category.

Nickel, silver and platinum have full, or nearly full, d-bands so PINES predicts that the plasmon energy will be lower than expected, since many of the d-electrons are tightly bound and have high energy transitions to the Fermi level. In fact plasmon energies seem to be more readily indicated when the number of free electrons per atom is equated to the valency. Using this approach PINES' qualitative reasoning can be seen to be fairly self evident since it is not very sensible to consider <u>all</u> of the d and s-electrons to be free in this case.

Both tungsten and tantalum fall into the centre of PINES' scheme, so he expects the plasmon energy to be fairly accurately given by taking all the d and s-electrons as free. Since this coincides with the metallic valencies, the simple approach again seems to be justified.

PINES expects all the transition metals to show rather broad plasmon losses, because of the d-electron interaction with the plasmon. For tungsten and tantalum he expects the broadest losses of all since in these cases there are both high and low energy transitions taking place.

As pointed out above the x-ray fine structure and the theoretical interband transitions of VIATSKIN should be very similar, since both give a description of the higher energy levels. Some order of agreement is apparent but only to such an extent that neither one could be taken as completely representative of the true structure. GAUTHE's work in this field included study of nickel, silver and platinum and his results and interpretations are discussed in chapter 5 alongside the present results.

As mentioned in the last section the cross-section for the excitation of an atomic transition is smaller than those for plasmon or interband excitation. Such transitions, however, may become significant for high energy losses. Explanation of these losses requires either this single loss mechanism or the successive occurrence of smaller losses. That atomic transitions are excited is now beyond doubt since the presence of the corresponding Auger electrons has been firmly established [30, 31, 54, 80 152-159] . It is therefore reasonable to expect to observe the primary event by a peak in the spectrum of characteristic energy losses.

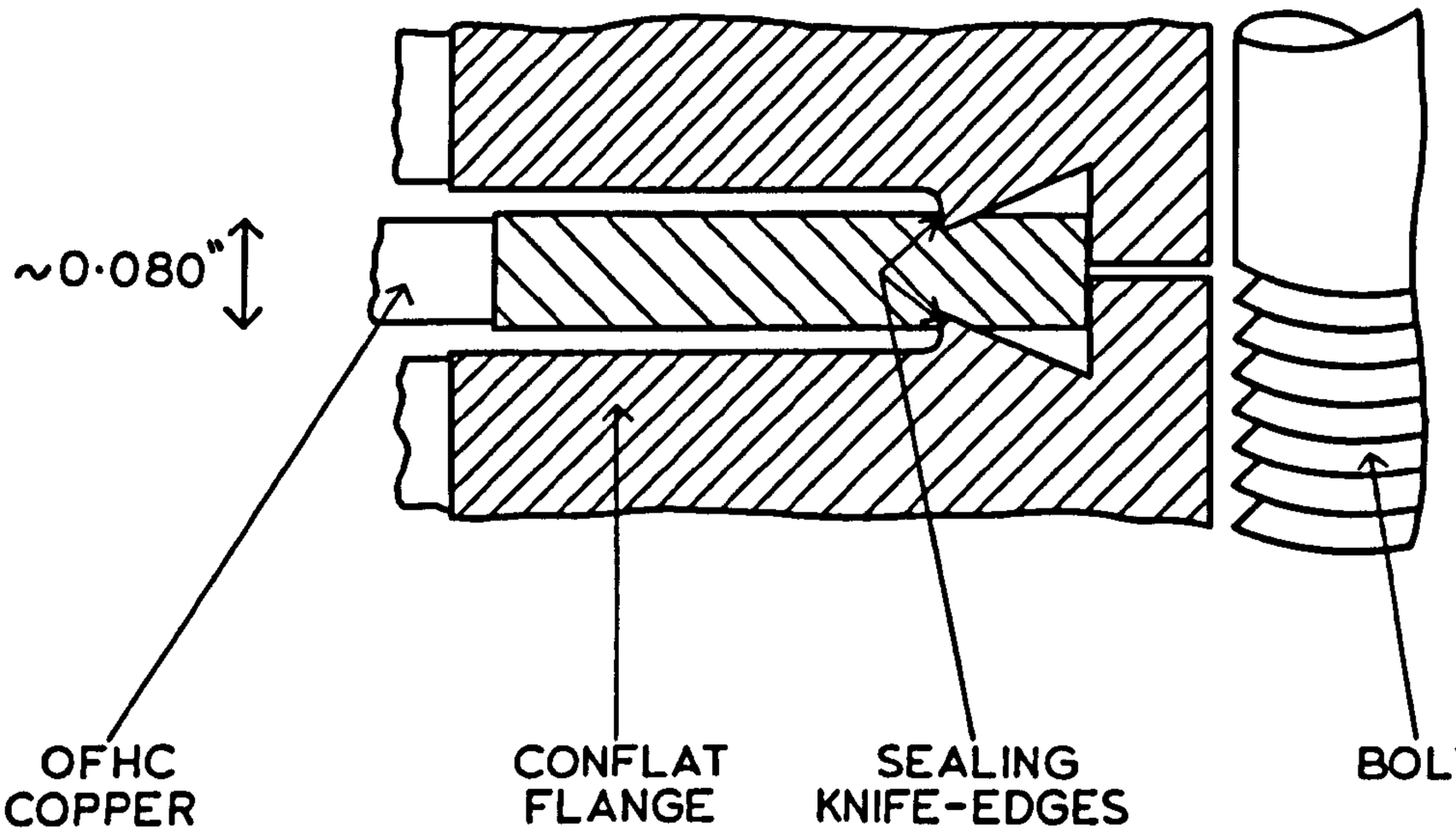

FIGURE 3.1 The Conflat Flange

CHAPTER 3

PRESENT EXPERIMENTAL APPARATUS AND TECHNIQUES

3.1 *Stainless steel*

Stainless steel is chosen as a vacuum material in preference to glass for a number of good reasons: better ultimate vacua are obtainable since steel is non-porous: the evacuated steel system can be baked in air to 450°C without detrimental affect to the steel, and thus it can be very well outgassed: the baked system is very clean internally; the system is mechanically and thermally very robust, the weakest point being the ceramic in electrical feedthroughs.

Although the steel system is opaque and is not as perfectly flexible as one of glass, these disadvantages can be minimised by a suitably wide choice of the many electrical and mechanical feedthroughs commercially available, and viewing ports of many types can be fitted in critical positions.

The major advantage of a metal system, however, is that it can be readily demounted and reconstructed and provided a metal gasket is used the vacuum seal at the flanges is not a source of contamination. The vacuum system used in this investigation had Varian "conflat" flanges throughout, which employ annealed copper gaskets of high purity. Their principle of operation is shown in Figure 3.1, and with little experience the sealing technique is virtually foolproof.

3.2 *Pumping System*

Ion pumps were chosen to produce the vacuum. The diode ion pump requires an initial evacuation of the system to about 10^{-2} to 10^{-3} torr, and thenceforth operates in various modes, pumping down to an ultimate in the 10^{-10} torr region. The initial evacuation was accomplished with a sorption pump: this is completely static in its operation, whereby some sort of molecular sieve such as zeolite or activated alumina, cooled to liquid nitrogen temperature, physically adsorbs the surrounding gas. The 8 l/s. ion pumps were then switched on and after a period of outgassing, during which they often became very hot, their mode of discharge changed. When the sorption pump was valved off, they then took over the task of pumping.

The diode ion pump is a Penning gauge made into an efficient pump. A discharge is triggered by a random electron and is confined between electrodes in a magnetic field which forces the electrons to spiral up the parallel electric field. The 8 l/s pump has a kilogauss magnet and a d.c. potential of 3 kV is applied to it. Spiralling electrons have a high probability of ionising neutral gas atoms, and the ions created move towards the cathode. Sputtering of the cathode material (usually Ti) takes place when the ions impact on the cathode, and the newly arrived ions may combine chemically with the freshly exposed metal or be buried by titanium at the anode[162]. Thus the gas phase is reduced, even the noble gases being pumped to some extent by the physical burying process.

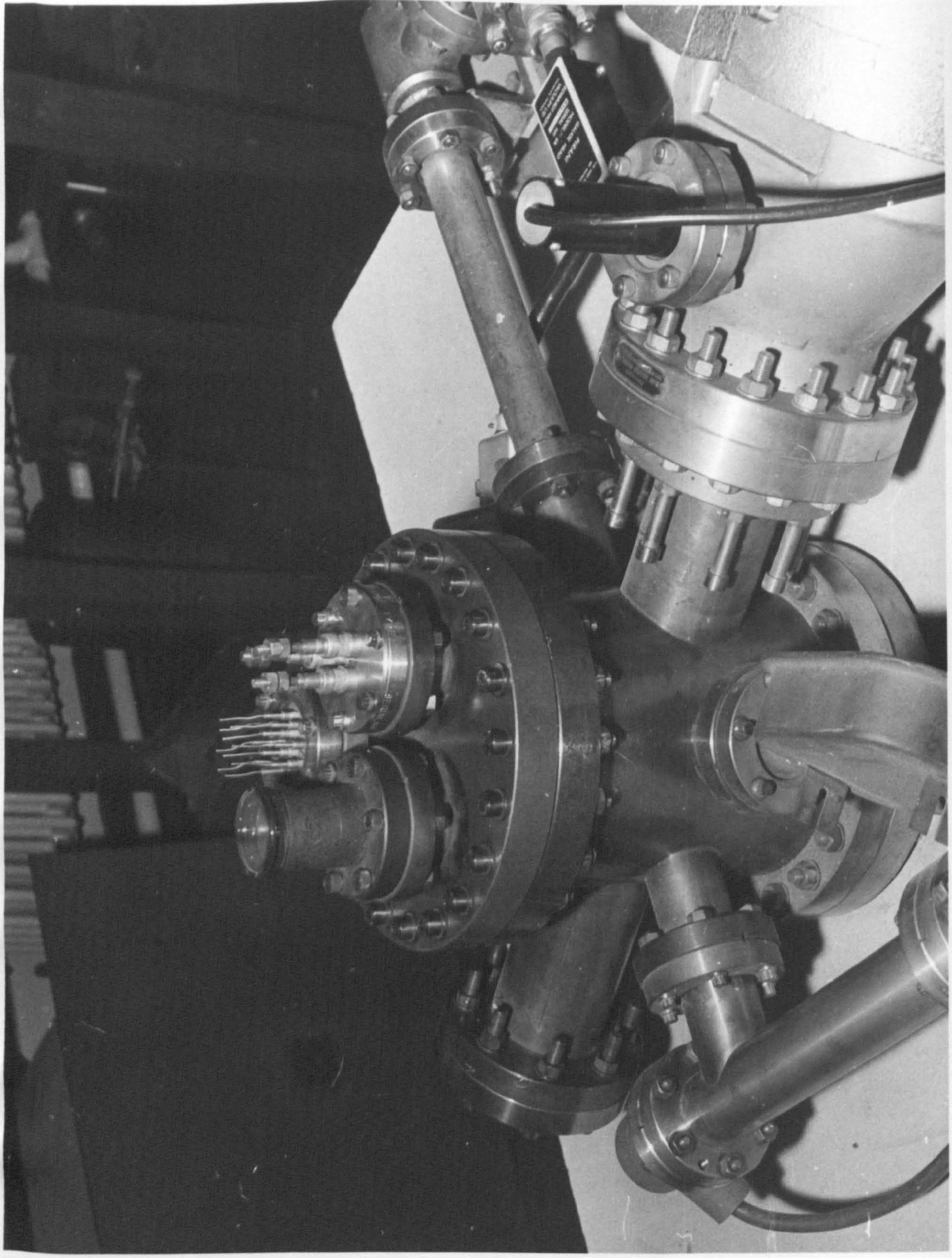

FIGURE 3.2

The other sorts of fluid-free pump as mentioned in Chapter 1 were not considered: the titanium sublimation pump requires a large chamber to itself and does not have a useful pumping speed before the environmental pressure has been reduced to about 10^{-6} torr. Hence an ion pump is needed in combination with a sublimation pump, and in fact such a unit is now marketed by ULTEK. The orbitron pump was not then in production, but had it been available it might well have been considered, despite a number of drawbacks, since it has a very high pumping speed and does not embody a magnet.

Late in 1965 one 8 l/s. ion pump was replaced by a 50 l/s. ion pump and the system at this stage may be seen in Figure 3.2. This afforded easier starting and enabled one to shorten pump-down time to 10^{-8} torr to about 24 hours in a previously baked system. To let the system up to atmospheric pressure dry nitrogen was bled into it, this also proving a useful technique to speed starting.

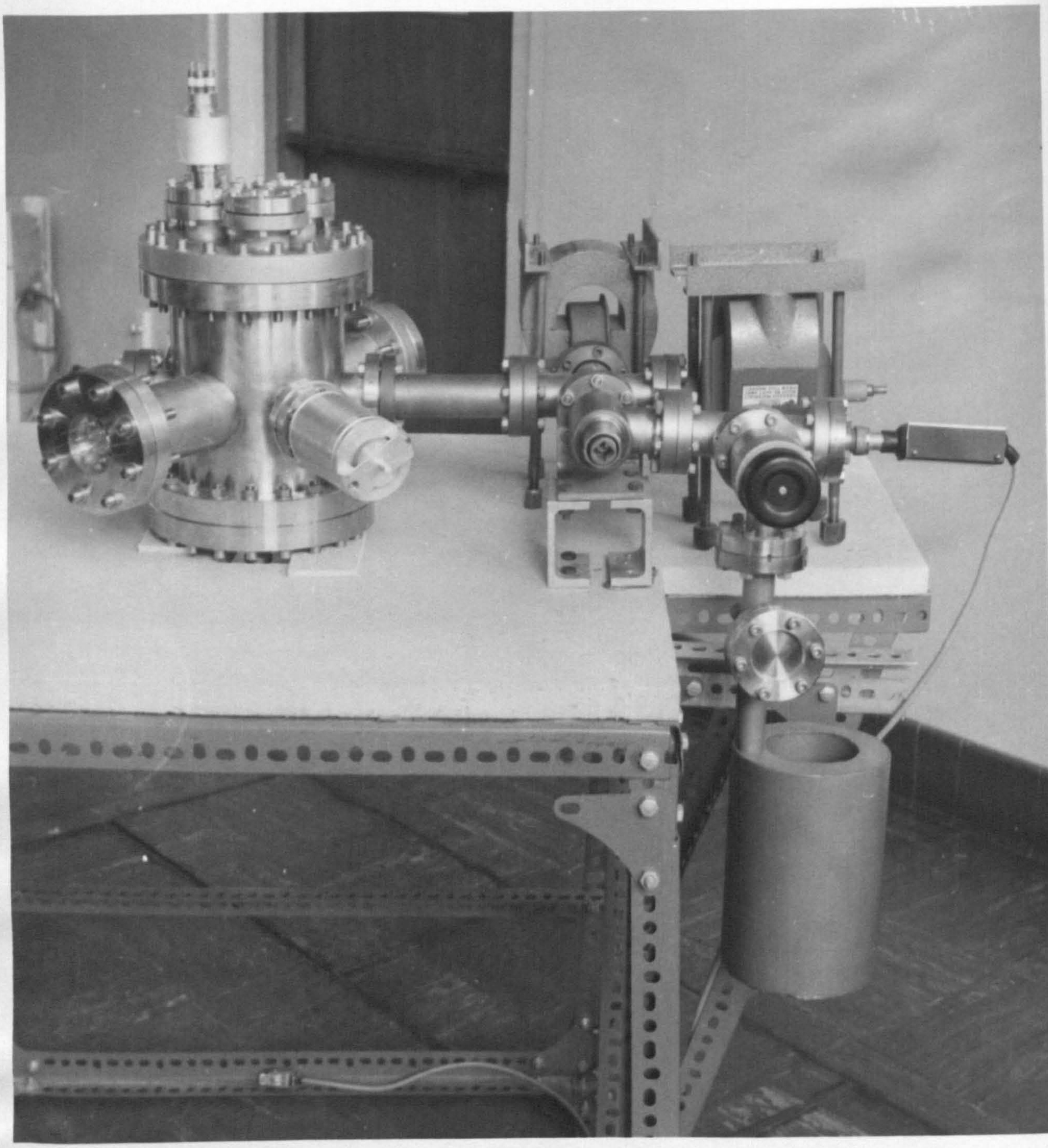

FIGURE 3.3

3.3 *Baking routine*

An early arrangement of the pumping system and manifold can be seen in Figure 3.3. Two ion pumps were employed to enable a cyclic baking routine to be followed [161]. The system up to and including the bakeable valve is enclosed in an oven and one of the pumps is switched off and baked out in an ancillary oven, while the second pump maintains a reasonable vacuum. After 24 hours or so the role of the pumps is reversed, and the ovens are taken off after a further 24 hours of baking. The outside of the vacuum system becomes slightly oxidised during the first bake to 400°C and turns a pale straw colour.

When the manifold arrived from FERRANTI it was pumped out to 10^{-6} torr and given a short bake. The pressure only fell to 10^{-7} torr, and hydrogen leak testing with a hypodermic "sniffer" revealed three leaks in welds. These were eventually cured by re-welding, and after a single cycle of baking the pressure was typically 5×10^{-10} torr (see Chapter 5).

After the system had received many of these thorough bakes it was found sufficient to use an internal bake-out. Mounted with no direct line of sight to critical surfaces such as target, viewing ports and insulating ceramics, a 1 kW tungsten filament was heated to half rating inside the vacuum system. Stainless steel being a rather poor conductor of heat, this proved an efficient way to get the heat where it was most wanted, and when the system was packed around with glass fibre the outside temperature could be raised to 350°C.

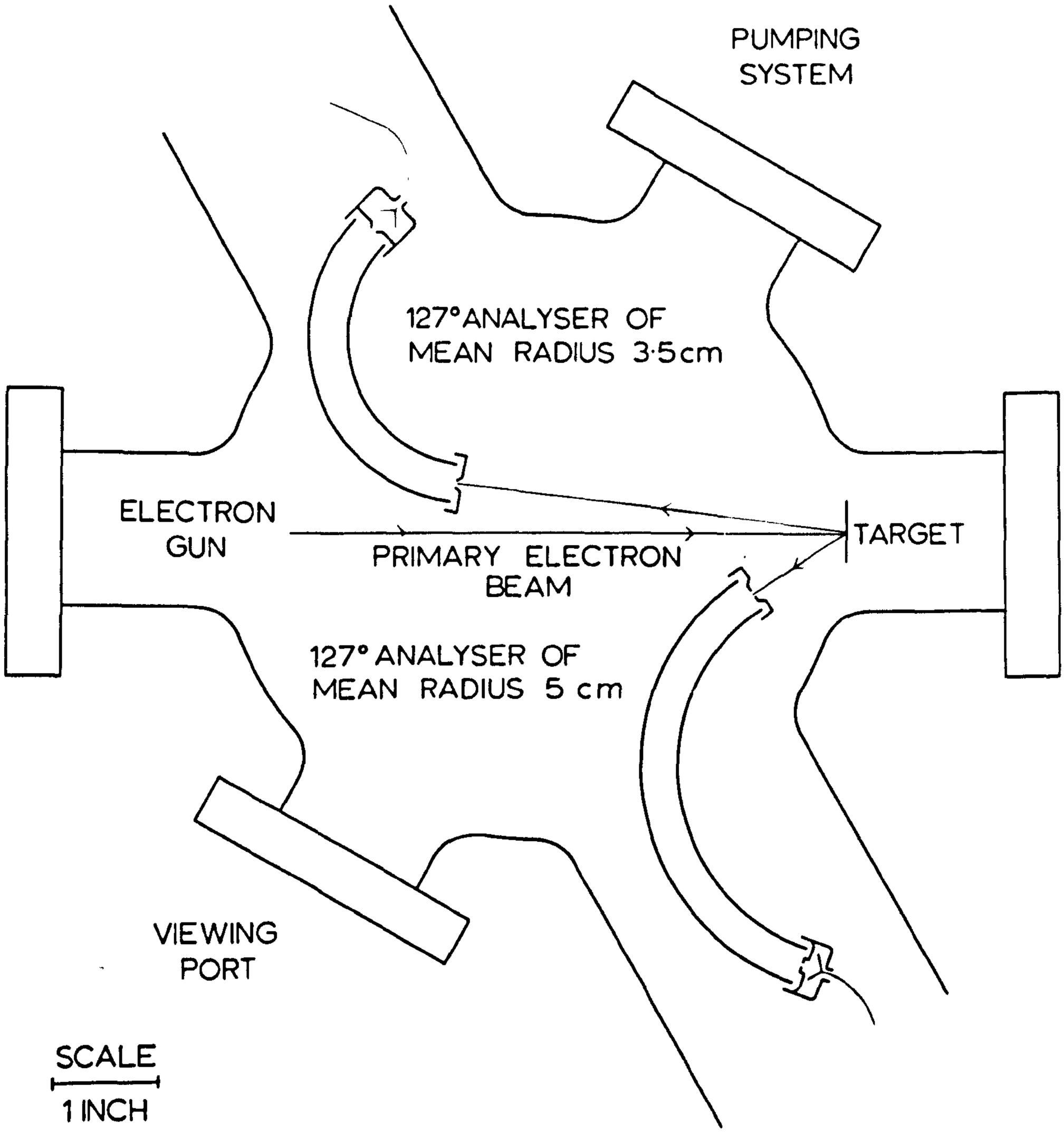

FIGURE 3.4 GEOMETRY OF THE FIRST 127° ANALYSERS WITHIN THE VACUUM CHAMBER.

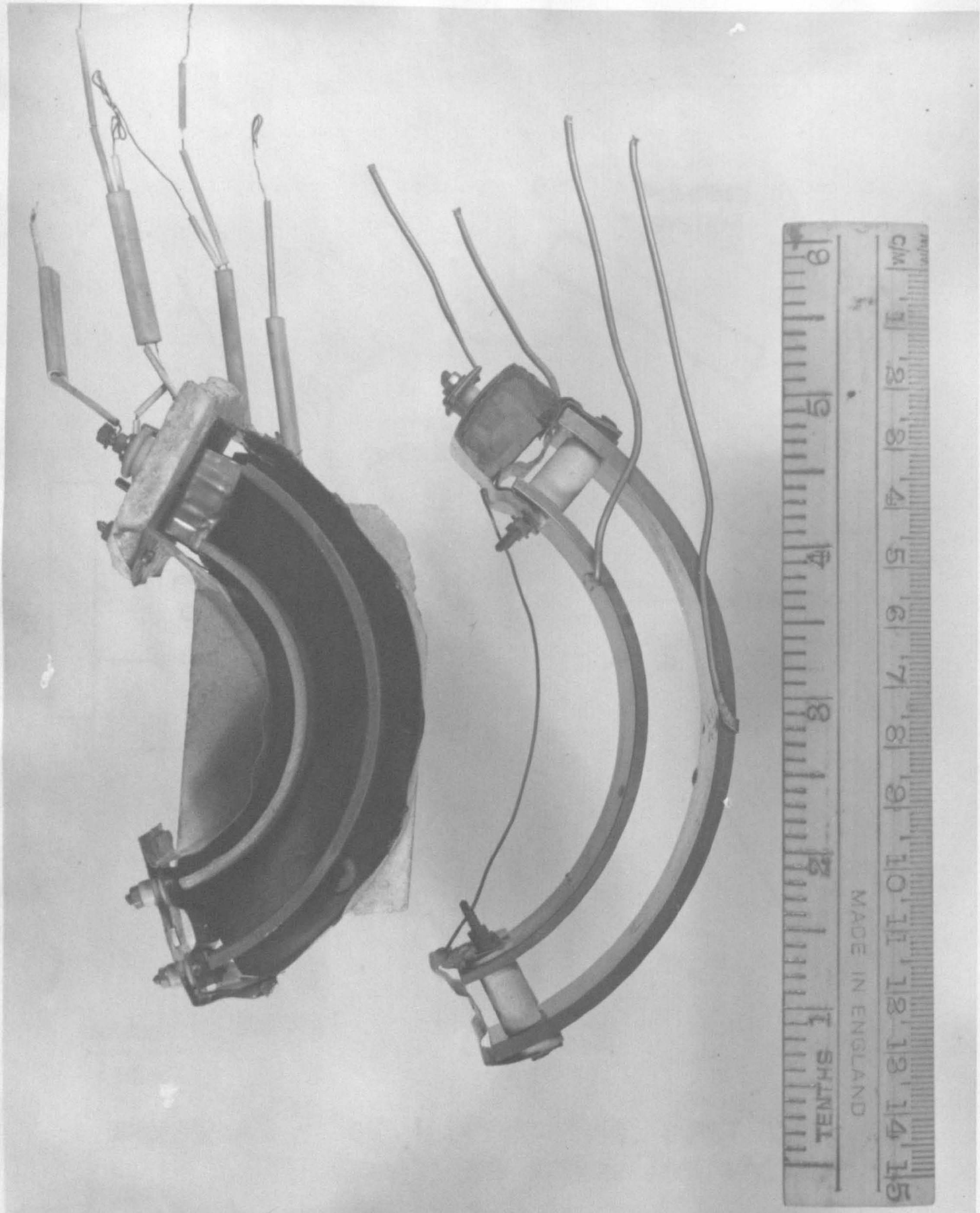

FIGURE 3.5

3.4 *First 127° analysers*

The interval up to the arrival of the manifold was used by the author to design and make a pair of 127° analysers, the intention being to use them as shown in Figure 3.4 to detect secondary electrons emitted from the target in two distinct directions. The plan was to use primary electrons with a potential of several hundred volts, and to reproduce the work of HARROWER as an initial trial. Using a 127° analyser HARROWER[30,31] had been able to obtain the CEL spectra of tungsten and molybdenum and observed evidence of Auger electron emission.

Each analyser was made from a pair of stainless steel tubes cut into 3 cm high cylindrical arcs of 127°C and mounted 1 cm apart with ceramic spacers, as shown in Figure 3.5. Their mean radii were 5 and 3.5 cms. Each had an entrance slit and the exit slit wrapped around a collector forming a faraday cage. The last items were all stamped out and formed from nickel sheet.

3.5 *Difficulties: magnetic shielding*

Experience with this first arrangement revealed several weaknesses in the apparatus:

(a) Although the stainless steel system itself was non-magnetic the stray fields from the ion pumps caused considerable deflection of the electron beams.

(b) The results from the 127° analysers showed that there were tertiaries being formed within the analysers and stray electrons were entering them through the top.

(c) The collecting cups in the analysers were not adequately shaped to capture all the electrons which fell on them.

To counteract the first difficulty a quantity of magnetic shielding known as "Netic" and "Co-Netic" shielding* was purchased. Netic material has a comparatively low permeability, but saturates at a high flux density, whilst Co-Netic has a higher permeability and a lower saturation density. Therefore they are used in alternate layers, the Netic material on the outside attenuating the external field to an intensity low enough to prevent saturation of the Co-Netic inner layer.

The main advantage of this material over the more conventional μ- metal was that it did not lose its properties when bent, soldered or drilled, and required no annealing. The ion pumps had heavy gauge

* (Made by the Perfection Mica Co., Chicago.)

Netic boxes made to enclose the magnets, and the rest of the system was isolated in a double enclosure of Netic and Co-Netic lowered over the apparatus in the form of a box. The residual magnetic field as measured by a sensitive Hall Effect probe (See Section 4.10) was less than 20 mgauss.

Described in the next section are the analysers which progressively surmounted the defects apparent in the first analyser design.

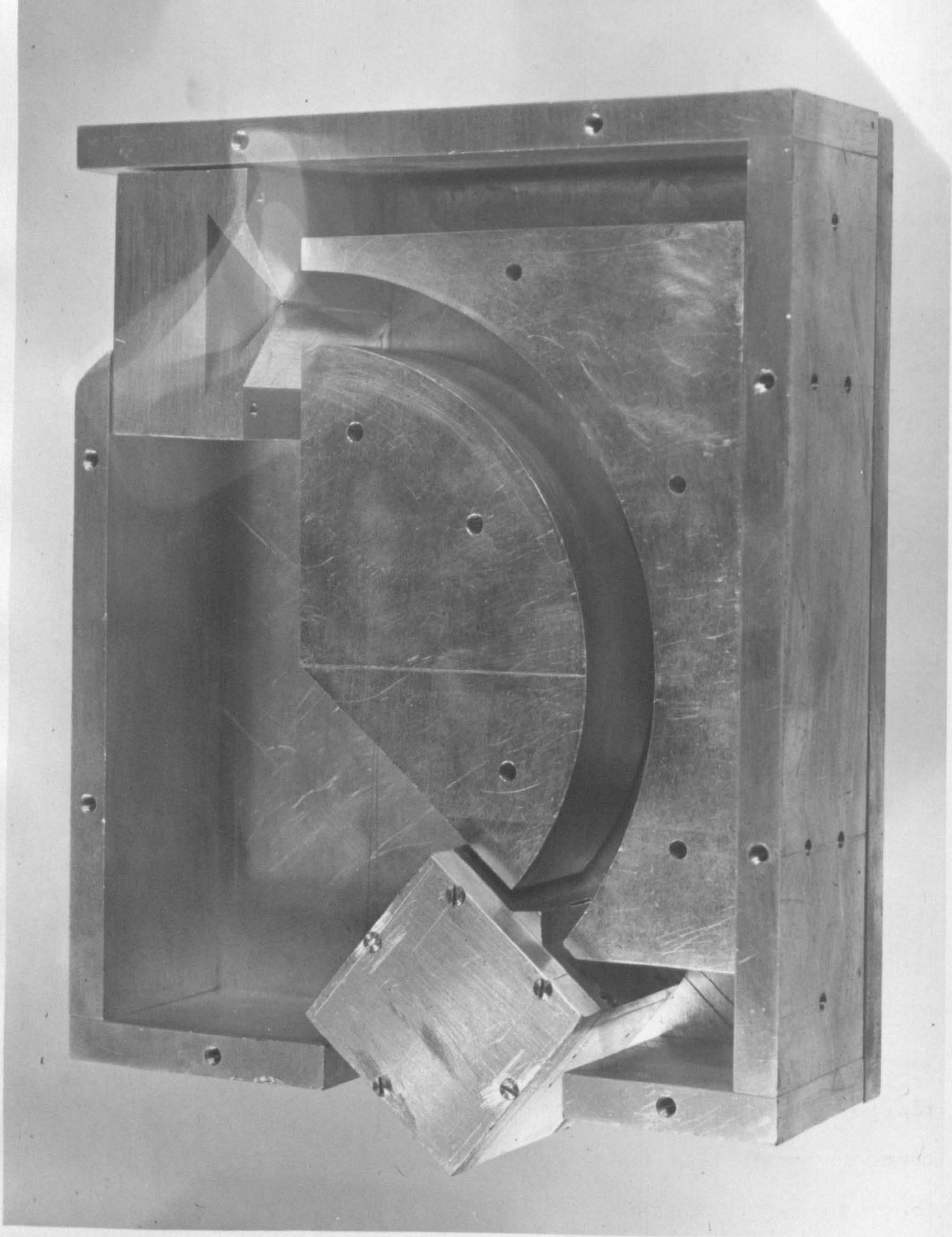

FIGURE 3.6

3.6 *More analysers*

The second type of analyser was constructed on a flat ceramic plate. The same kind of cylindrical arcs were given a sputtered coat of TaC on the inner faces, and were bolted down onto the plate. Similarly supported were the entrance and exit slits, and the collector was a U-shaped pice of nickel also with a coating of TaC. These coatings were very rough in character, having the texture of medium grade sandpaper, and this fact contributed to the low secondary yield of the material[22]. The whole of the analyser was then surrounded with a nickel shield to prevent the entrance of stray electrons. The results obtained using this analyser were more satisfactory and are present in Chapter 5

The third and final type of analyser was machined entirely out of dural. This material is non-magnetic and has a low yield ($\delta<1$), thereby reducing the number of tertiaries scattered from the arc walls to a minimum. The arcs were milled out of a single piece of metal to an accuracy of better than 0.001" and subtended an angle at centre of 131^{o}. The positions of the final slit of the entrance apertures and the exist slit defined the required $127^{o}17'$, each of them projecting between the arcs. These items were all bolted to a base plate, with fine adjustment possible in their positions, the arcs being located on ceramic washers to provide electrical insulation. The base plate formed the bottom of a shielding box which completely surrounded the analyser but for the entrance apertures and collector configuration. Figure 3.6 shows the complete assembly with box lid removed.

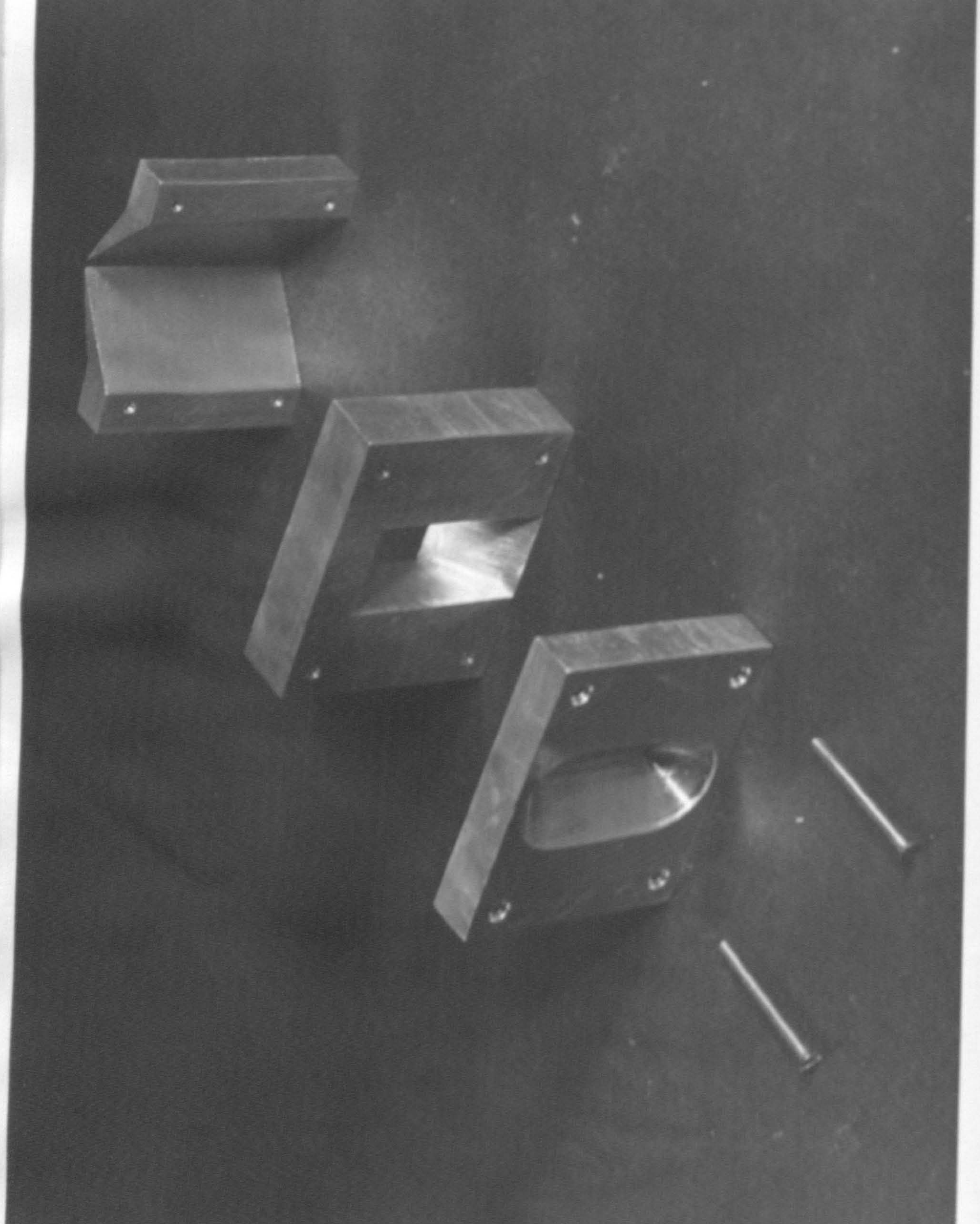

FIGURE 3.7[a]

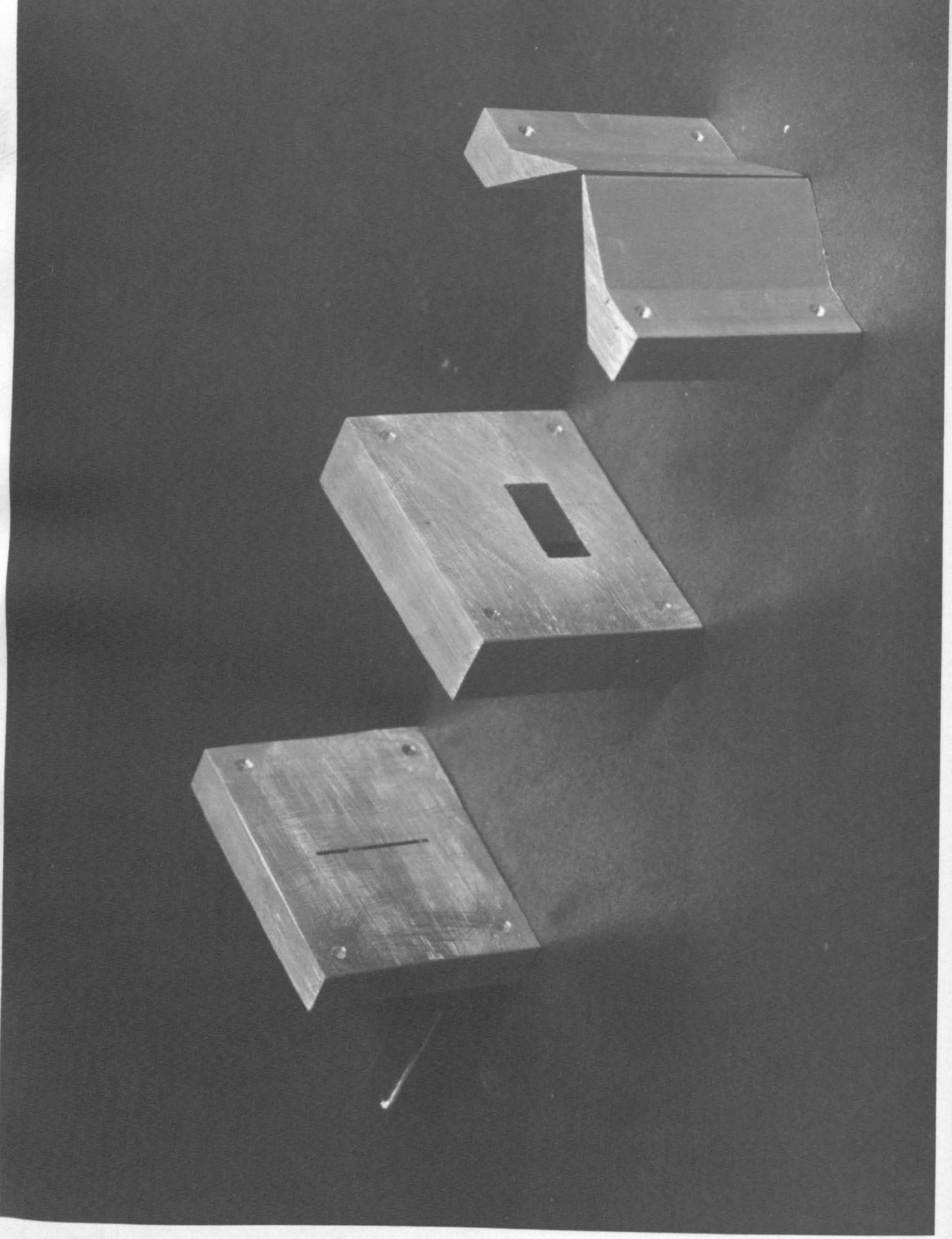

FIGURE 3.7[b]

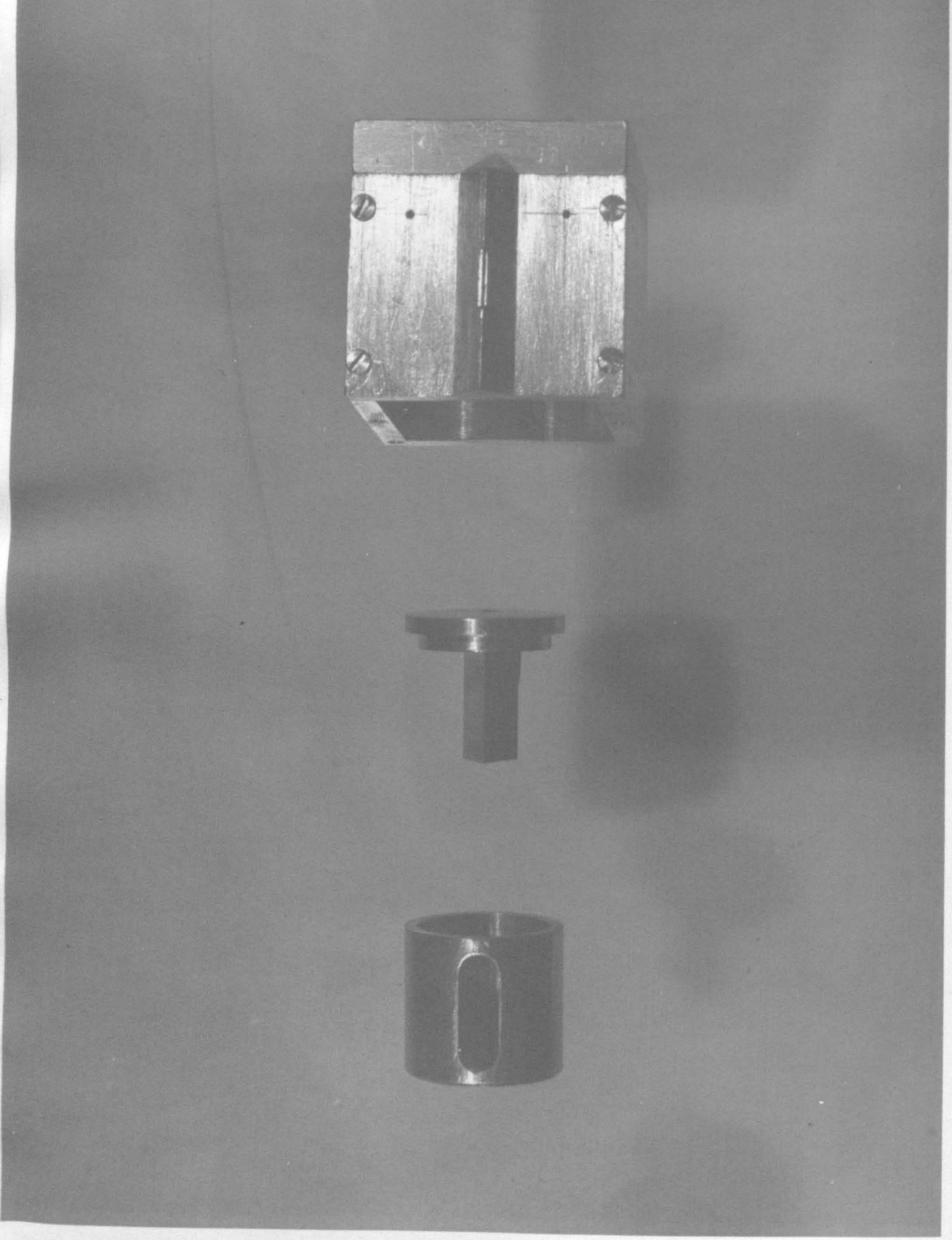

FIGURE 3.8

Exploded views of the entrance apertures are shown in Figure 3.7. The purpose of the apertures was to:

(a) define a narrow slit width (0.01")

(b) define a small entrance aperture angle (± 2°)

(c) distort the field between the plates as little as possible

(d) inject electrons along an anode (earth) potential line.

Theoretically attainment of these objectives gives a resolution at half peak height of about 0.6%.

As can be seen from the photographs the entrance slits were made up of several pieces bolted together. The outer two slits defined slit width and angular aperture, and the V-shape of the final slit distorts the radial field less than if it had been a flat plate. Adjustment of the final slit permitted the electrons to enter along the earth line, in this case a calculated 0.01" toward the outer (negative) arc from the point midway between the arcs. In order that the limited height of the analyser arcs ($\frac{1}{8}$") should be of least consequence, the central section of the aperture arrangement defined a fixed $\frac{1}{4}$" slit height centred at the half height of the arcs where the fringe fields were minimum. The final slit was adjustable in width in order to gain better resolution or intensity.

The collector was entirely enclosed in a separate shielding box which included the 0.01" exit slit. Electrons passing through the exit slit entered a relatively wide slit in the cylindrical collector, where escape of tertiaries was suppressed by a triangular pillar at the centre of the cylinder Figure 3.8.

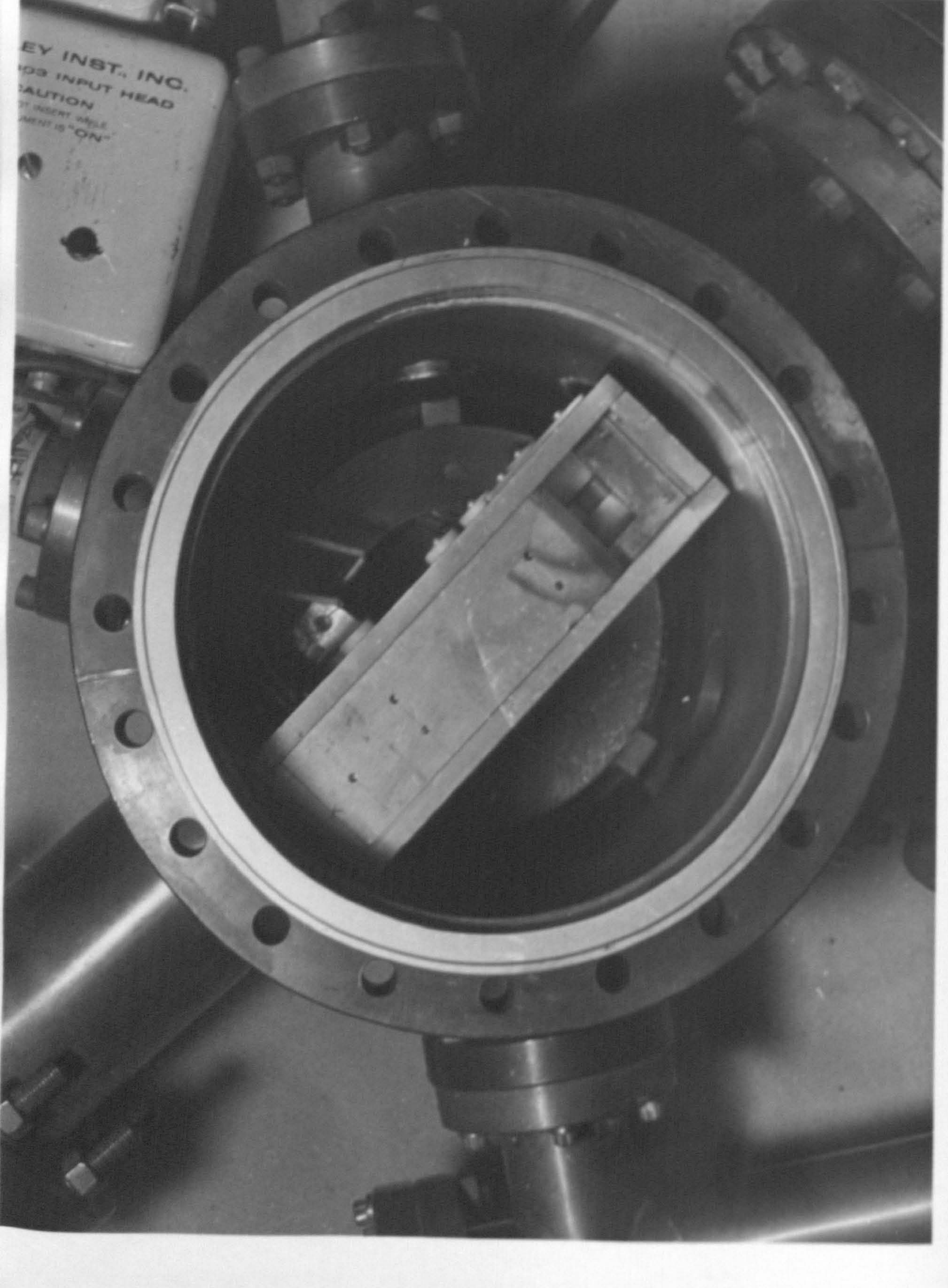

FIGURE 3.9

The analyser had a larger mean radius (5.18 cm) than the previous ones, and was mounted, as shown in Figure 3.9, with the entrance slit facing vertically upwards. This faced directly into one of the targets, as described in Section 3.8 which, being angled at 45°, allowed electrons specularly reflected from a horizontal gun to enter the analyser.

Most of the measurements reported in this thesis were made using this analyser.

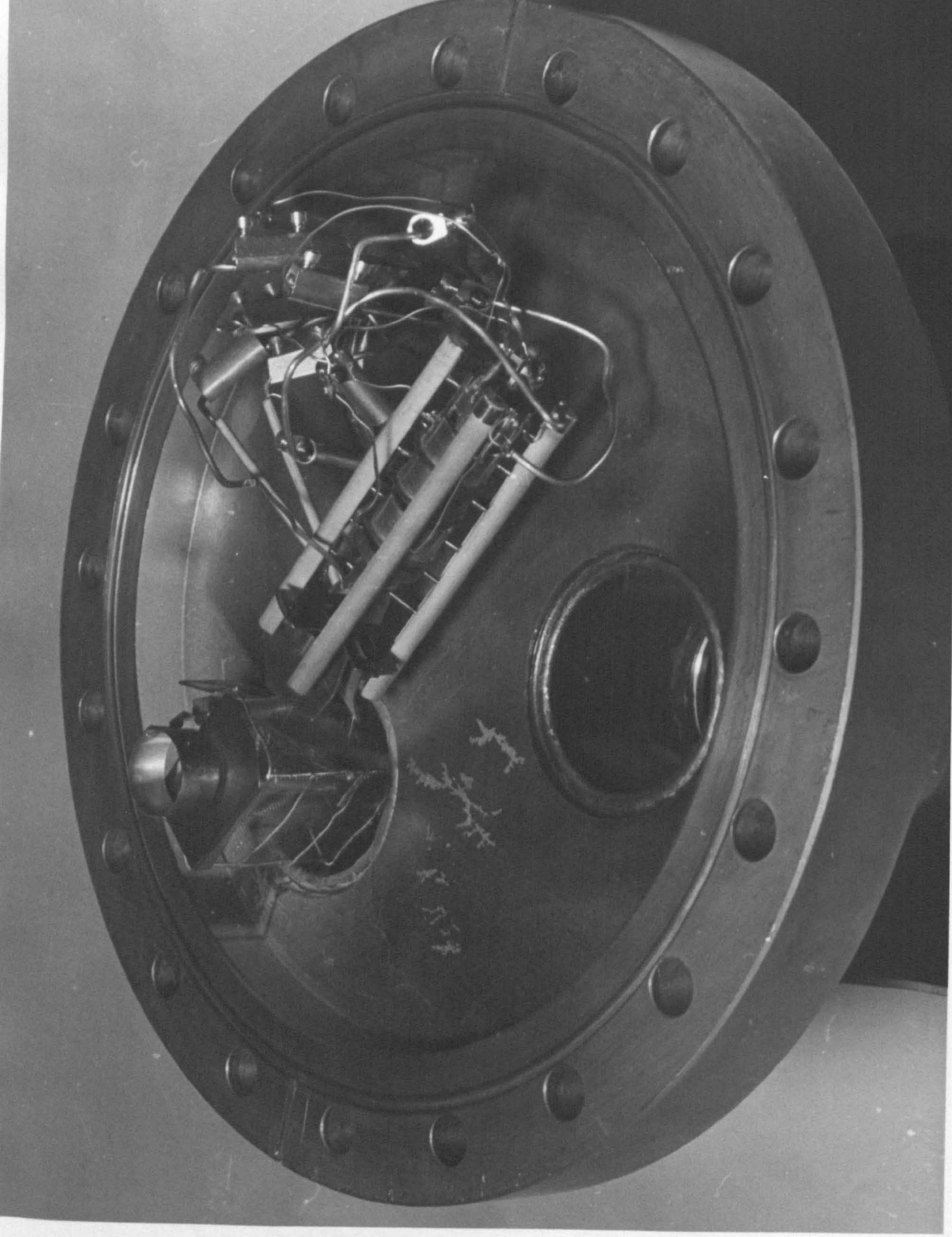

FIGURE 3.10

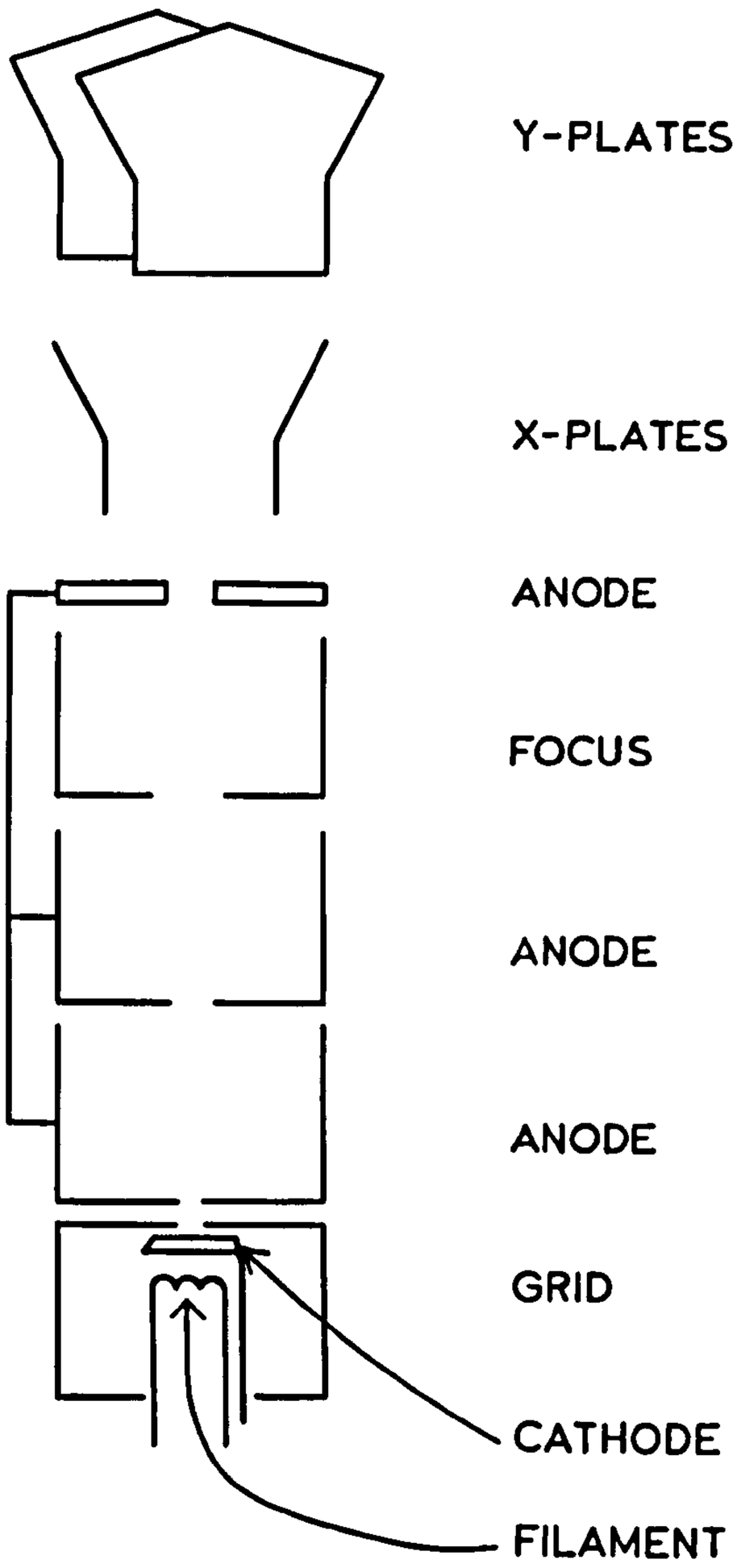

FIGURE 3.11 Schematic Diagram of the Electrodes in the Electron Gun

3.7 Electron gun

The source of primary electrons was the electron gun used in a Mullard DG7-32, a small oscilloscope tube. A photograph of one of these guns mounted on an electrical feedthrough is shown in Figure 3.10 A maximum operating voltage of 500 V was recommended for the tube, but in practice the nude gun was found to give satisfactory electron beams in the range 50 - 1500 volts.

Electrons were extracted from an indirectly heated oxide cathode through an immersion lens formed in the grid aperture (Figure 3.11). After one cross-over the accelerated electron beam entered a retarding einzel lens which performed the final focussing. A beam of low divergence and about 1 mm diameter was aimed at the target placed between 1 and 10 cm away. The position of incidence could be varied by means of X and Y deflection plates which made up the last part of the gun.

It was found that with care the oxide cathode would stand several exposures to atmosphere after activation with little or no deterioation in emissivity, before replacement became necessary.

With a good cathode the primary current was usually between 1 and 10 μA.

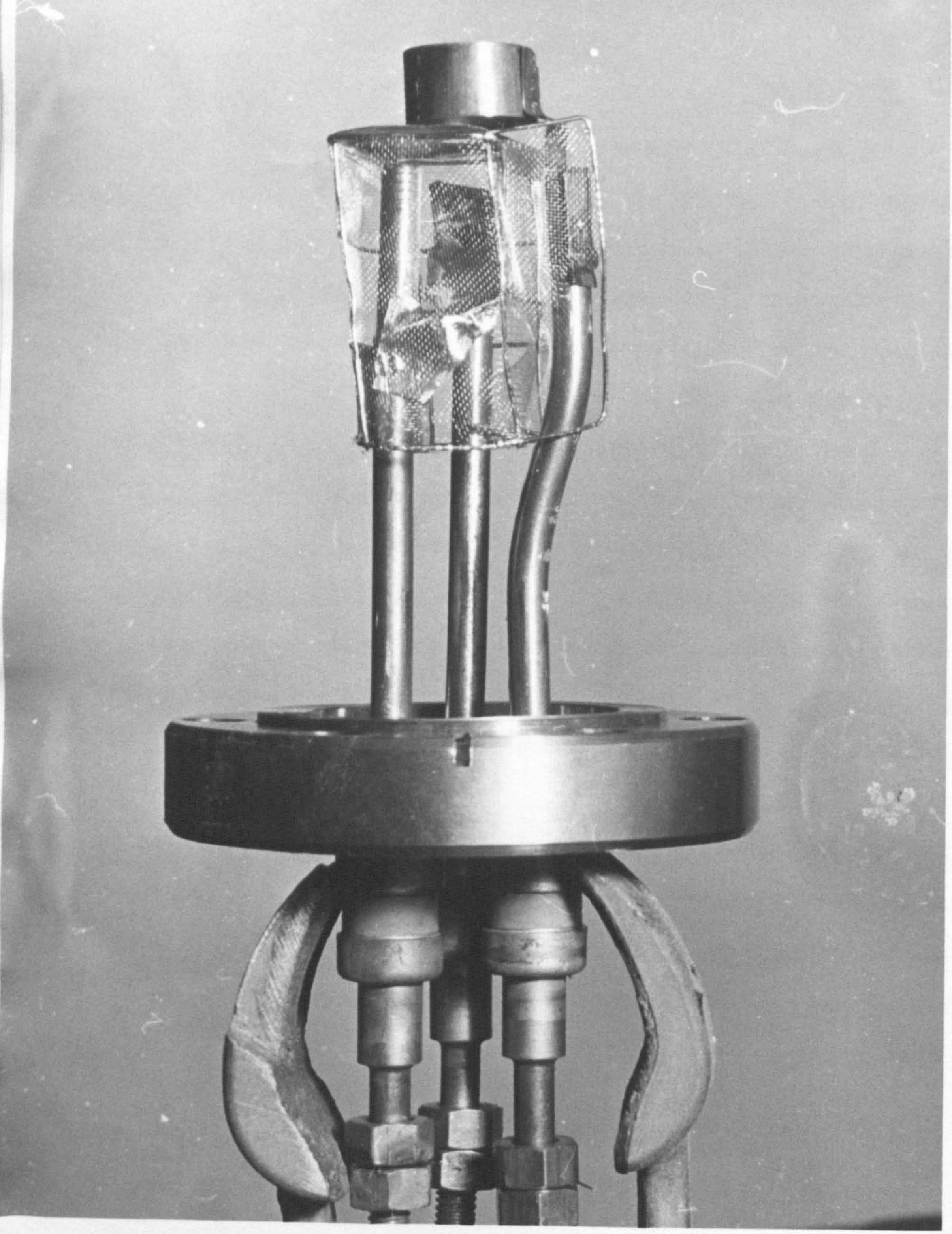

FIGURE 3.12

3.8 *Target assemblies*

All the targets used in these experiments were 4-5N grade polycrystalline strips and received a simple cleaning procedure prior to mounting within the vacuum system: first, degreasing in trichlorethylene (AR), then a light acid etch and thorough washing in de-ionised water.

Nickel was chosen as the first target material, then tungsten to correspond with HARROWER's work, and subsequently platinum, tantalum and silver were used. Platinum had the interest of being one of the substances whose main CEL was at variance with the simple plasma theory. Tantalum had not been done by anyone other than KLEINN[68]. All these metals bar silver had the advantage that when they were mounted on high current feed-throughs they could be readily outgassed and further cleaned by resistance heating. Silver had been investigated by a large number of experimenters but its plasma loss was by no means clear. Silver having the ability to wet tantalum it was mounted in a strip on top of a tantalum backing with the intention of heating it just to melting point when it would collapse forming a film over the target surface.

When 45^{o} incidence of primaries was employed in conjunction with the third analyser it was found necessary to surround the target with a cube of fine steel mesh (95% transparent). As can be seen in Figure 3.12 the primaries could penetrate one face of the cube and strike the target: but since the face on the analyser side had been replaced with a metal sheet, secondaries could only escape through a 0.4 cm hole in this direction. The emerging beam was naturally diverging and found

itself on the axis of a saddle lens which focussed it into the front entrance of the analyser. This new technique not only presented the analyser with what it required in theory but also stepped up the current reaching the analyser collector by an order of magnitude. The mesh shield around the target was separately earthed, and together with the analyser aperture formed the outer elements of the saddle lens. The central element was a short cylinder of tantalum (1.5 cm long, 1.5 cm diameter), the negative voltage on which was synchronously swept with analyser arc voltage. The mesh shield prevented this changing voltage from altering the point of incidence of the primaries on the target.

3.9 *Vacua*

To measure the degree of vacuum obtained there was an EDWARD's Pirani gauge on the sorption pump side of the bakeable valve, which gave a rough indication when it was sensible to start the ion pumps. When they are in operation the current flowing through the ion pumps is very nearly directly proportional to the pressure. With good calibration this reading corresponds closely to the "true" pressure over the range 10^{-5} to 10^{-8} torr. To extend the range of pressure measurement, and make leak detection more easy, a cold cathode Penning gauge was bought from GENERAL ELECTRIC. This instrument operates in the range 10^{-4} to (a specified) 10^{-14} torr, having a hot filament "trigger" which can be momentarily fired if and when the discharge goes out at low pressure. This was the weakest point of the instrument as this filament was not replaceable, and subsequently when the filament blew two years later the instrument was of little use as a vacuum gauge.

It was appreciated however that "true" pressure measurement required detailed knowledge of the quantities of each particular species of gas. Also it was realised that a thorough knowledge of the constituency of the ambient gas phase linked with carefully controlled target treatment would provide the practical basis required for reproducibility of results.

From the outset then there was interest in residual gas analysis, and even before the manifold arrived some experience was gained in setting up and using an omegatron. This work will not be discussed here however, since, in common with most forms of RGA the omegatron embodied ~~of a strong magnet; it was not desirable to introduce magnetic fields~~

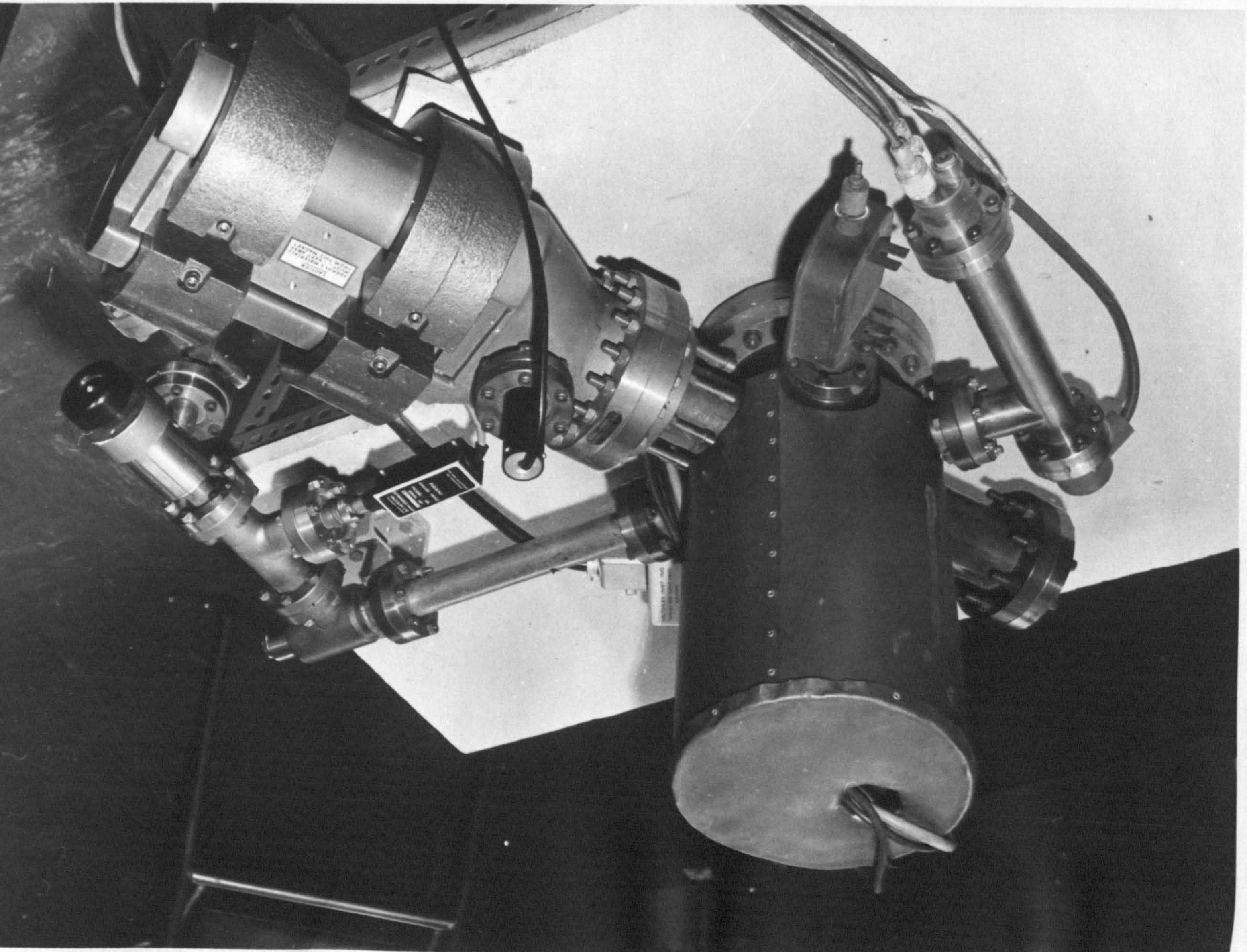

FIGURE 3.13

. a strong magnet: it was not desirable to introduce magnetic fields and enhance shielding problems. In later stages of the work a VARIAN "Quadrupole RGA" was fitted, together with the newly arrived 50 l/s ion pump, and was ready for the third analyser. The complete assembly is shown in Figure 3.13with one layer of Co-Netic shielding over the main part of the manifold.

The physics of the quadrupole is presented in Appendix B, and it will suffice here to describe the basic structure and operational techniques. The quadrupole, as its name suggests, consists of four parallel rods of circular cross-section, and in this case some 10 cm in length. They are arranged about an axis at the vertices of a square as shown in Figure B.1(see Appendix).

Ions normally incident on a circular entrance aperture positioned on the axis can move stably down the "filter" only if they have an *M/e* ratio lying within the narrow range defined by the d.c. and a.c. voltages applied to the rods. Such ions may then pass through the exit aperture and either be collected directly in a faraday cup or strike the first anode of an electron multiplier. The ions are created by a gas electron bombardment source and accelerated up to 120 V at the entrance aperture. There is no magnetic field required and a linear mass spectrum of the residual gas may be displayed on an oscilloscope or recorder by suitably chosen sweep rates of the d.c. and a.c. voltages.

If the d.c. voltage is switched off the quadrupole passes all the ion species more or less independent of *M/e* ratio. Thus another form of total pressure measurement was available which made the loss of the GE gauge less critical.

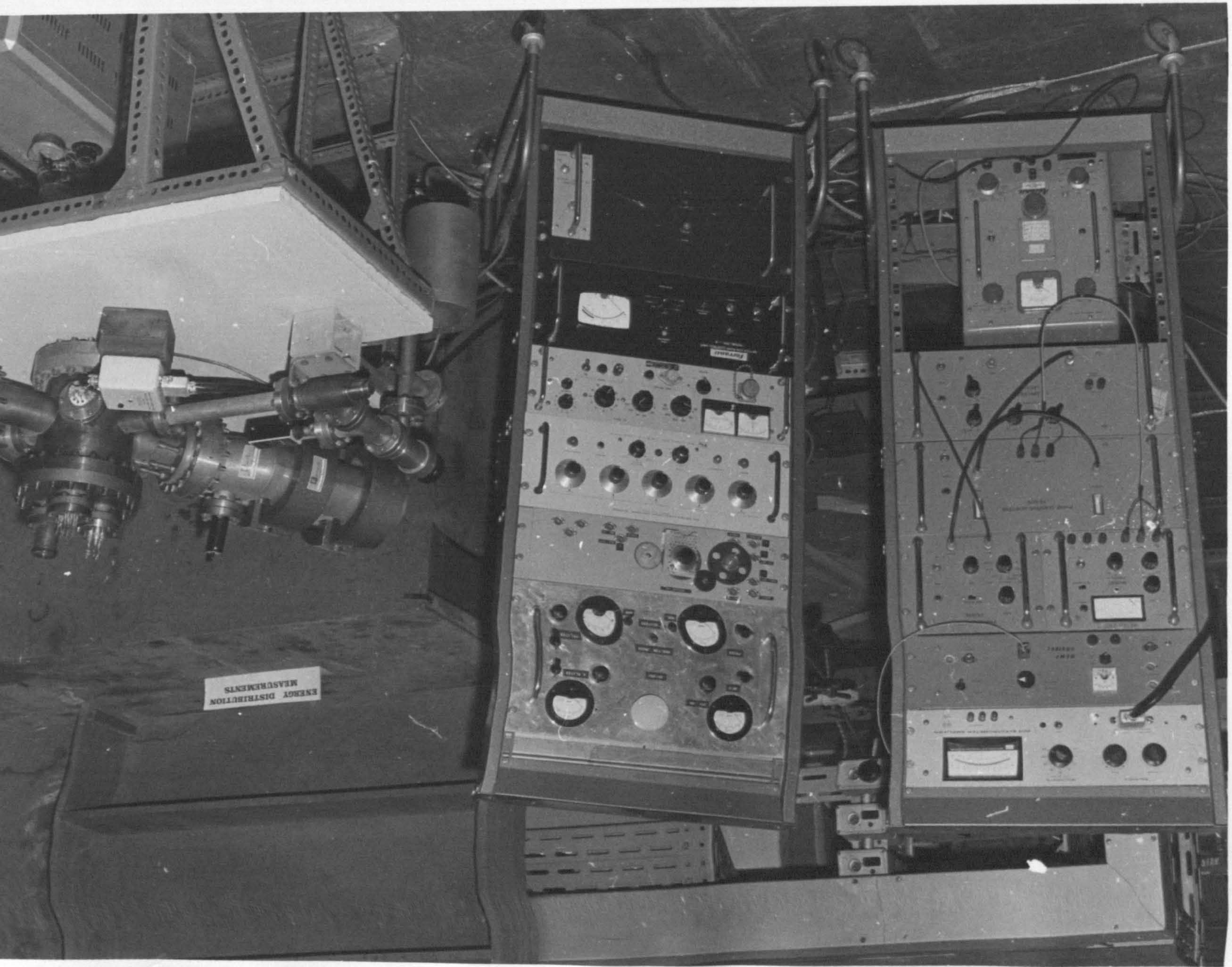

FIGURE 4.1

FIGURE 4.2

FIGURE 4.3

CHAPTER 4

INSTRUMENTATION

4.1 *Disposition*

This chapter is devoted to a description of the specifications and operation of the many instruments which were used in the investigation.

The general disposition of the laboratory in summer 1967 may be seen in Figures 4.1 and 4.2 . The cylindrical manifold will be recognised in Figure 4.1 sitting on a Marionite base supported on a Dexion framework. On the left of the system are rack 1 and rack 2. In Figure 4.2 the QPSA system can be seem with rack 3 on its right and rack 4 on the left.

The instruments can be divided into two main groups: those purchased from commercial companies, which will receive only a cursory description, and those which were built by the author which will be given a more detailed treatment, despite their relative simplicity. Instruments of the first group will be dealt with in Sections 4.2 to 4.7.

4.2 *Ion Pump controls*

An 8 l/s ion pump control unit appears near the base of rack 1, shown in detail in Figure 4.3. It supplies a stabilised 3 kV to the pump anode and the single metre may be switched to read log scale pressure, anode voltage, and decade ranges of discharge current from 500 mA to 5 μA. The 50 l/s pump also uses 3 kV but since it has a larger electrode area its power supply is similar but heavier.

4.3 *D.C. voltage generators*

Very stable d.c. voltage supplies were an important requirement for the work. In several cases dry batteries were used but two power packs provided a wide range of finely adjustable voltage. They may be seen immediately above the ion pump control unit in the middle of rack 1.

The lower one, a John Fluke 413C power supply, usually provided the accelerating voltage for the electron gun. It has two polarities and a range of voltage settings from 0 to 3111 V with a quoted resolution of 2 mV and 'resetability' of ± 0.05%. A crude voltmeter gives an indication of the voltage setting and a second meter displays the current being drawn up to 20 mA.

The power pack above the 'Fluke' was the Keithley 241 regulated voltage supply. It provides a twin positive and negative output either of which can be earthed to give a single polarity, or they may be 'floated' about an earth established outside the unit. Most frequently it was used in this last mode, acting as the source for the analyser arc voltages. With maximum setting of 1000 V its lowest range switches from 10 to 90 mV and there is a fine uncalibrated adjustment in the next decade.

4.4 *Quadrupole supplies*

The remaining power packs came in a unit as the supplies for the Varian quadrupole RGA. They may be seen in the lower half of rack 3. The control unit, third from the bottom, has a meter scaled up to 50 which follows the spectrum scanning in mass numbers. In fact the quadrupole has two ranges of scan 0 to 50 and 0 to 250 amu, the latter one being of little importance, once the cleanliness of the systems had been established. The scan has completely variable limits, and the rate of scan in the 0 to 50 amu range can be chosen from 1 msec. to 30 sec. per amu. At any moment during the scan the press of a button restarts the scan again from the lower limit.

A feature of the quadropole, as shown in Appendix B, is the 'trading off' permissible between sensitivity and resolution. A ten turn potentiometer at the bottom of the control panel determines the required resolution. At the bottom left of the panel are the controls over the thoria coated iridium filament in the electron bombardment source which are normally adjusted to provide 1 mA of emission. They could be turned up high to give some 30 mA of emission current in order to outgas the ion source, which was usually necessary after the system had been let up to atmospheric pressure.

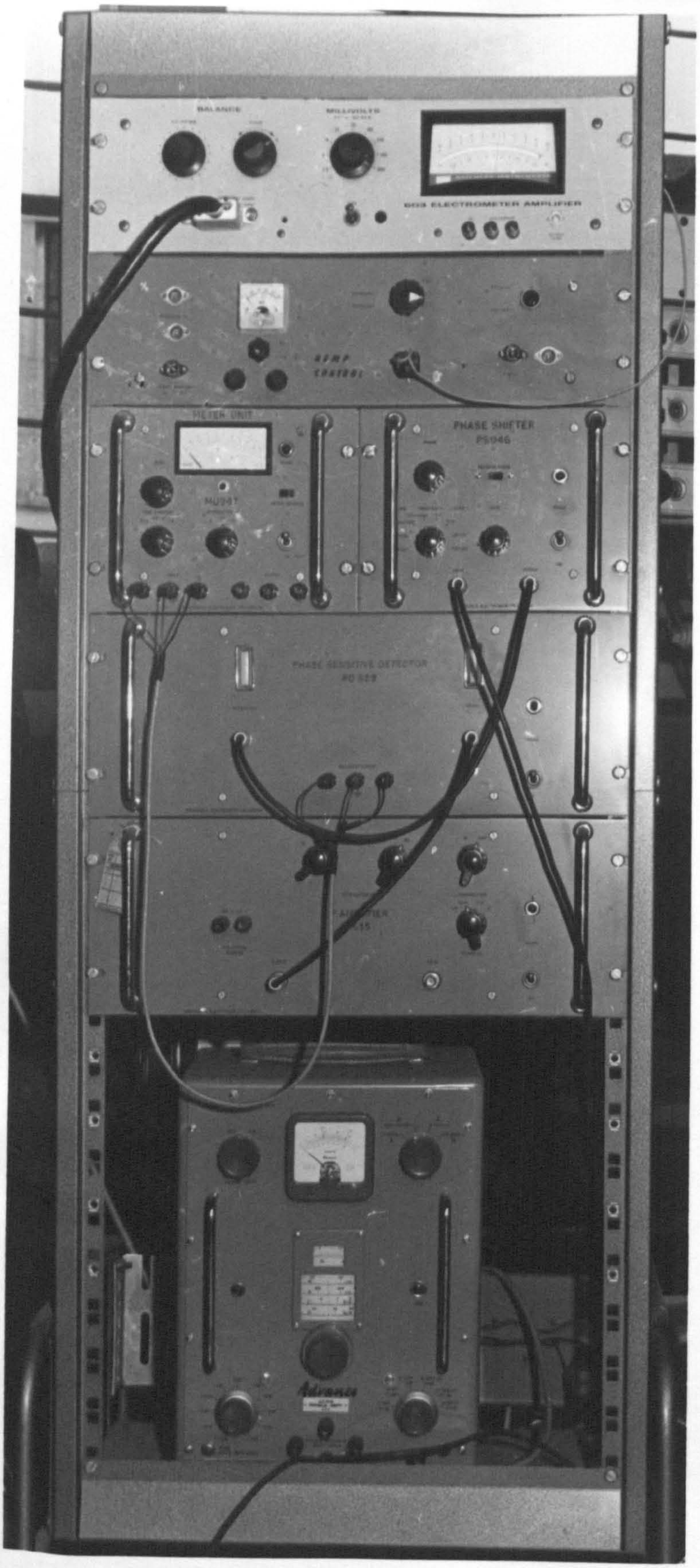
BALANCE
MILLIVOLTS
903 ELECTROMETER AMPLIFIER
METER UNIT
MU941
PHASE SHIFTER
PS946
PHASE SENSITIVE DETECTOR
Advance

FIGURE 4.4

4.5 *Electrometer Amplifiers*

Essentially there were three electrometer amplifiers involved in the measurements, although only one was so called. Consisting of a direct-coupled d.c. amplifier with a large amount of feedback each one had very high input impedance and was able to respond to fairly rapid changes in low level signal. More precise figures are given as each is discussed in the following subsections.

4.5.1 The main part of the Keithley 603 electrometer amplifier may be seen at the top of rack 2 in Figure 4.4 and its preamplifying head at the end of a 24 feet cable is shown next to the vacuum system in Figure 4.1 It amplifies voltages from d.c. to 50 kHz and displays d.c. measurements from 2.5 mV to 1 V fsd on the single meter. Suppression of up to 1 V d.c. is provided to permit detection of low level signals above a large background. When required in its current measuring mode its input impedance of 10^{14} Ω becomes valuable, and the appropriate high resistor is inserted into the preamplifier.

By this means currents in the 10^{-11} to 10^{-12} amp range were fairly easy to measure providing care had been taken in placing electrostatic shielding around the vulnerable connection to the vacuum system. Within the vacuum system too, shielding was required to reduce the capacitative pickup from other internal connections and prevent the collection of stray electrons. Naturally the system was well earthed to avoid interference from external sources, but nevertheless noise was still a

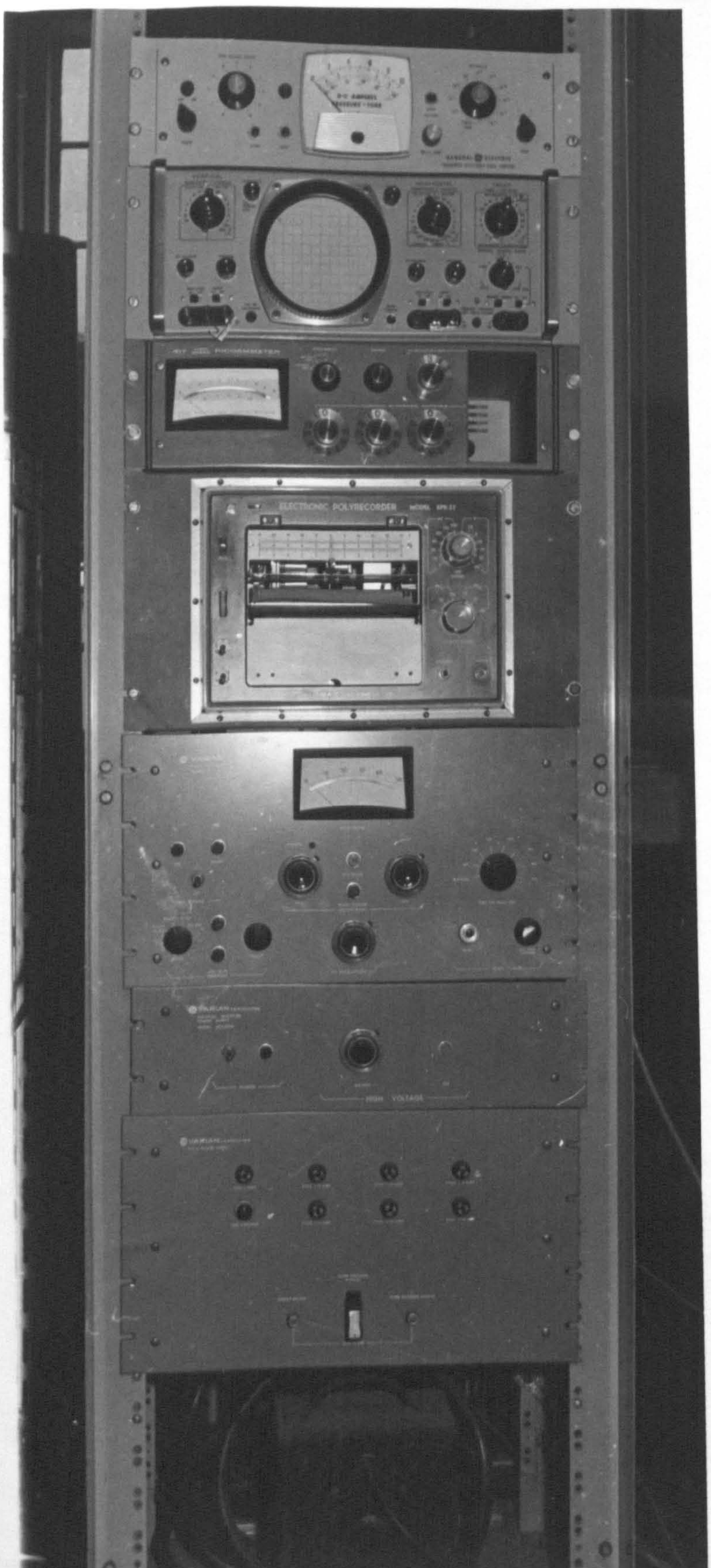

FIGURE 4.5

problem on the more sensitive ranges.

The electrometer was usually used to measure the collector current from the analysers, and it provided a 10 V output for recording purposes.

4.5.2 A Keithley 417 picoammeter was used to measure the target current and the ion current from the quadrupole. It is the third instrument down in Figure 4.5 , its preamplifying head being withdrawn from the case. Like the Keithley 603 this can be attached to a long extension cable, the head containing its own high resistors which can be switched to measure currents in the range 10^{-13} to 3×10^{-5} amp fsd. It has a zero suppression like the Keithley 603 and is fairly fast in its response, 1 second on the 10^{-13} amp range (50 pf. output). To cut down noise the head has a filter network which can be switched on, though of course this reduces the bandwidth. At the rear an output of 3V is available for recording purposes.

4.5.3 The GE gauge control can be seen as the top unit in rack 2 (Figure 4.5). It provides a 2 kV supply for the gauge head and trigger heating current when necessary. The collector current is amplified by an electrometer circuit whose input resistors may be switched on the front panel. The measured current can lie between 10^{-4} and 10^{-13} amp fsd and this is the reading displayed on the meter.

To obtain pressure readings from this assumptions have to be made about the nature of the residual gas: if nitrogen then one divides the scale reading by 2.5 and so on.

As mentioned in the last chapter there are some weak features in this instrument: another one is the poor nature of the connection between vacuum head and cable terminator. When the trigger filament finally blew, though that was the end of a vacuum gauge, an adaption was made to use the electrometer side to measure ion or electron currents.

4.6 *PSD equipment*

The phase sensitive detection equipment, a Brookdeal PD629, was principally used in conjunction with the RPSA. It was housed in rack 2 (Figure 4.4) and used by the author in connection with a Hall effect magnet probe (HEMP), which is discussed below in 4.10. This phase sensitive detector (PSD) can operate up to 100 kHz but the HEMP purposes about 70 Hz was used.

No detail of the theory of a PSD will be given beyond saying that it is a sophisticated electronic switch which permits detection of only that part of the signal in phase with a reference signal. Thus by some means one modulates the signal with the chosen frequency and the PSD rejects noise of significantly different frequency.

4.7 *Oscilloscope and chart recorders*

Very useful as a general purpose instrument in connection with the eradication of noise, and in conjunction with the PSD, was the 301 C oscilloscope made by Hewlett Packard. It is shown in Figure 4.5 second from the top of rack 3.

Two chart recorders were used in the investigation. The first was a Moseley Autograf 680M, and the second a Japanese Polyrecorder made by Toa electronics (Figure 4.5). Both instruments have a wide range of paper speed and sensitivity and comparable response speed (2 Hz fsd). The Autograf has the advantage of an event marker which can be operated remotely from the instrument. Both recorders have an input impedance greater than 2 M Ω.

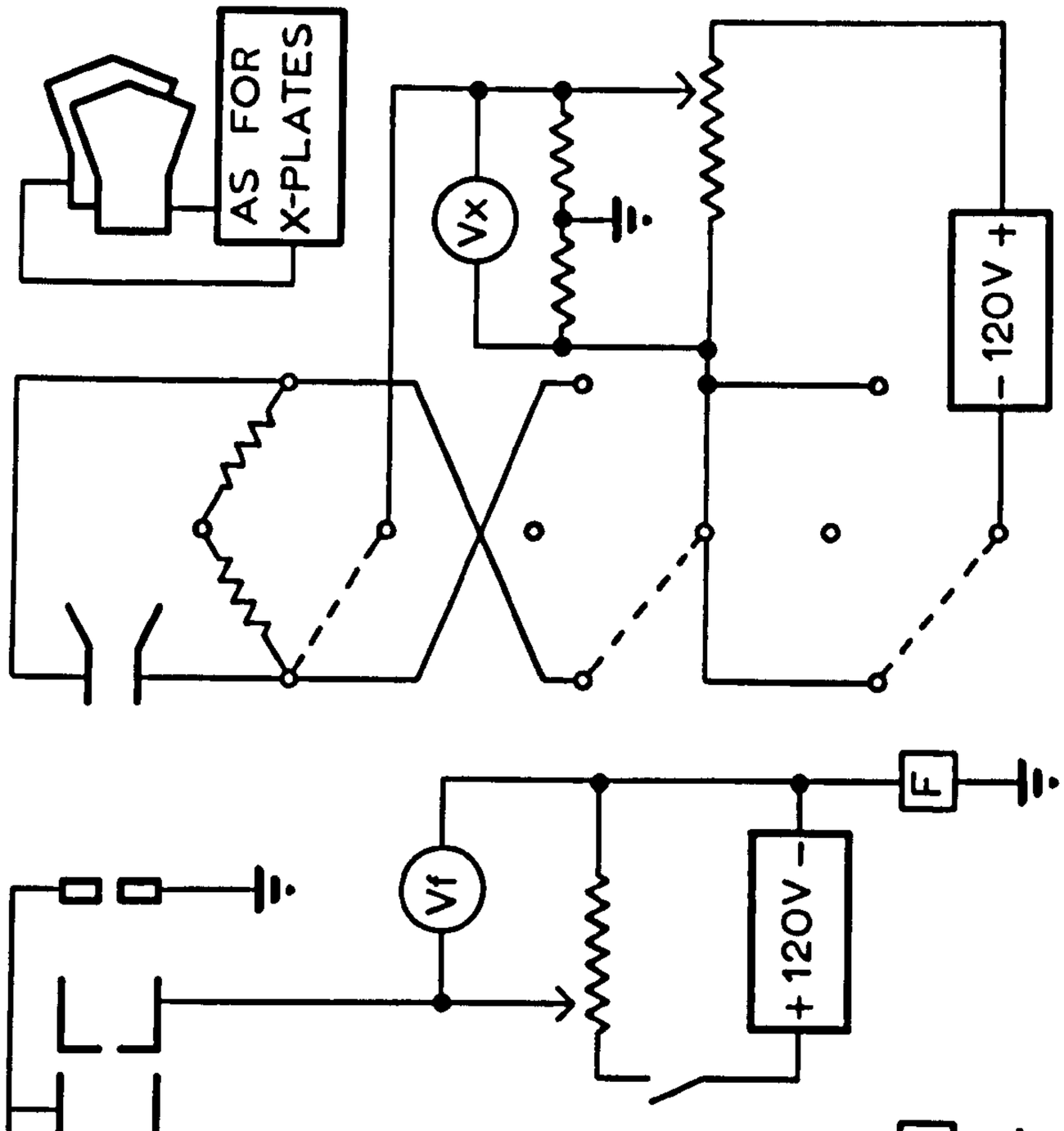

FIGURE 4.6 Circuit of Electron Gun Control (See Figure 3.11)

4.8 *Electron gun control*

This is the first of the pieces of equipment specially built by the author. It was built in order to control and monitor the electron beam within the vacuum system. It was put in the top of rack 1 (Figure 4.3) and contains four 120 volt dry batteries and the controls for the voltages on the grid, focus, and X and Y plates of the primary electron gun. These voltages are carried to the gun via a ten-way electrical feedthrough in the vacuum system. The voltages are also taken in parallel to a Mullard DG7-32 oscilloscope tube which is mounted in the front plate of the control box.

This arrangement permitted the virtual observation of the focussing and deflection of the primary electron beam in the vacuum system. Also, by observing the changes in target current as one scanned the beam around, one could draw the apparent shape of the target on the face of the oscilloscope and thereby make selection of the point of incidence.

The circuit diagram is given in Figure 4.6. The gun was operated with the heater and cathode held up to negative potential, and thence the electrons were accelerated down to earth potential. This negative potential, supplied by the Fluke power pack to common points in the diagram, is indicated by a boxed F . A 12 V heavy duty battery, housed in a shielded box beneath the vacuum system, supplied the 0.3 A to the filament which was centre tapped to the Fluke voltage. The grid was operated at a potential negative to the cathode in order to control the immersion lens and form a small object cross-over. This

negative difference between the grid and cathode was shown on a meter and called the grid voltage (Vg). After acceleration down to earth potential the electron beam had to surmount a saddle field formed by a cylinder whose potential was varied positively from cathode potential. This difference was called the focus voltage (Vf) and displayed on another meter.

The electron beam then accelerated down to earth again on the far side of the saddle and passed through an earthed anode aperture of 0.15 cm. On the far side of this lay the X and Y deflection plates which, when needed, held voltages either side of earth. A three layer wafer switch enabled the polarities to be reversed and the voltage difference between either pair of plates was shown on the appropriate meter

4.9 *Magnetic probe control*

A Hall effect magnet probe (HEMP) was bought from Siemens (FC 34) in order to investigate the effectiveness of the magnetic shielding. This device is made of a thin layer of indium arsenide and has a sensitivity of 145 μV/amp gauss. However the resistive component at zero field introduces a false voltage (Vz) of the order 1000 μV/amp, and since there was interest in measuring residual fields with intensity well under a gauss, clearly careful techniques would be needed. With the normal control current of 200 mA passing through the 15 mm long crystal some 600 mV are generated, and the contacts sensing the Hall voltage (Vh) only have to be misaligned by 0.005mm to produce such a Vz.

Using a d.c. control current one can eliminate Vz by making two measurements of any field: with the field in one direction the voltages may combine to give (Vz + Vh), and when the field is reversed (probe rotated) the voltages will subtract to give (Vz - Vh). Subtraction of these two readings leaves one with 2 Vh from which one can deduce the field intensity, knowing the sensitivity of the probe.

Another problem was anticipated, however, for in fields of the order 30 mgauss even this very sensitive probe would produce only about 1 μV. Therefore, since the same arguments apply to the elimination of Vz in a.c. as in d.c., the PSD equipment was brough in to remove noise difficulties. The HEMP control was built with all this in mind and had the facility of operating a probe d.c. or a.c. with very

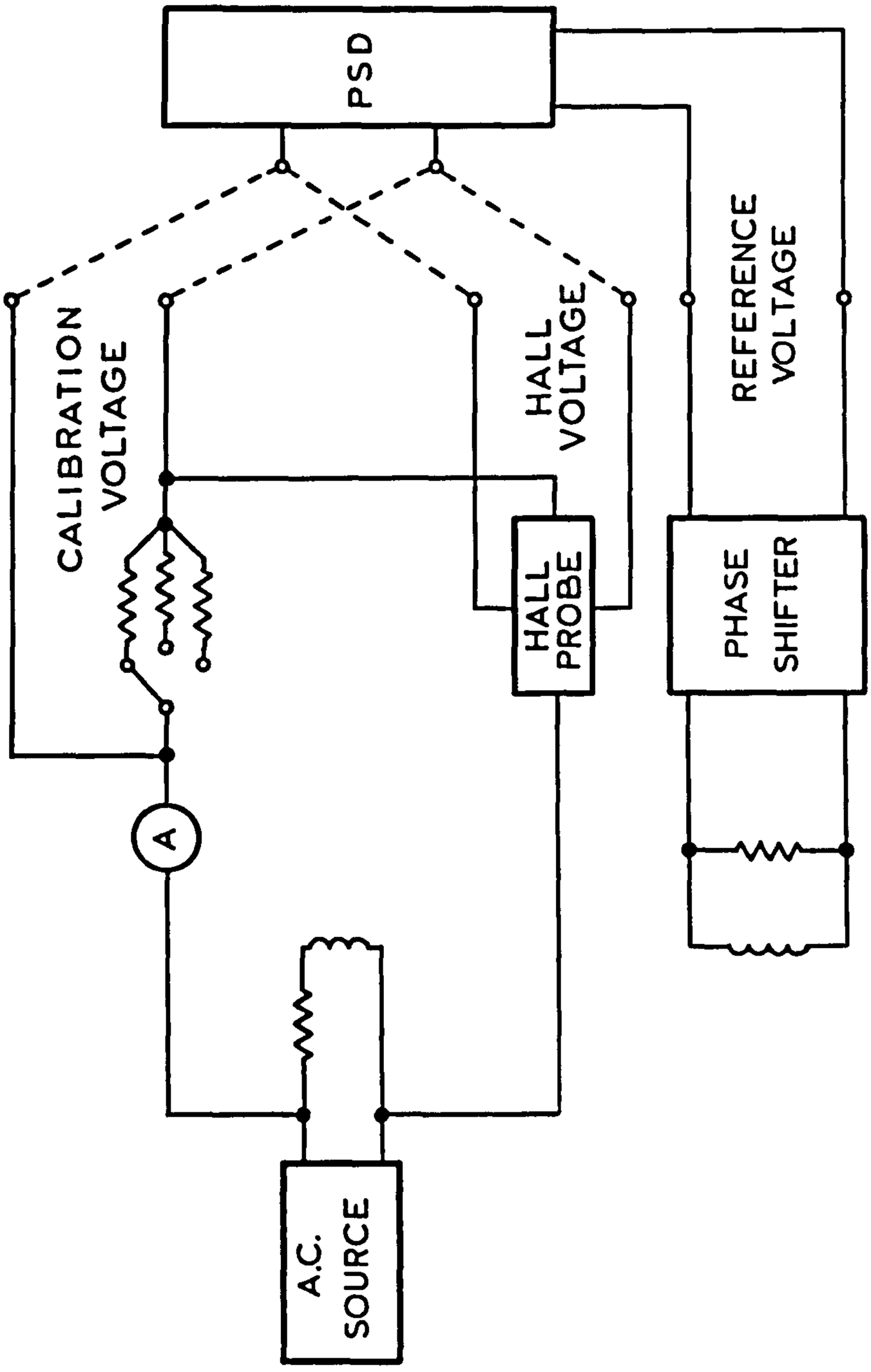

FIGURE 4.7 HEMP Control Circuit

simple circuitry, as shown in Figure 4.7.

A signal generator fed power into a transformer, the loaded secondary of which provided the reference signal for the PSD via the phase shifter. In parallel with the primary winding the control current was drawn, to go in series through the probe, ammeter, and one of a number of standard resistors.

The voltage generated at the Hall contacts was fed into a low frequency amplifier which passed the signal onto the PSD. The deflection of the meter was noted and the NEMP control switched to 'calibrate' to compare the reading with the known voltage dropped across one of the standard resistors. Then the probe was rotated and the procedure repeated.

In this way, taking quick readings to avoid temperature effects, no difference greater than 0.6 μV was detected and, after a set of calibrations with standard magnets had confirmed a sensitivity of 150 μV/amp gauss ± 3%, it was concluded that the residual magnetic field within the Netic and Co-Netic shields was not greater than about 20 mgauss.

4.10 Gears

Over the three year period of the investigation proper, the scanning of the arc voltages gradually developed into a fairly length set of meshing gears. The final version can be seen in Figure 4.3 just beneath the gun monitor apparatus. Concealed behind the panel was a reversible Citenco electric motor of variable speed which drove the wheel on the right. The next wheel rotated the shaft of a ganged pair of fifteen turn helipots. These were precious items each being 1 MΩ and standing the several hundred volts required for the arc voltages. A rotation indicator on the front of the shaft gave a good indication of the output voltage for the helipots were linear to ± 0.025%, but when accuracy was required a valve voltmeter was connected to a test socket. The third gearwheel was merely a jockey driving the final wheel on the left which operated another similar but single helipot. This scanned the voltage on the focussing ring (Vr), the central element in the crude saddle lens which focussed the secondaries down into the analyser.

4.11 Curve Resolver

The Dupont 310 curve resolver played an important role in the analysis of some of the results. (The author was able to use this instrument through the courtesy of the Company during a visit to London). The Curve Resolver is a special purpose analogue computer for the rapid resolution of overlapping peaks in experimental curves. To accomplish this the instrument generates a series of component peaks and synthesises a sum curve matching the original data. The operator determines the type of distribution (Gaussian, Lorentzian, etc.) which he requires the component peaks to follow, and then visually puts in up to ten of these functions at any position along the X-axis. He then can vary the height, width, and skew of each peak independently until the automatically generated sum curve fits the experimental curve to his satisfaction.

One snag with the technique is that generally no experimental curve will have a unique breakdown into component peaks, although a solution which requires the minimum number of peaks is readily obtainable. In practice it relies upon the operator knowing to some extent the type of solution he seeks.

As far as the results reported in this thesis are concerned the component peaks were assumed to be Gaussian, and the solution sought was generally the one requiring the least peaks. Effectively the Curve Resolver improved the resolution of the CEL spectrum and enabled the author to place the position of the peaks more accurately.

FIGURE 5.1. Quadrupole analysis of unbaked system at ~ 10^{-8} torr.

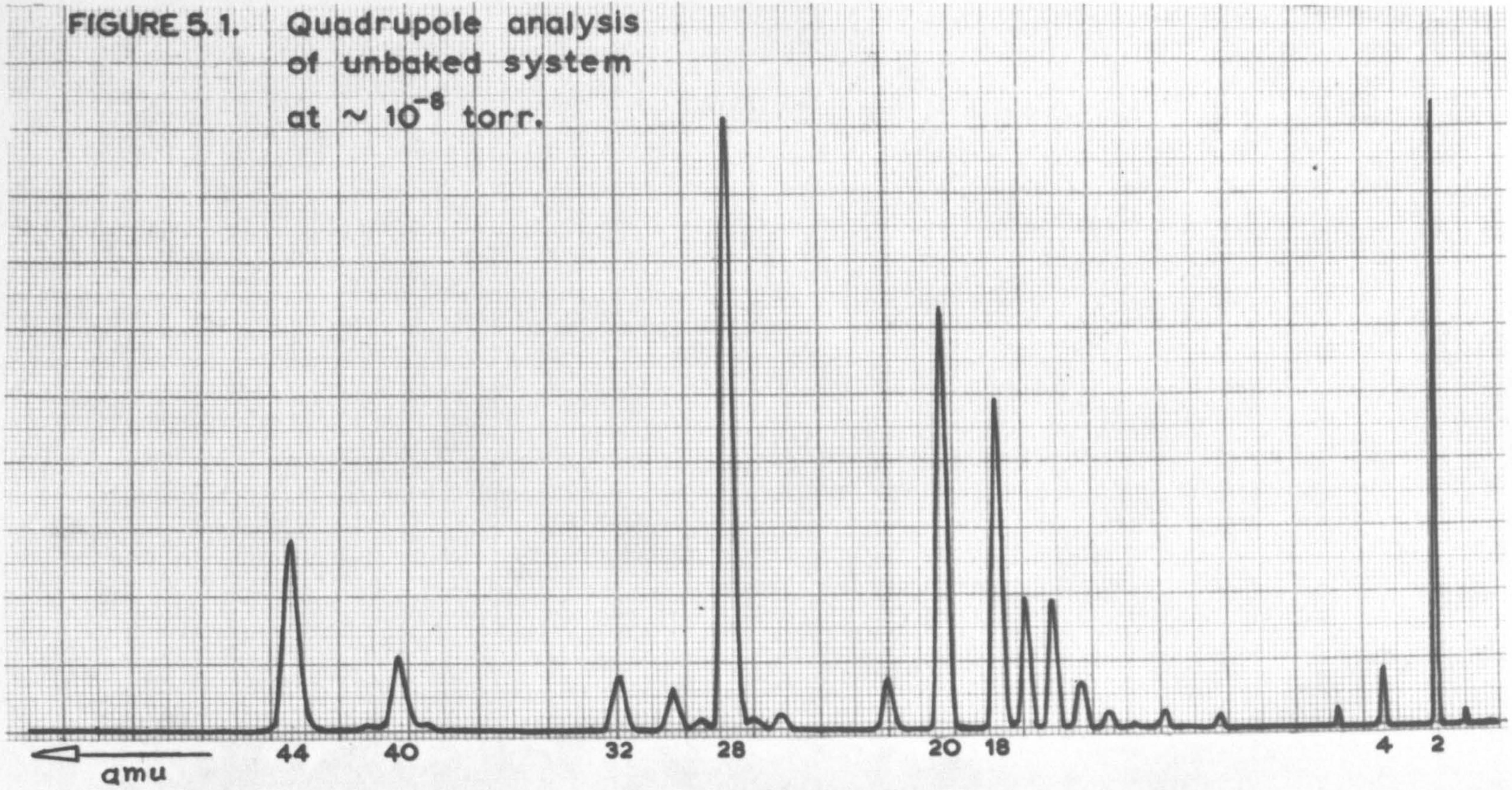

CHAPTER 5

PRESENTATION AND DISCUSSION OF RESULTS

5.1 *Residual gases*

Use of the quadrupole RGA made it possible to give an accurate analysis of the residual gas atmosphere surrounding a metal target. Some attempts were made to determine which gases were evolved when a target was heated but they were not concluded: using the given apparatus it was necessary to heat the target rapidly to prevent the radiation and thermal conduction causing a substantial outgassing of the target supports and surroundings. The trouble was that rapid changes of gas pressure were not compatible with the relatively slow spectral scan rate of the quadrupole RGA. Although a procedure could have been worked out (see reference 52) the problem was not pursued since it did not lie within the strict terms of reference: ' to record CEL in known residual gas atmosphere'. This indeed was carried out and the gas analyses so obtained are described below.

The slow process of baking the vacuum system was followed with the aid of the quadrupole. In Figure 5.1 can be seen the typical residual gas spectrum of an unbaked system at about 10^{-8} torr. The calculations required to derive the actual gas pressures are described in Appendix B, and some results are presented in Table 5.1. The temperature was gradually raised by increasing the power to the internal bake-out filament and typically reached 270^{o}C in 265 hours. Then the filament was switched

FIGURE 5. 2. Quadrupole analysis of system after bake-out.

Pressure ~ 5×10^{-10} torr.

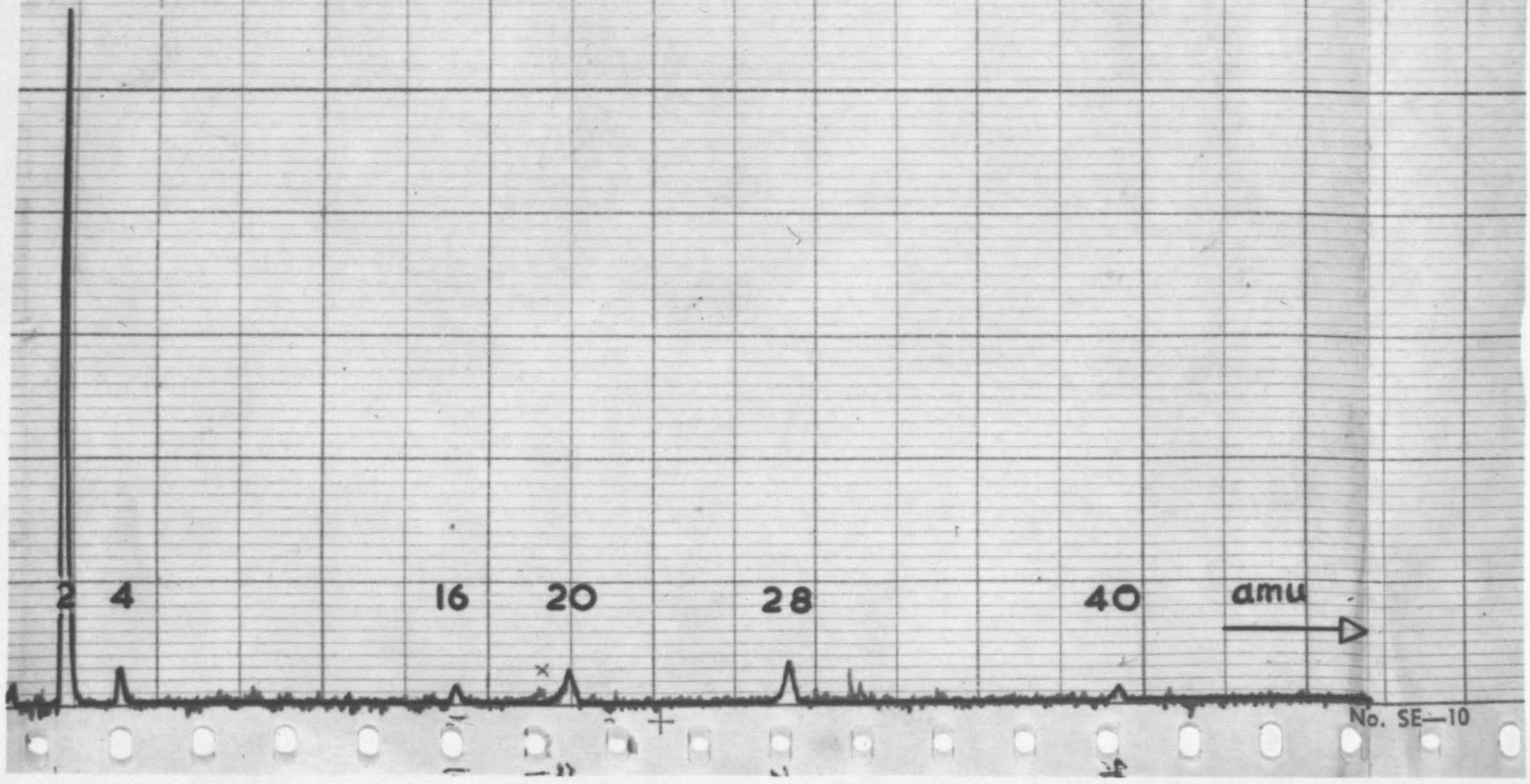

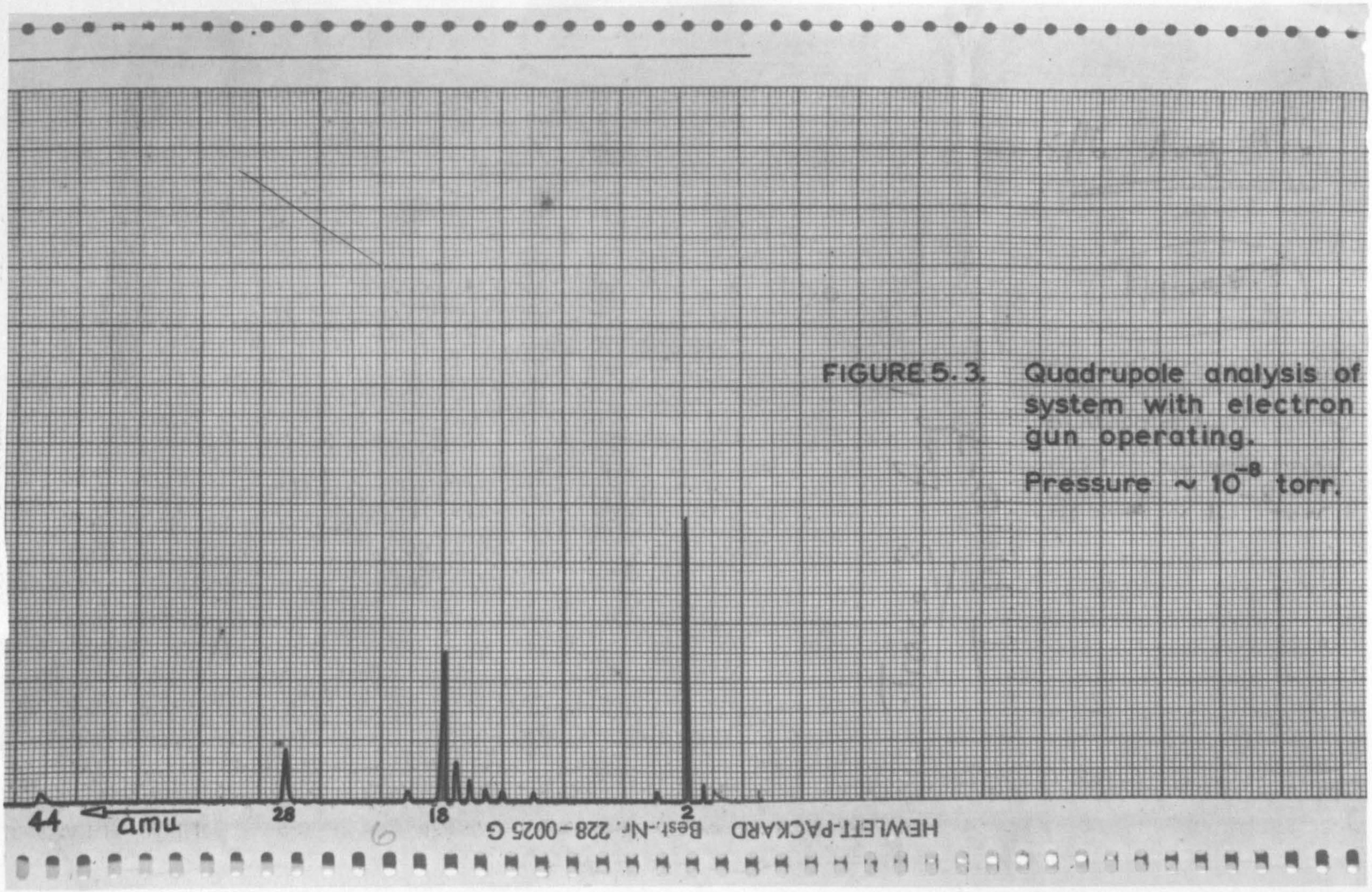

FIGURE 5.3. Quadrupole analysis of system with electron gun operating. Pressure ~ 10^{-8} torr.

TABLE 5.1

ANALYSIS OF RESIDUAL GASES (x 10^{-10} to give torr)

Gas	H_2	He	CH_4	H_2O	Ne	CO	N_2	C_2H_6	O_2	Ar	CO_2	Others	Total
Before Bake	78.2	4.0	2.1	14.0	7.7	3.7	3.7	1.1	1.2	0.9	3.2	6.0	125.8
After Bake	4.67	0.15	0.04	-	0.04	0.03	-	-	-	0.01	-	-	4.94
Gun On	75.0	1.0	0.9	14.0	0.5	1.6	-	-	-	-	0.5	3.0	96.5

off and Figure 5.2 shows the residual gas spectrum when the system had cooled to room temperature again. The total pressure was about 5×10^{-10} torr.

It can be seen that the relative proportions of gas have changed remarkably. Some of the residual gases, H_2O, N_2, O_2, C_2H_6 and CO_2 could not be detected and so had partial pressures less than 0.01×10^{-10} torr. The dominant gas was H_2 which had a pressure 95% of total and, neglecting the rare gas content, the remaining gases were CH_4 and CO which had a joint partial pressure of only 1.5% total. The presence of CH_4 is most likely due to the combination of the residual hydrogen with the carbon evolved from the tungsten lamp filament.

Switching on the electron gun filament raised the pressure and the equilibrium residual gas spectrum taken with an electron beam of 10^{-6} A is shown in Figure 5.3. It is analysed into partial pressures in the last row of Table 5.1. Apparent once again were H_2O and CO_2, but H_2 was still the predominant gas at 78% of the total.

For a complete explanation of these changing partial pressures one would have to consider a wealth of sources and sinks of gas. However, the most important sources of gas were: the ion pumps (162-165): the filaments for bakeout, gun and quadrupole; and the other metal, ceramic and glass surfaces exposed to the vacuum. All these sources were also sinks of gas under differing pressure and temperature conditions.

For the present purposes it is sufficient to say that the vacuum conditions obtaining during the experiments described, were such that the relative abundancies did not alter appreciably with time or target material.

5.2 *General remarks*

The spectra presented in the following sections are the original traces reproduced photographically to appropriate page size. With the equipment described in the last chapter it was possible to sweep the analyser voltage in either direction and the CEL spectra so obtained were identical to within the errors of measurement. Tabular values of the losses were calculated as the mean of the results from several traces and the errors quoted are the mean deviations of these results.

At the outset of the investigation the field of research covered the entire energy spectrum of secondary electrons: from the peak of "true secondaries" up to the reflected primary peak and its associated CEL peaks. For this reason the first few spectra include the true secondary peak, but as it soon became clear that 127° analysers were comparitively poor tools to study such low energy electrons, later work was confined to the CEL end of the spectrum where energies were usually in excess of 200 eV.

The results are categorised under the various target materials in historical sequence and, after summary in tabular form, are discussed with reference to theory and the results of other workers.

The symbols in the theory column of the tables may be understood as follows:

A : loss involving an atomic transition

B : loss involving a band transition (VIATSKIN {144})

X : loss involving a band transition as shown by X-ray spectrum

nFr : n multiple losses due to collective oscillation of r electrons per atom (plasmon losses)

L : lowered, or surface, plasmon loss.

The values of these losses for the particular metals investigated here, have been summarised in Table 2.2

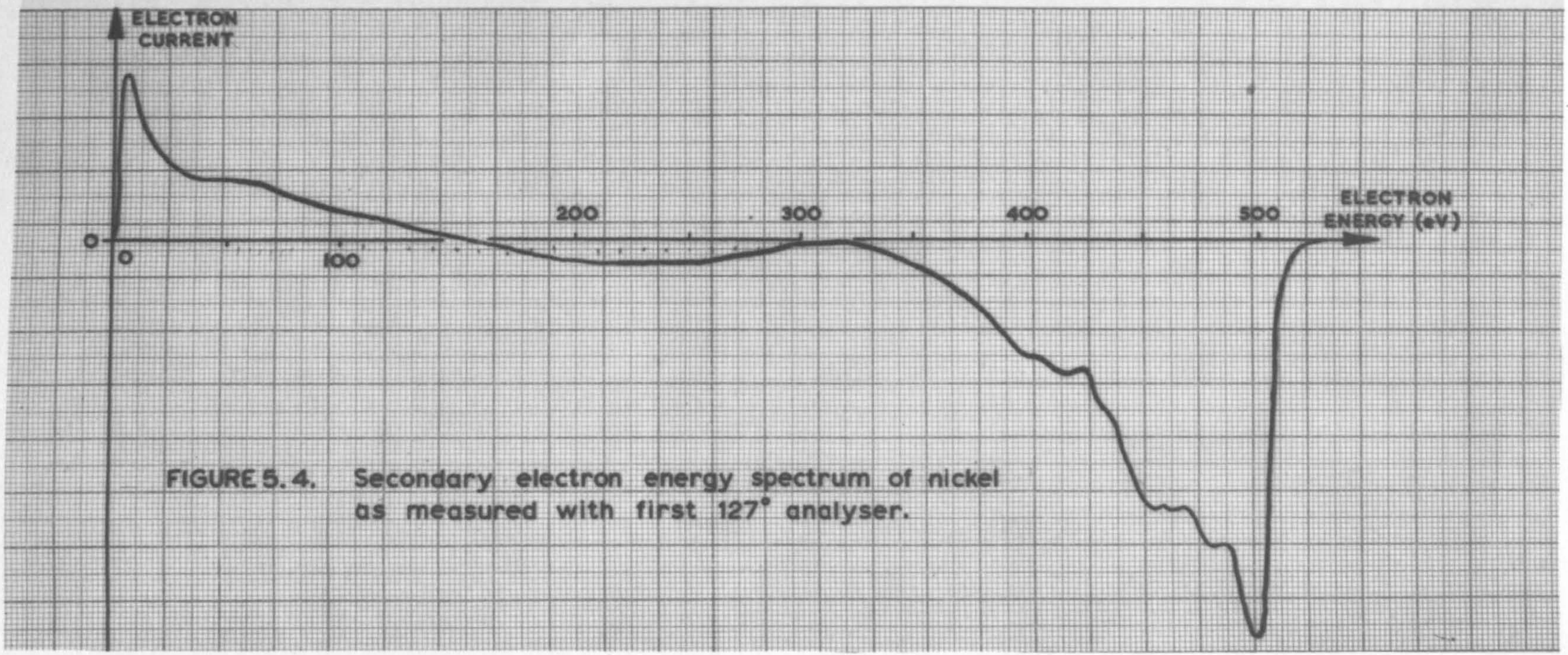

FIGURE 5.4. Secondary electron energy spectrum of nickel as measured with first 127° analyser.

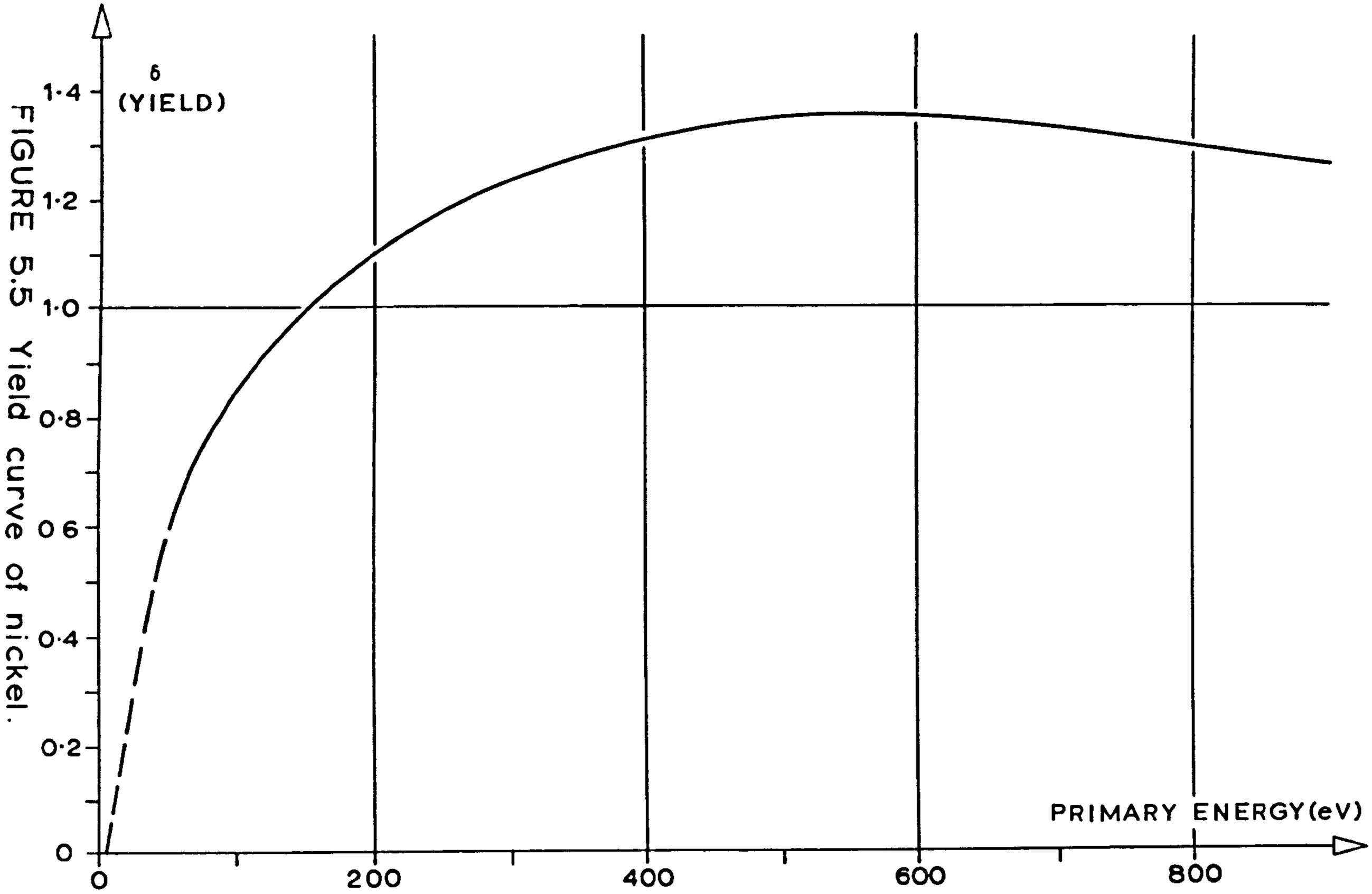

FIGURE 5.5 Yield curve of nickel.

5.3 *Nickel*

As noted in Chapter 3 the first type of 127° analyser gave results which served mainly to point out design difficulties. Nickel was chosen as the first target material and a specimen trace of the energy spectrum appears in Figure 5.4. A normally incident primary beam was used and the analyser collected electrons scattered through 150°. The spectrum looks rather odd since the elastically reflected peak of 500 eV is inverted: the explanation is that for fast moving electrons the nickel collector in the analyser lost more electrons than it gained, the yield curve of nickel rising up to $\delta_{max} = 1.4$ at 550 eV, as shown in Figure 5.5.

Suppose that x electrons of a particular energy were incident on the collector; then if one assumes that all second generation secondaries were lost, there was a charge of $-\delta x$ leaving the collector. Hence the charge registered was $-(1-\delta)x$ for any particular energy. Thus when the energy was such that $\delta < 1$ the current was of apparently incoming electrons, but when $\delta > 1$ the current became positive, implying a loss of electrons. By the trick of dividing the registered current by $(1-\delta)$ at all energies one can get back to x itself and effectively turn the high energy end of the spectrum the right way up.

Another complication, as pointed out in Appendix A, is that the 127° analyser discriminates against slow electrons. Correction for this can be made by dividing the collector current by the energy being passed by the analyser.

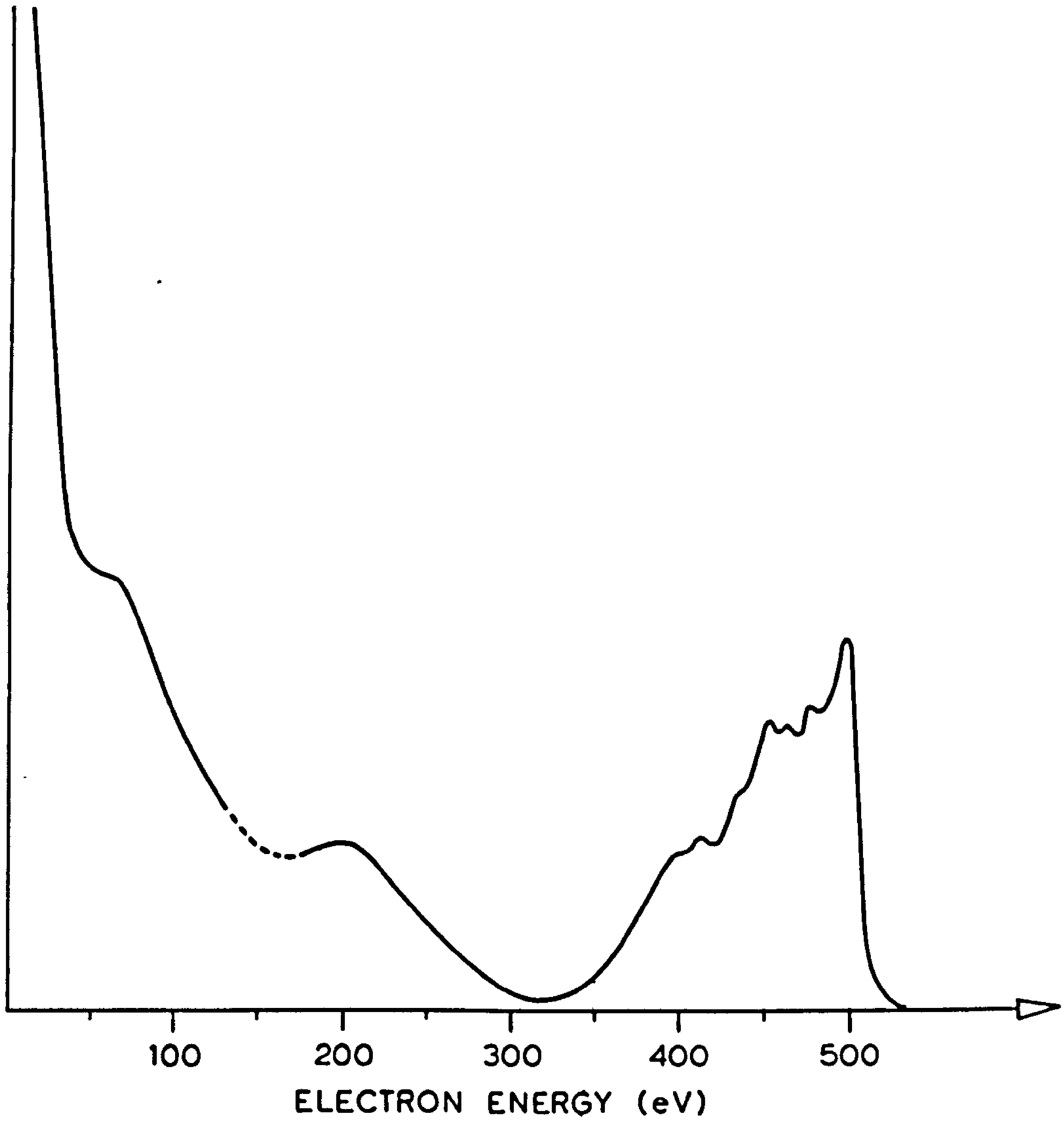

FIGURE 5.6 Corrected energy distribution of nickel.

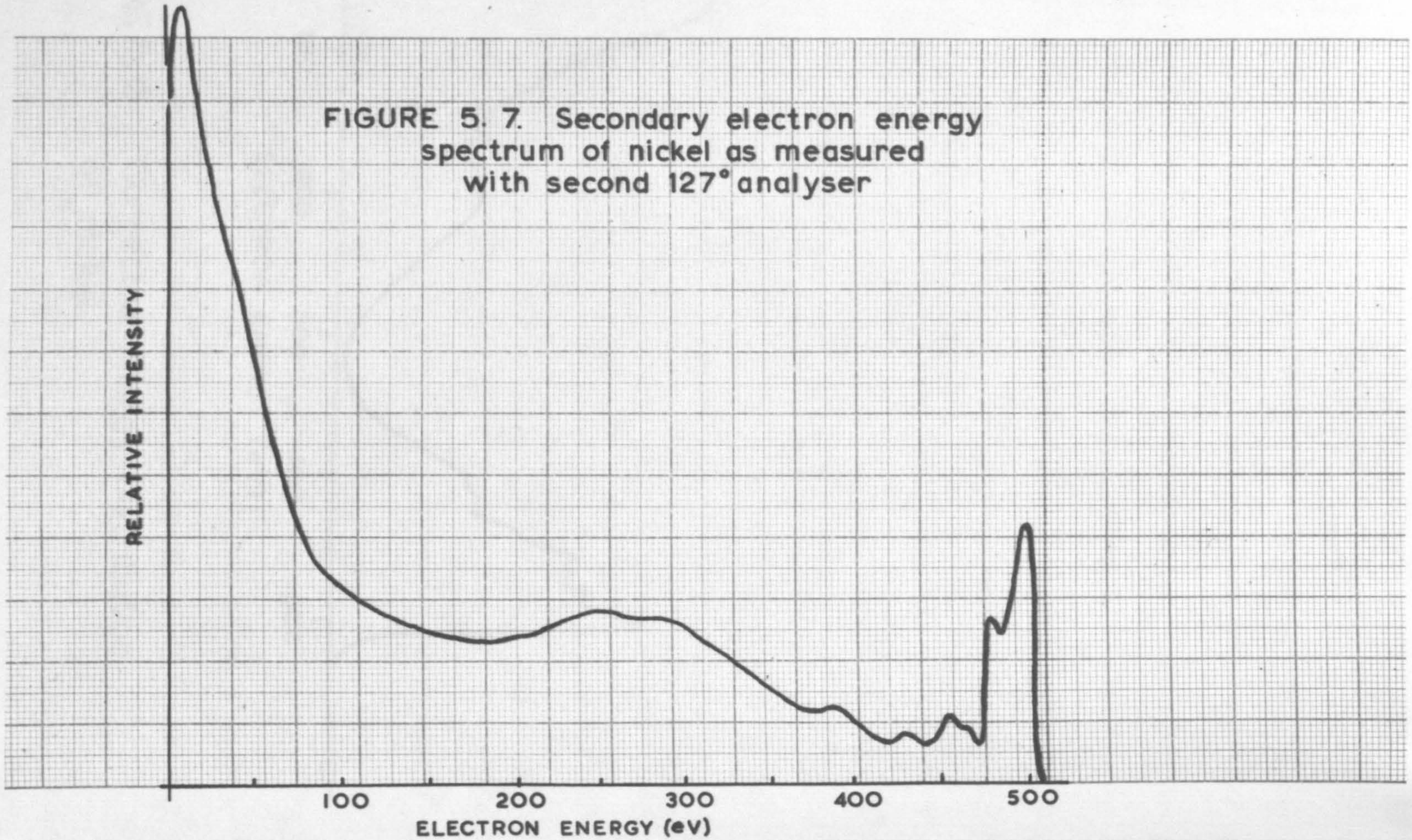

FIGURE 5. 7. Secondary electron energy spectrum of nickel as measured with second 127° analyser

The result of dividing the experimental trace by V(1-δ) for all energies is shown in Figure 5.6. The overall shape of the spectrum is rather better, the peak corresponding to the true secondaries having the accepted proportions. Nevertheless the detail of the CEL region leaves a lot to be desired for most of the spectral peaks are mere inflexions in a poorly resolved hump. The magnitudes of these CEL are given in Table 5.2 but it is to be noted that owing to their widths it was difficult to place them more accurately than ± 6 eV towards the high loss end.

The next measurements were made with an analyser of the second type, as described in Chapter 3, but before any tantalum carbide coating had been applied to the arcs or collector. Instead, a fine mesh grid was placed between the exit slit and collector, the voltage on this being swept synchronously with the analyser arc voltage. The magnitude of this voltage permitted the electrons being passed by the analyser to reach the collector, but impeded the escape of tertiaries from it.

While the spectra were much improved, the current collected always being of electrons and the resolution somewhat better since slit widths had been reduced to 0.5 mm from 1 mm, there was still a strange feature. As can be seen in Figure 5.7 a diffuse bump appeared centred at about half primary energy, and it remained here for the range E_p = 250 eV to 800 eV. Since this bump vanished with the TaC coated analyser it was ascribed to tertiaries from the zero loss peak being scattered around between the arcs and collected at an anomalous arc voltage. The measured

TABLE 5.2

ENERGY LOSSES IN CEL SPECTRUM OF NICKEL (eV)

Lang	Marton + Leder	Watanabe	Gauthé	Robins + Swan	Analyser 1	Analyser 2	Theory
	5.8	6.5		> 4.3			2.4 (X)
	9.4			8.3			7.7 (X)
15	13.2	12.0					12.2 (B) 15.7 (X)
	17.6		20.6	19.5			17.5 (X) 19.4 (P3)
24.2	23.4	22.5			22	22.9	24.4 (B) 22.5 (P4)
			26.5	26.4			27.2 (X)
			32.6		35	34.4	
47.5		45.0	42		45	45.7	45.0 (2 P4) 45.7 (X)
			52				48.8 (B)
				63	67	68.6	66.9 (A) 67.5 (3P4)
					89		90 (4P4)
					100	106.8	111 (A)

resolution of the second type of analyser was only 4% and as can be seen at least one loss peak overlaps the primary peak. The positions of the loss peaks are shown in Table 5.2, the mean deviation going from 0.8 eV near the primary peak to just over 5 eV for the high losses. The results of previous workers are contained in references (37, 59, 60, 69 and 73).

As discussed in Chapter 2 the case of the transition metals is a particularly difficult one for the plasma theory to handle. Nickel usually exhibits a valency of 2 or 3 and this number of free electrons per atom would give energies of collective oscillation P2 = 16 eV and P3 = 19 eV respectively. However, if one takes all the 10 electrons in the 4s and 3d orbitals together, and supposes their low binding energy leaves them free to oscillate, then one obtains P10 = 35 eV. Clearly either extreme is unreasonable and the present results imply that about 4 electrons per atom are sufficiently free to participate in collective oscillation. In fact there is an excellant fit between four of the loss peaks observed and multiples of a basic loss P4 = 22.5 eV.

A loss at about 35 eV has been observed by only one previous worker and it is difficult to explain its origin: possibly it represents successive excitation of volume and surface plasma oscillations, the latter being modified by surface conditions.

The highest loss observed at about 100 eV had not been reported previously. Due to its width the peak was difficult to locate accurately

but there was not doubt of its presence. It could be the loss suffered by a primary electron in raising an electron in the M_1 level to the conduction band although X-ray data (147) shows this level to be 111 eV below the Fermi level.

The two most recent workers, ROBINS & SWAN and GAUTHE were unable to find the 22.5 eV loss but observed two losses at about 20 and 26 eV which they surmised were detected by previous workers only as an unresolved peak in the 23 eV region. It is possible that they are correct for the resolution of the analyser used in this work might well not have distinguished two such losses. However it is to be noted that MARTON & LEDER were able to resolve even closer losses in the spectrum and yet saw only a single peak at about 23 eV. Perhaps all that can be said is that the present results fit in well with previous work and that an analyser with better resolution would be able to reveal smaller losses and settle the question of the 23 eV loss.

FIGURE 5.8 C E L spectrum of tungsten measured by second analyser: sensitivity of (b) is 2·5 times that of (a)

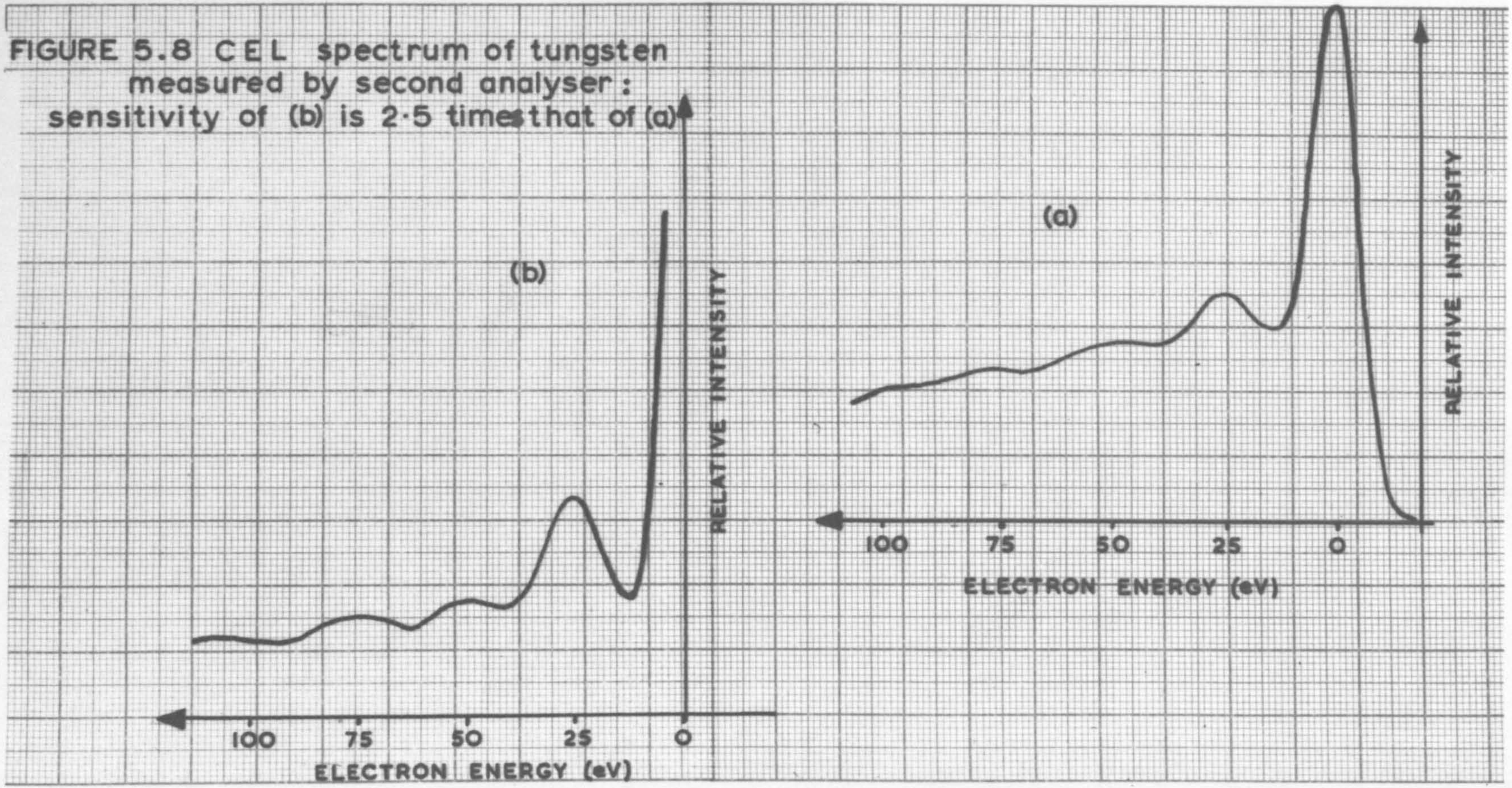

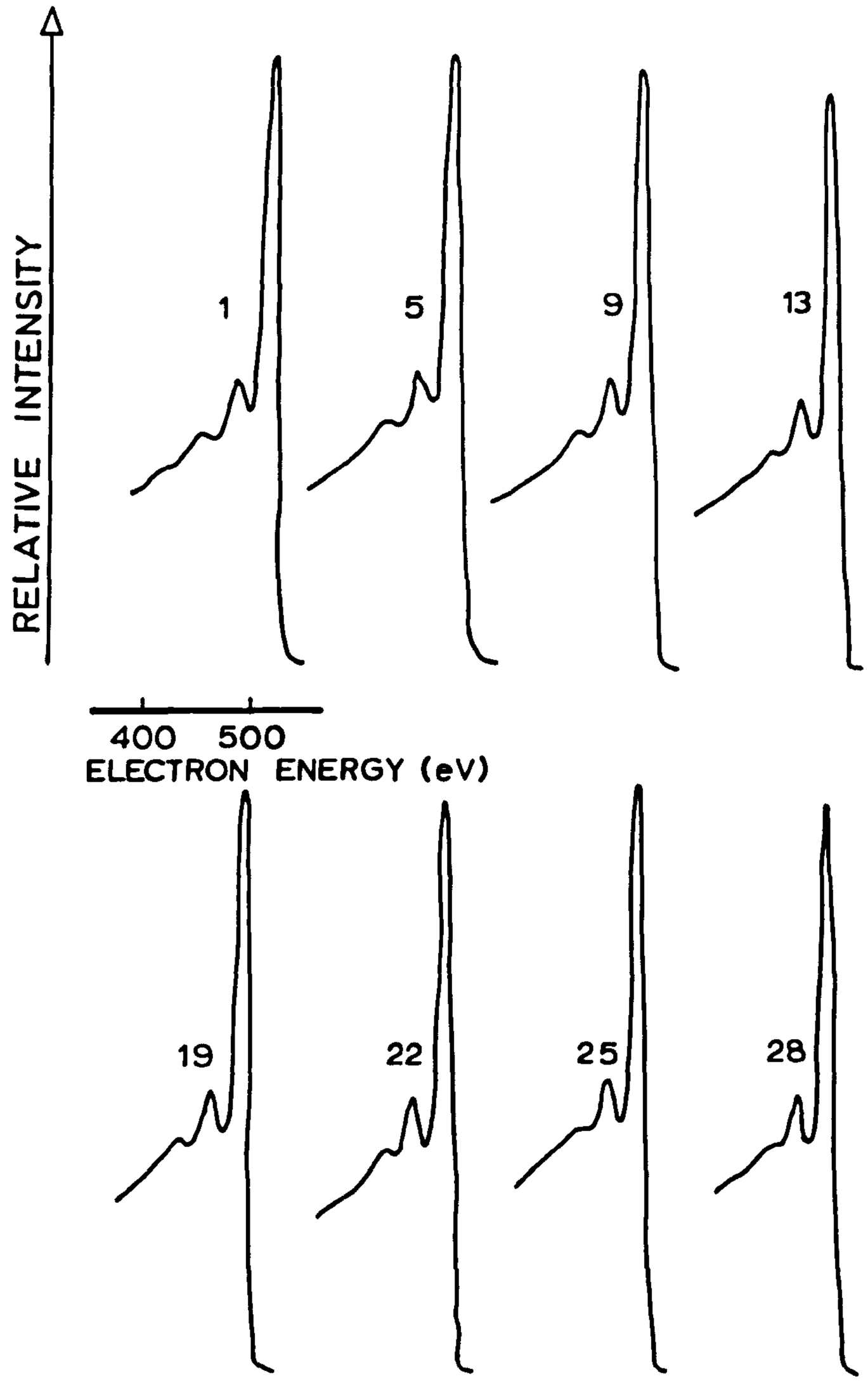

FIGURE 5.9 Succession of CEL spectra of tungsten showing progress of contamination. The number above each spectrum gives the time in minutes after outgassing.

5.4 *Tungsten 1*

When the TaC covered analyser arcs and collector were put in the vacuum system it was decided to change the target material to tungsten which could be very well outgassed by resistance heating. At this stage also the investigation was turned away from the low energy part of the spectrum, where only faint indications of Auger emission had been detected, and concentrated on the CEL part.

The system was given a 450°C bake for 48 hours and then the target outgassed for some 5 hours at low red heat by passing a current of 10 amps a.c. Some fine clear traces were obtained as shown in Figure 5.8, but gradually over an hour of continual measurements the quality deteriorated to such an extent that only the first two losses could be discerned. It was found that further heating of the target restored the original clarity and resolution. Thus, although the background pressure with all the equipment operating was below 10^{-8} torr, it was apparent that some sort of contamination of the target was still taking place.

Several sets of fast CEL spectrum scans were made to investigate the progress of the phenomenon and a selection from one set can be seen in Figure 5.9. At the begining of each set a heavy current was passed through the target raising it to white heat (~ 1800°C by optical pyrometer) for about a minute, during which interval a puff of gas was given off: the pressure rose to above 10^{-7} torr and swiftly sank back to 2 x 10^{-8} torr. When the heating current was switched off the pressure slowly fell further to about 8 x 10^{-9} torr. Each set of scans was begun four or five seconds after the current was switched off and continued for about half an hour.

Initially some four loss peaks were visible, but after a minute a third was barely showing. After twenty minutes the second loss peak, whilst still clearly present, had reduced to an inflexion..

A paper was published by POWELL et al. in 1958 (32) on the effects of contamination on the CEL spectrum of tungsten. They were able to remove contamination by heating the tungsten to 1500°C and found that it would remain in this condition if kept at a temperature of about 400°C. The contamination in their case however was carbon, the untrapped oil pumps producing a vacuum of about 3×10^{-5} torr. If the target was allowed to cool to room temperature it took only six minutes for the loss spectrum to become radically altered. The tungsten peaks vanished and new ones corresponding to carbon CEL appeared. Happily such gross contamination was never observed in the present experiments and it is probable that the contamination observed here was hydrogen, carbon monoxide or water vapour (43-52, 166-169).

The remainder of the tungsten measurements was made with a hot target a low d.c. current just making it glow (~ 600°C by optical pyrometer). Under these conditions the pressure gradually rose to about 2×10^{-8} torr as the target feedthrough became warm. Under these conditions no sign of deterioration was observed in the traces and, despite the slight increase in noise level, spectra were recorded with a very sensitive electrometer (50 mV/10^{10} Ω). With this sensitivity the zero loss peak was off scale, so the position of this peak was noted on a less sensitive scale, and the losses calculated from it can be seen together with other results in Table 5.3.

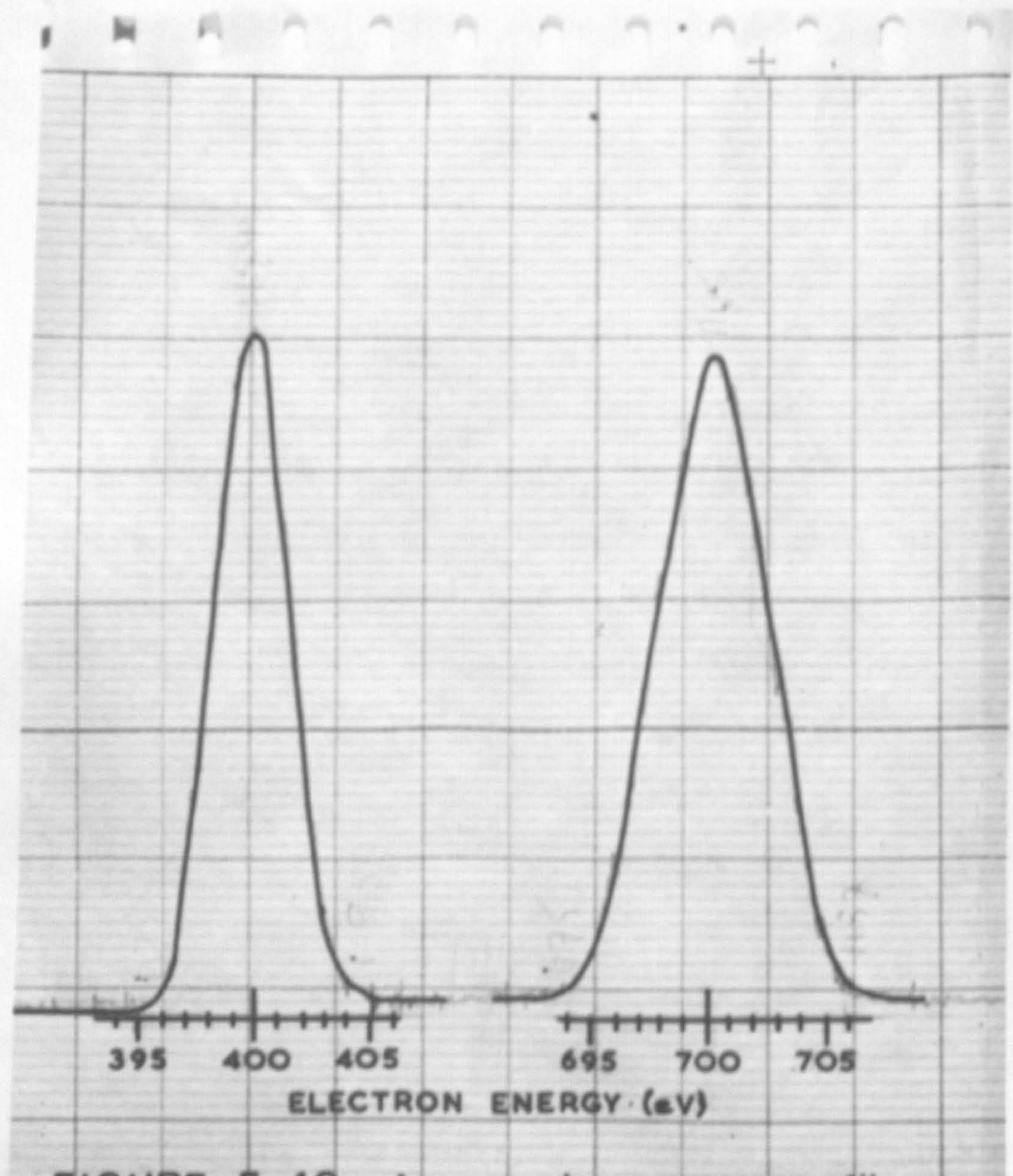

FIGURE 5.10 Apparent energy profile of two primary electron beams of mean voltage 400V and 700V

5.5 *Analyser characteristics*

It was at this stage that the other analysers (see Chapter 1: intermediate image filter lens, BOERSCH analyser) were made and tested. Whilst electrons fired directly into them from a gun could be detected, the much lower currents of secondary electrons were elusive and some six months were spent in gaining valuable experience and no real results.

The third 127° analyser was then designed and built, and on completion the first move was to test its resolution. The electron gun was mounted so that it fired directly vertically downwards into the analyser aperture and the apparent energy width of the beam was measured. The beam energy profiles were found to be nearly triangular, as can be seen in Figure 5.10. Taking the position of the maximum as the voltage set on the gun, the analyser factor (see Appendix A) came out to 2.45 ± 0.01 comparing satisfactorily with the designed 2.5. The mean FWHM of the profiles was about 0.88 ± 0.1% of the beam energy, as compared with a designed 0.6%. This width, of course, was made of several components over and above that due to the resolution of the analyser itself (19). The beam of primary electrons was not mono-energetic: the thermal energy available at the oxide cathode operating at 1000°C theoretically would provide some 0.3 eV of spread: the beam current at 10^{-5} A would have broadened this further to 0.5 eV perhaps: and then there were the various unaccounted aberrations of the gun lenses and analyser which could have introduced transverse velocity components.

The first trials of the new analyser using a tungsten target were

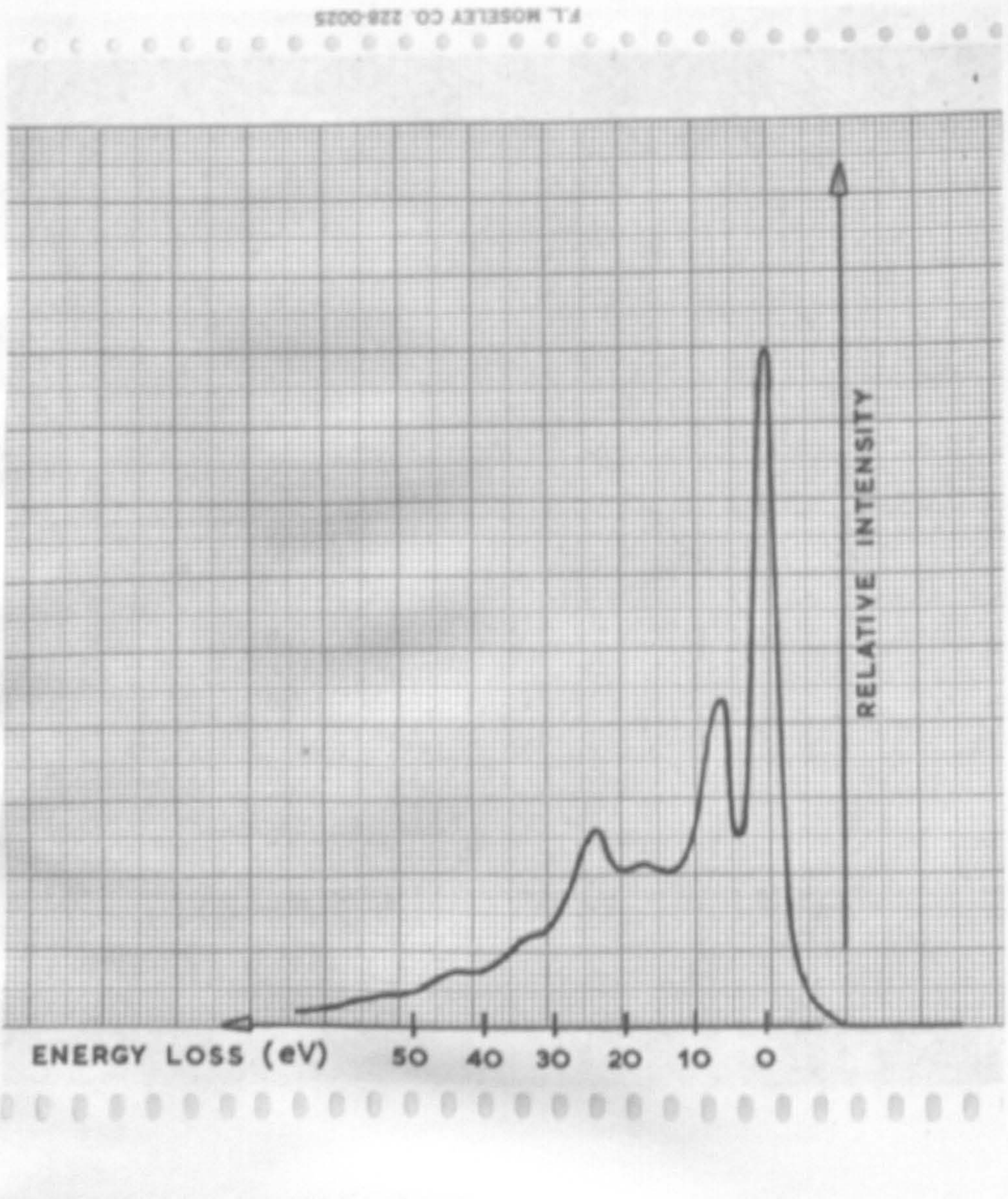

FIGURE 5. 11. CEL spectrum of tungsten.
Primary energy 300 eV.

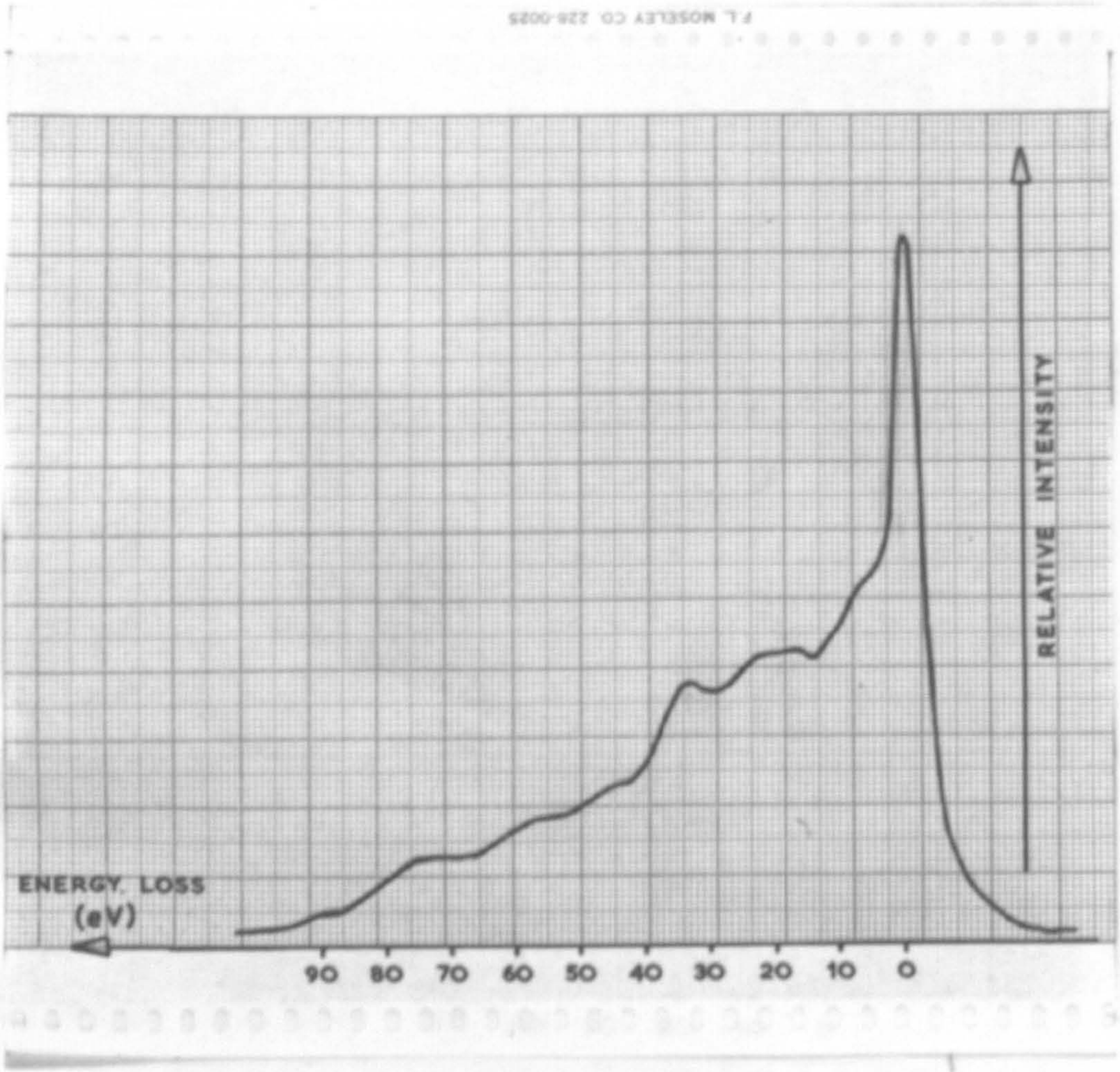

FIGURE 5. 12 (a) CEL spectrum of tungsten.
Primary energy 400 eV.

FIGURE 5.12 (b) CEL spectrum of tungsten.
Primary energy 400eV.

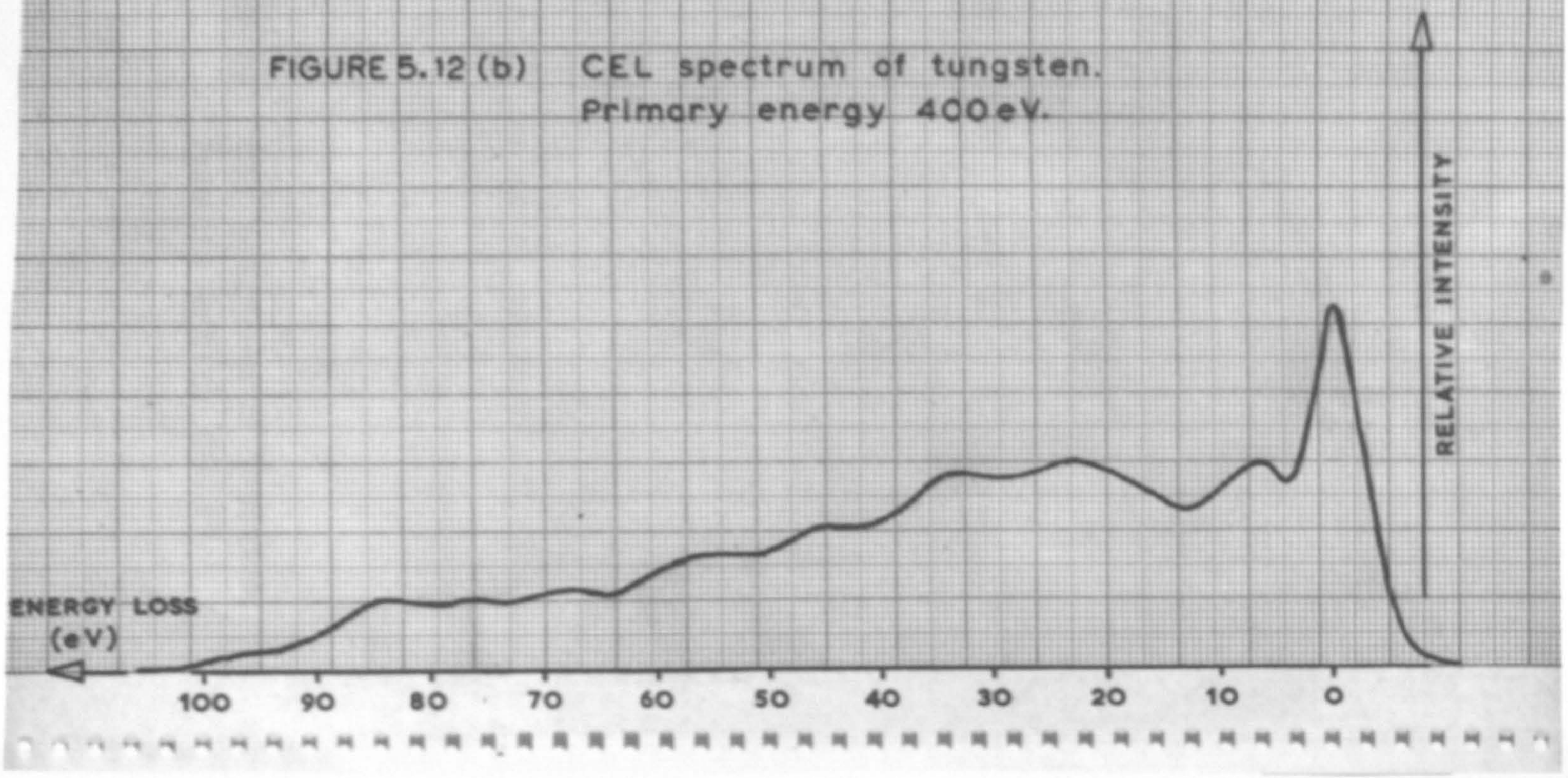

FIGURE 5. 13 CEL spectrum of tungsten.
Primary energy 400 eV.

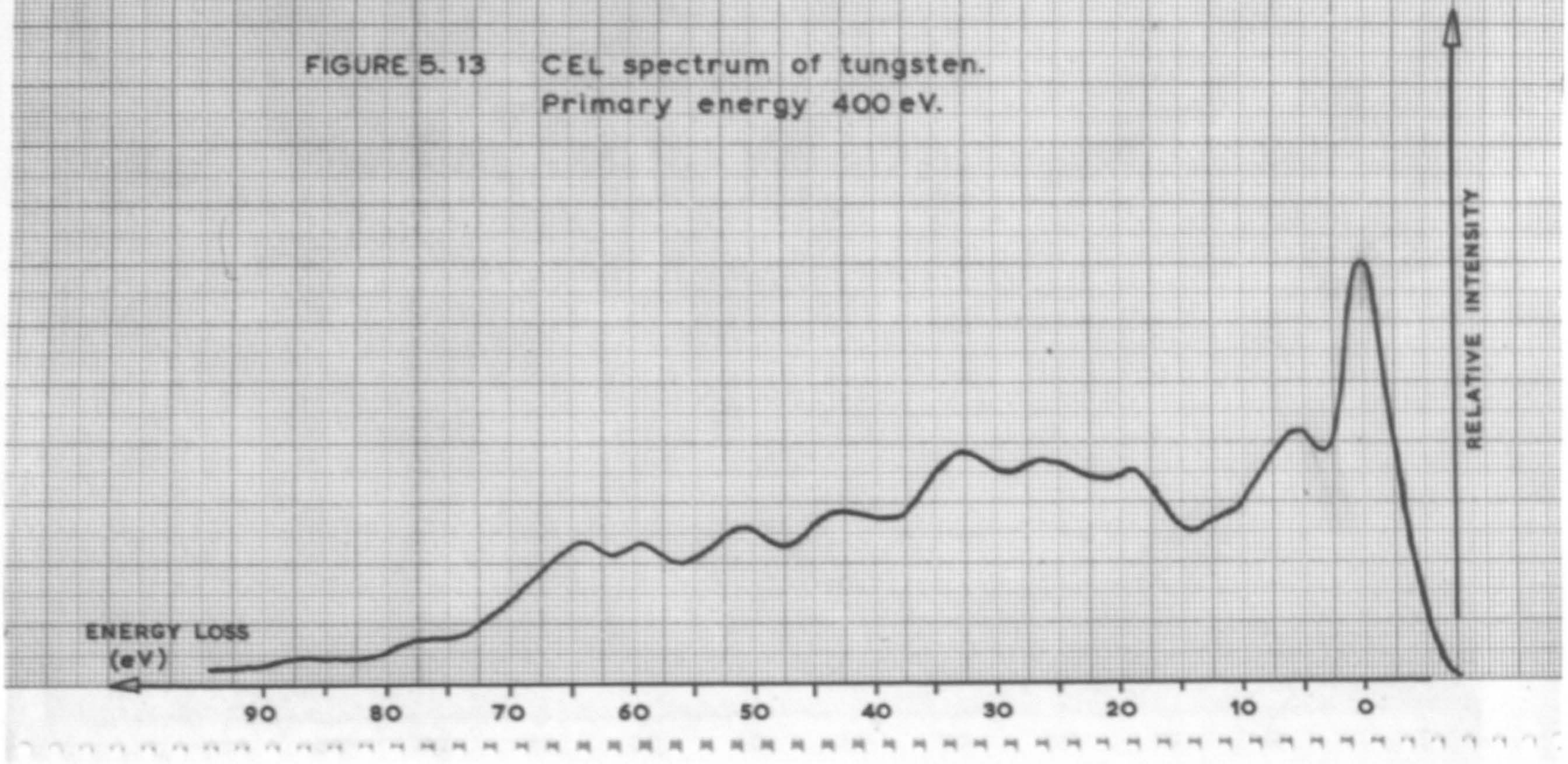

TABLE 5.3

ENERGY LOSSES IN CEL SPECTRUM OF TUNGSTEN (eV)

Harrower	Powell et al.	Scheibner + Tharp	Fig 5.8	Fig 5.11	Fig 5.12(a)	Fig 5.12(b)	Fig 5.13	Average Energy Losses	Theory
				6.5	6.6	6.8	5.7	6.4 ± 0.3	
14.8	10.6	12.5		17.3	17.2	23.6	17.8	17.4 ± 0.2	16.2 (L) 15 (B)
26.8	24.3	23.5	24.7	24.4	24.6		25.1	24.7 ± 0.2	22.8 (P6) 26 (A)
		35		33.9	33.6	33.8	32.5	33.5 ± 0.5	30 (B) 31,34 (A)
46.4	43.3	43		44.6	45.0	45.2	43.2	44.5 ± 0.6	45 (B) 42.1 (P6 + L) 43 (A)
	52.8	53.5	50.0				51.0	50.5 ± 0.5	49.4 (2 P6)
58.0					57.0	56.2	57.9	57.0 ± 0.6	60 (B)
					67.8	67.0	65.0	66.6 ± 1.1	66.8 (2P 6 + L)
			74.0		75.0	76.2	75.8	75.2 ± 0.8	74.1 (3 P6) 73 (A)
88.0					88.2	84.1	87.5	86.6 ± 1.7	

5.6 Tungsten 2

At first the new focussing ring was kept at some steady negative voltage (Vr) suchthat one of the peaks in the spectrum was maximised. Figure 5.11 shows a trace taken with a 300 V primary beam and electrometer sensitivity of 100 mV/10^{11} Ω. Vr was chosen to maximise the reflected primary peak and some five loss peaks are discernable. Figure 5.12 shows two traces taken with a 400 V primary beam and maximising (a) the zero loss peak with Vr = 250 V, and (b) a low intensity peak some 33 eV from the zero loss peak with Vr = 244 V. Figure 5.13 shows a repeat of the last trace made with a more negative grid voltage on the electron gun and using greater electrometer sensitivity. A remarkable number of peaks is visible and their positions are noted in Table 5.3 (the results of other workers are quoted from references 30, 32, 80).

The first tungsten measurements were made with normally incident primaries and secondaries scattered through 150°. These have been collected as all of a type under the column headed Figure 5.8. The three losses appear to be close to multiples of about 25 eV, which is near the loss predicted by the simple plasma theory (PG = 22.3 eV) but closer to the losses observed by other workers. Hence these losses may be ascribed to a volume plasma loss involving an average of about six electrons per atom.

All the other figures were produced from the results of the third analyser using 45° incidence and 90° scattering angle. This arrangement would make a surface plasma loss a more probable event (134, 146, 170, 171) and this expectation was fulfilled. A lower loss peak was found at about 17.4 eV, a remarkably close fit to the $L = \frac{1}{\sqrt{2}} \times P$ formula which gives

L = 17.5 eV, taking the value P = 24.7 eV. Whilst this might be thought fortuitous, it can be pointed out that the errors of observation were very small, and that the fit is an indication of the cleanliness of the tungsten surface.

With this orientation the volume plasma peaks were less pronounced and from the table it can be seen that the peak at about 50 eV was rarely resolved from its close neighbours; that at 75 eV was small but more readily distinguished, although some of its intensity may have come from a nearby ionisation event.

The losses observed at 44.5 eV and 66.6 eV could be explained as being combinations of volume and surface plasma losses: P + L = 42.1 eV, 2P + L = 66.8 eV. The peak at 44.5 eV however fits better with an ionisation of an electron in the O_2 level (43 eV), or it may be associated with an interband transition of 45 eV (144).

At the 400 V primary voltage used in figures 5.12 and 5.13 it was often difficult to differentiate the volume and surface plasma losses. Figure 5.12(b) was the only one where it was impossible and the sum of the two peaks yielded a single broad one at 23.6 eV. Generally though, the higher the primary energy the greater the primary current and the number of peaks observed. The limit of the analyser resolution usually kept the primary energy in the 200 - 500 eV region.

An interesting find was the prominent loss at 6.4 eV which has not been reported by previous workers, and its presence cannot be explained on the basis of the previous arguments. The loss at 33.5 eV had not been

seen before at the time these experiments were done, but has since been observed by SCHEIBNER & THARP (79). Its position is very close to an interband transition and to the energy required for the ionisation of the N_6 or O_3 levels which might well give rise to such a peak. The remaining losses at 57.0 eV and 86.6 eV were also found by Harrower, but they can receive little justification on present theoretical grounds.

FIGURE 5. 14. CEL spectrum of tantalum.
Primary energy 400 eV.

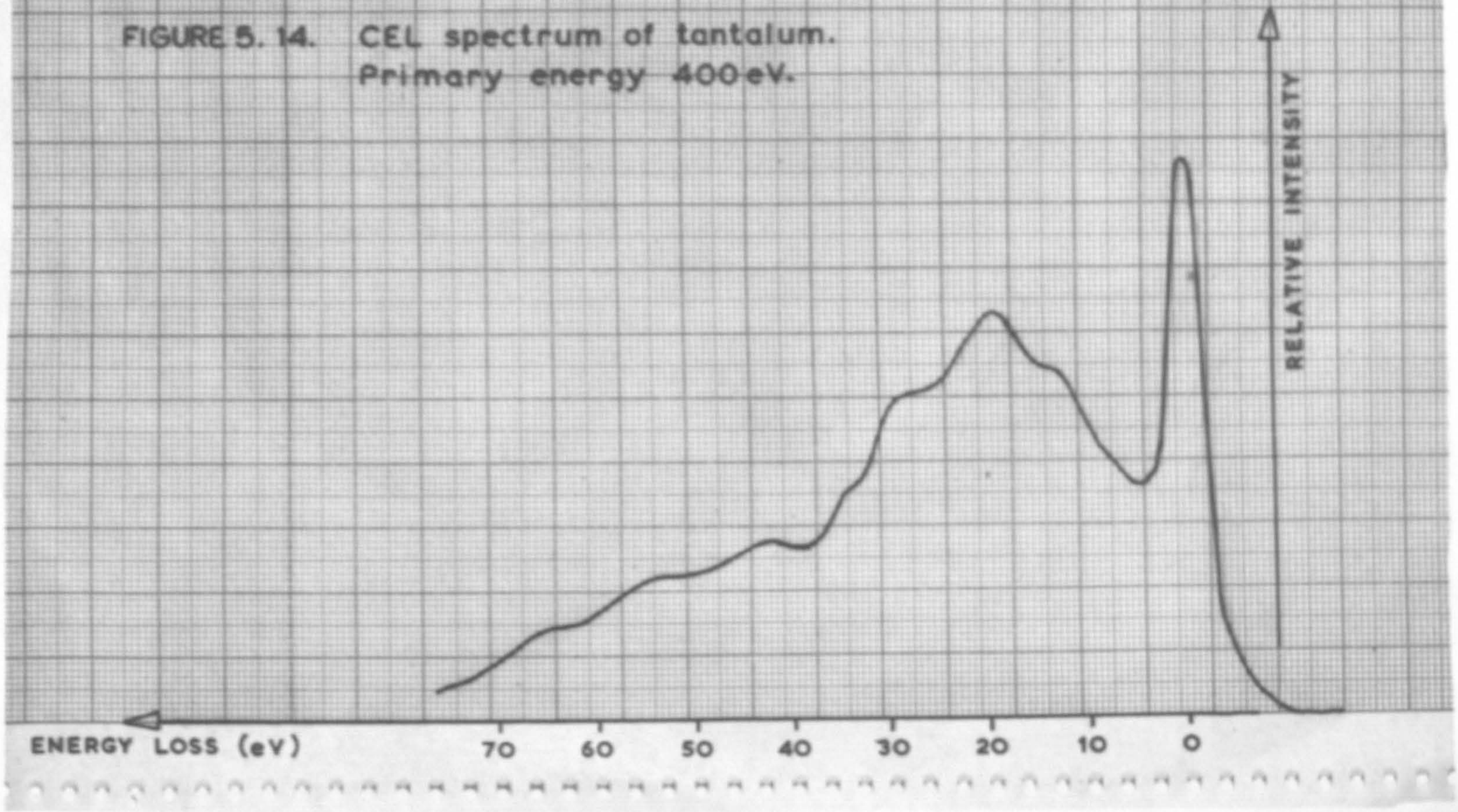

TABLE 5.4

ENERGY LOSSES IN CEL SPECTRUM OF TANTALUM (eV)

Kleinn	Thomas	Average Energy Losses	Plasmon Theory	Other Theory
	7.9 12.4	13.8 ± 0.8	13.8 (L)	13.6 (B)
19.7	20.1	19.7 ± 0.7	19.5 (P5)	18 (A) 20 (A)
		29.6 ± 1.5		27.2 (B) 23 (A)
		(34.2 ± 0.2)	33.5 (P5 + L)	
47.7	47.7 ?	43.4 ± 1.5	39.4 (2 P5)	39 (A) 40.8 (B)
		54.5 ± 0.6	53.2 (2 P5 + L)	54.4 (B)
		(58.9 ± 0.1)	59.1 (3 P5)	
		(66.7 ± 1.5)		65 (A)

5.7 *Tantalum*

When this metal was put in as a target a modification was made to the scanning gears to enable the voltage on the ring (Vr) to be swept synchronously with arc voltage. It was found that to obtain maximum current through a range of electron energies Vr had to be varied linearly. By a curious coincidence, with a short focussing ring than before, Vr was approximately equal to the electron voltage.

The CEL spectra obtained from tantalum were all recorded with cold targets: following the initial outgassing no change in the spectra was observed during several hours of working. The tantalum spectra, shown in Figure 5.14, was very different from the tungsten one in that only two losses appeared as peaks above a diffuse background. The average values of these and the other detectable losses are given in Table 5.4.

A rather large mean deviation of the results is apparent: this is because the loss peaks were very broad and the losses visible as inflexions were on sharply sloping backgrounds. The losses in brackets were only observed in 30 to 40% of the spectra owing to this resolution difficulty.

The main peak was observed at a loss of about 19.7 eV, very close to the P5 = 19.5 eV of the simple plasma theory, and

identical to the result of KLEINN (68) the only previous experimenter. The results of THOMAS (22) using the RPSA system at Keele are also tabulated: he found the main peak at about 20.1 eV. This peak may thus be ascribed to a volume plasma loss, with the five valence electrons per atom being free to oscillate. Some of the intensity and width of this peak may, however, be due to the ionisation of core electrons in the N_6 and N_7 levels. The low lying 13.8 eV loss fits excellently with the formula $L = \frac{1}{\sqrt{2}} \times P$ for the surface plasma loss.

Immediately above the volume plasma loss appeared a peak at about 29.6 eV. This can be identified with the ionisation of an electron in the O_3 level. Most of the other losses fit fairly well into combinations of volume and surface plasma losses as indicated in the table. The one at 66.7 eV can be matched with the ionisation of an electron in the O_1 level.

FIGURE 5. 15 Resolved CEL spectrum of silver
Primary electron energy 400 eV

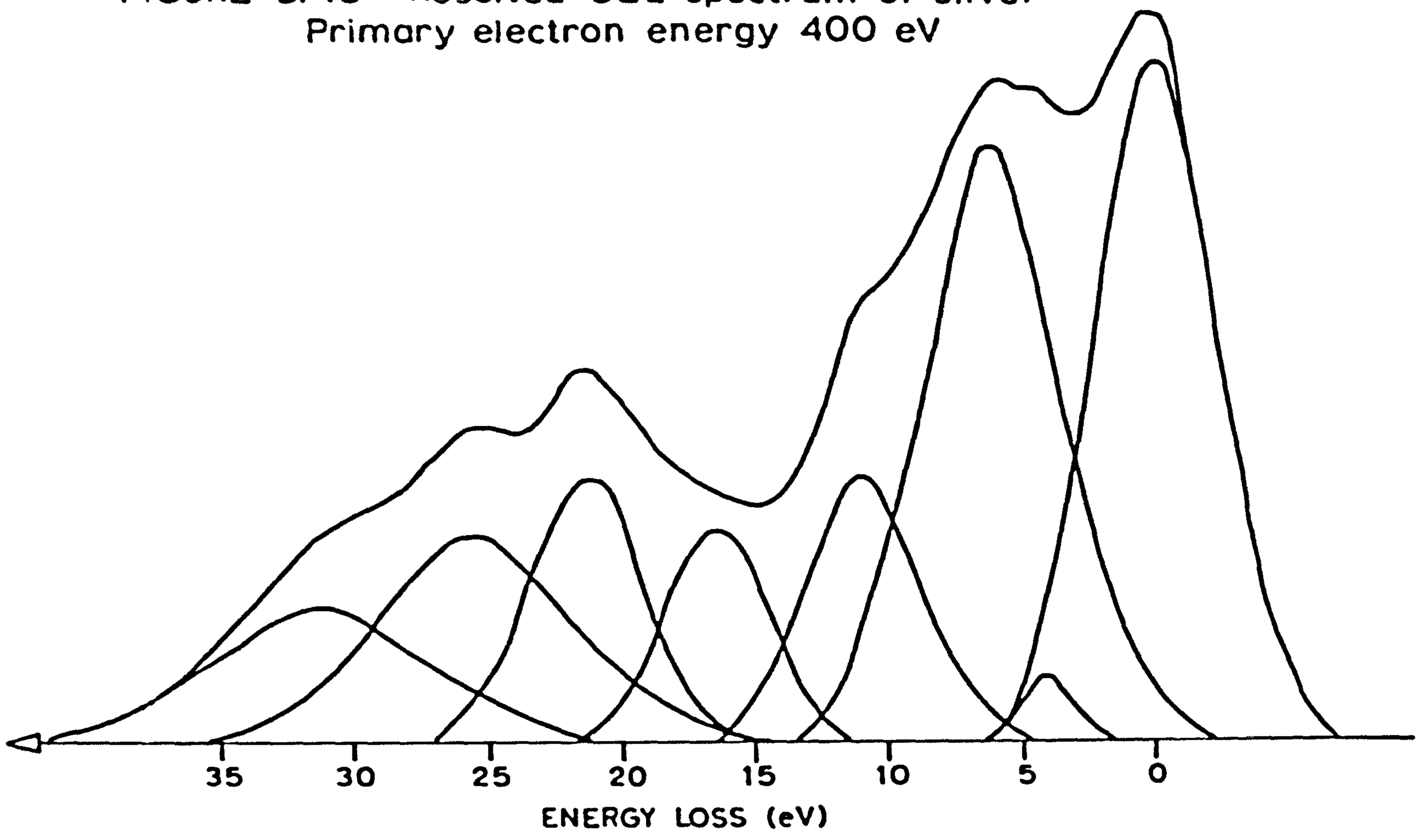

TABLE 5.5

ENERGY LOSSES IN CKL SPECTRUM OF SILVER (eV)

Gauthé	Jull	Marton et al.	Robins	Rudberg	Thomas	Average Energy Losses	Theory
	3.3	3.4	4.1	4.6	4.1	4.2 ± 0.2	3.9 (B) 3.75 (P.hybrid)
7.5	6.8	7.0	7.3	7.4	8.6	7.3 ± 0.5	8.9 (B) 7.5 (P1 mod)
	14.3				13.5	12.6 ± 0.6	
		16.7	17.2		16.7	16.6 ± 0.5	17.0 (X) 17.8 (B)
22.1	23.8				23.4	21.9 ± 0.4	
26.0		24.8	25.0	24.8	25.5	26.0 ± 0.6	24 (X) 26.7 (B)
			33.5		33.5	32.0 ± 0.8	33 (X) 35.6 (B)
36.0						37.5 ± 0.8	35.6 (B)
43.0	44.8				43.1	43.1 ± 0.9	44 (X) 44.5 (B)
						47	

5.8 *Silver*

The results from silver look much more interesting. With techniques continually improving it was just possible to resolve the loss at 4.1 eV with a 400 V primary beam. The nearby dominant loss of about 7 eV almost obscured it however, as can be seen in Figure 5.15. This is one of the traces analysed with the aid of the Dupont Curve Resolver which was invaluable in pin pointing the true positions of peaks which appeared on sloping backgrounds.

The results were obtained after gently heating the silver on its Tantalum backing. Unfortunately the intention of melting the silver to form a film over the backing was not realised: the silver melted but always ran down the 45^{o} sloping target to form a blob on the lower end, from which emission could not be observed for geometrical reasons. However after the gentle heating (to about 500^{o}C) no short term change with time was observed, indicating that whatever contamination there was, took place very quickly.

The positions of the loss peaks are given in Table 5.5, together with the results of some previous workers, (16, 22, 67, 73, 83, 193). The errors quoted are the mean deviations of the losses as measured from five Curve Resolver analyses.

The losses can be seen to be substantially identical with those measured by THOMAS and the whole table shows reasonable agreement

from worker to worker. Losses are apparent at intervals of 4 to 5 eV from zero up to nearly 50 eV from the reflected primary peak. With this complexity it would be vain to attempt a definitive correlation with theory, but some of the main features may be given a tentative interpretation according to the following scheme

The loss at about 22 eV has been ascribed to plasmon interaction, but the optical measurements of PHILIPP et al.(126-128) show a strong plasmon-like resonance with energy 3.8 eV which they describe as a hybrid resonance resulting from the cooperative behaviour of both the d and conduction electrons. They also find that the plasmon energy derived from free valence electrons (Pl = 9.0 eV) is depressed in energy by strong interband transitions to about 7.5 eV. Thus both the lower losses observed here may be ascribed to a modified Pl and a hybrid plasmon resonance.

In support of this view much other optical evidence may be set out (119, 120, 123), in particular the fact that light radiation corresponding to 3.75 eV has been observed emanating from electron bombarded silver. This may be due to the decay of collective oscillations, although there is an alternative: it may be transition radiation as discussed by RITCHIE and ELDRIDGE (117). These authors show that photon emission is to be expected not only at energies in the neighbourhood of the plasmon energy, but also around band transition energies. They associate the structure in

the optical area at 3.8 eV with the existence of an interband transition: electrons from the maximum in the N(E) curve for the d-band are raised to the Fermi level. There is optical evidence to support this possibility (118,172), so one can alternatively ascribe the lower loss as due to a band transition rather than a hybrid plasmon.

Fine structure near the K-edge of the X-ray absorption spectrum (see Chapter 2) corresponds very well with four of the losses observed here, which therefore supposes the translation of valence electrons to unoccupied levels above the Fermi level. These four losses are also close to the energy required for several band to band transitions, as predicted by VIATSKIN (144), and this tends to confirm the interpretation.

The four remaining losses occurred at roughly integral multiples of 12 eV, but this may well be coincidental: neither can they be explained satisfactorily justified on the basis of combinations of plasma oscillation losses for, although a fair fit could be made, the relative amplitudes and widths render it implausible (see Chapter 2).

FIGURE 5.16 (a) CEL spectrum of platinum immediately after outgassing. Primary energy 400 eV.

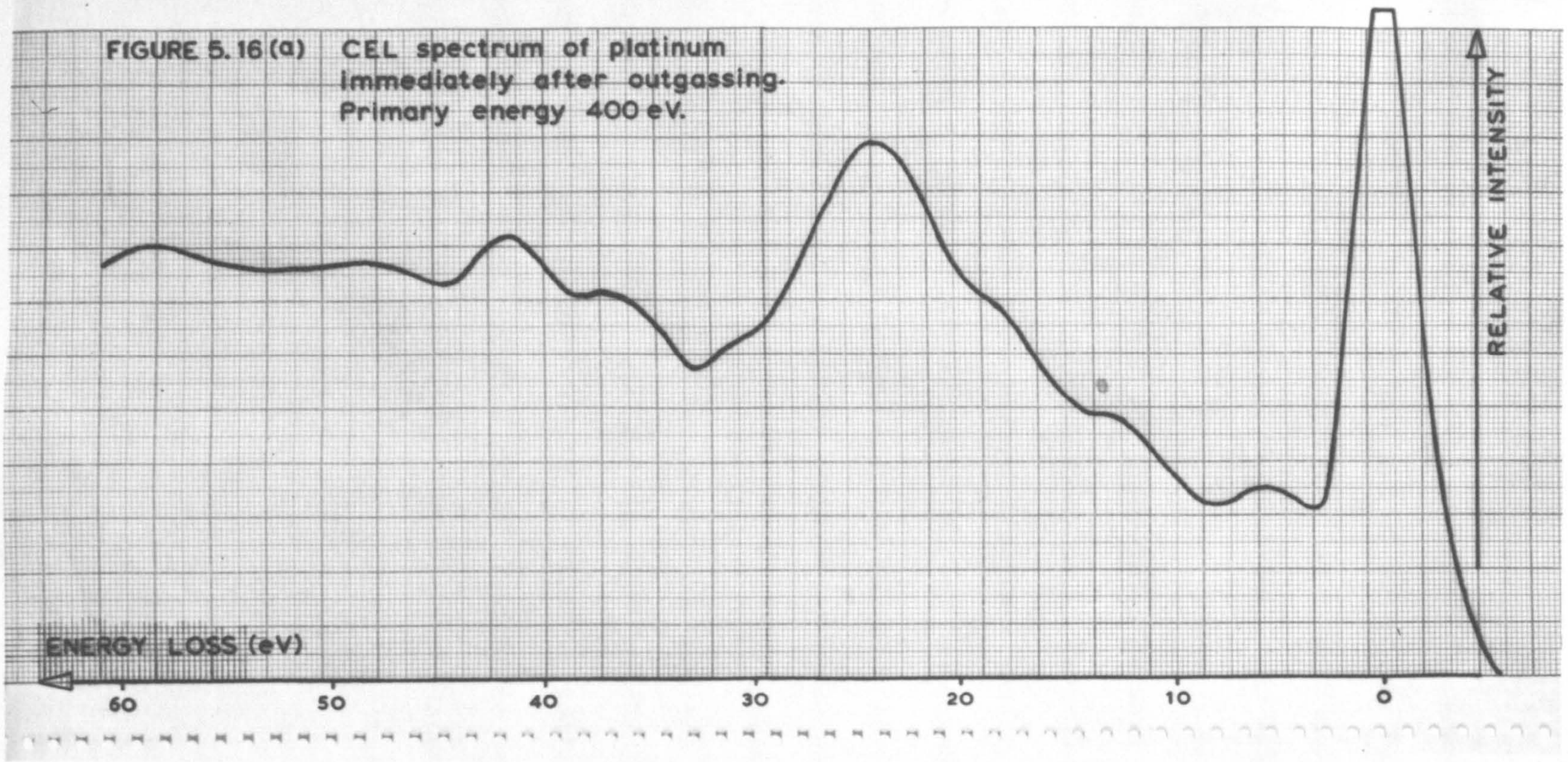

FIGURE 5.16 (b)
CEL spectrum of platinum
12 minutes after outgassing.
Primary energy 400 eV.

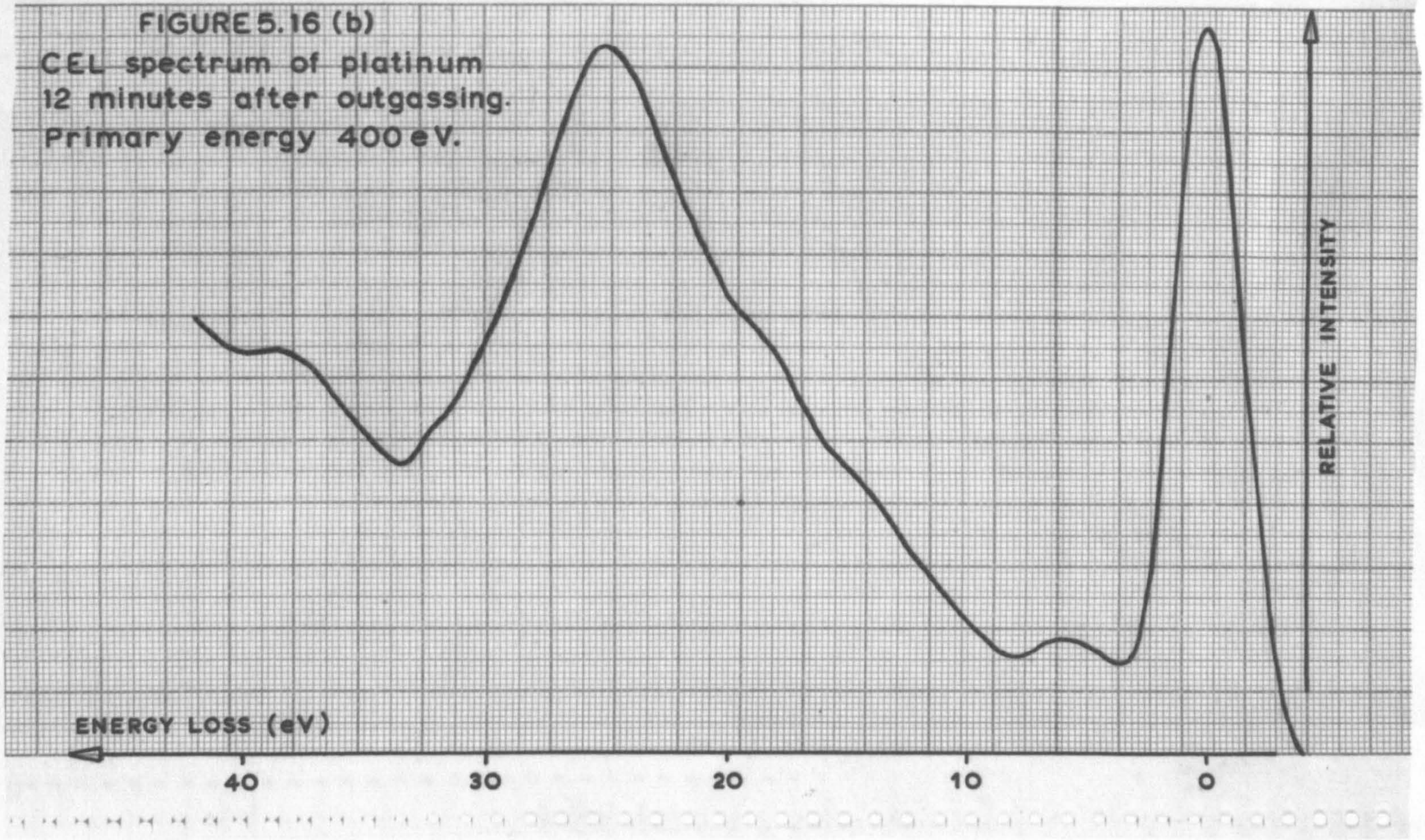

5.9 *Platinum*

The platinum target could be well outgassed by resistance heating, and it is significant that in this case some changes in the spectrum were observed, apparently due to contamination. Figure 5.16(a) shows a spectrum taken immediately after a 15 minute heat to about 1500°C, and Figure 5.16(b) is a spectrum taken 12 minutes later. The peak representing the 24 eV loss noticeably rose with time, blurring out the positions of the neighbouring losses. More prolonged heating to higher temperatures did not reduce the intensity of the loss below that of Figure 5.16(a). The conclusion is that this loss must be regarded with suspicion, even though it has been observed by all previous workers (see Table 5.6): it may represent a volume plasma loss as has been suggested by POWELL and the fact that it increased in intensity with time may signify the growth of some surface contamination which gave rise to a similar loss. Alternatively it may solely represent the presence of contamination, the vestiges of which were very difficult to remove.

Since this spectrum, like that of the silver, occurred on a sloping background (due to a small leakage current at the ceramic seal) the Dupont Curve Resolver was used to sum Gaussian curves

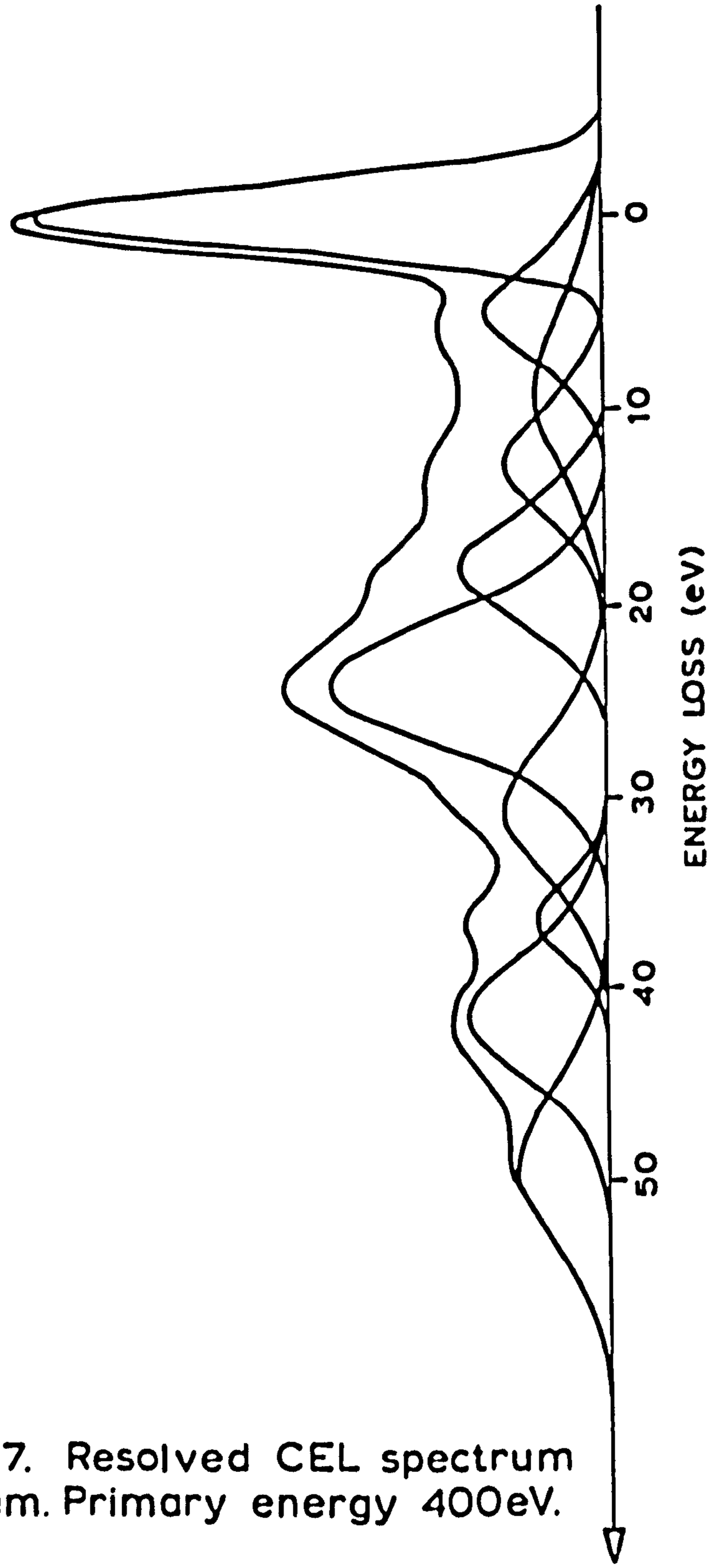

FIGURE 5. 17. Resolved CEL spectrum of platinum. Primary energy 400eV.

TABLE 5.6

ENERGY LOSSES IN CEL SPECTRUM OF PLATINUM (eV)

Gauthé	Kleinn	Hollenstedt	Powell	Rudberg	Average Energy Losses	Theory
	5.2		6.2	6.2	5.5 ± 0.4	3.3 (X)
				9.4	(9.5)	9.7 (B)
		14	14.3		13.2 ± 0.3	13.5 (L)
18.5					18.6 ± 0.4	19.1 (P4) 19.4 (B) 20.3 (X)
23.9	22.6	22.4	24.4	24.8	24.4 ± 0.3	20.3 (X)
30				33.7	31.5 ± 0.5	29.1 (B) 31.8 (P4 + L)
37					37.5 ± 0.4	37.2 (2P4)
47		46			42.0 ± 0.3	45 (A)
					50.1 ± 0.6	48.5 (B) 50.4 (2P4 + L) 53.3 (X)
		61.4			59 ± 0.8	55.8 (3P4) 58,62 (A) 58.2 (B)
					71 ± 1.4	68 (A) 69 (3P4 + L)

TABLE 5.6

ENERGY LOSSES IN CEL SPECTRUM OF PLATINUM (eV)

Gauthé	Kleinn	Mollenstedt	Powell	Rudberg	Average Energy Losses	Theory
	5.2		6.2	6.2	5.5 ± 0.4	3.3 (X)
				9.4	(9.5)	9.7 (B)
		14	14.3		13.2 ± 0.3	13.5 (L)
18.5					18.6 ± 0.4	19.1 (P4) 19.4 (B) 20.3 (X)
23.9	22.6	22.4	24.4	24.8	24.4 ± 0.3	20.3 (X)
30				33.7	31.5 ± 0.5	29.1 (B) 31.8 (P4 + L)
37					37.5 ± 0.4	37.2 (2P4)
47		46			42.0 ± 0.3	45 (A)
					50.1 ± 0.6	48.5 (B) 50.4 (2P4 + L) 53.3 (X)
		61.4			59 ± 0.8	55.8 (3P4) 58,62 (A) 58.2 (B)
					71 ± 1.4	68 (A) 69 (3P4 + L)

and a sloping straight line. Figure 5.17 shows the analysis of the spectrum shown in Figure 5.16(a), the background having been suppressed. Table 5.6 gives the positions of the peaks thus resolved and compares them with the results of previous workers (36, 68, 73, 194, 195).

The loss at 18.6 eV is the most intense and it is probable that this is the volume plasma loss since, taking the most common valence to 4 to represent the number of free electrons per atom, P4 = 19.1 eV. If this is the case then the loss at 13.2 eV could well be the sruface loss.

POWELL ascribes the lowest lying loss to an intraband transition. The loss noted at 9.5 eV has been observed previously by RUDBERG but its large width as found in the present work, and its insignificance as regards the summed shape of the spectrum, make its existence questionable.

As for the rest of the loss peaks the fit with the X-ray fine structure is not particularly good, but combinations of volume and surface plasma losses are very much better. The only explanation for the loss found at 42 eV is the ionisation of an electron in the O_3 level.

CHAPTER 6

SUMMARY, CONCLUSIONS AND SUGGESTIONS FOR FURTHER WORK

6.1 *Summary*

The CEL spectra of five transition metals have been measured using a number of 127° electrostatic analysers. The primary energy was always in the range 300 to 600 eV, and the spectra were taken of electrons 'reflected' from polycrystalline metal strips. Usually the electrons had been scattered through 90° [45° incidence] from the primary direction.

Very pure target materials were used and after chemical cleaning the metals were thoroughly outgassed by resistance heating within the vacuum.

The vacuum conditions were such that the total pressure during spectral recording was below 10^{-8} torr, and at no time was any visible target contamination observed. In fact residual gas spectra showed that the organic content was less than 1% of the total ambient pressure, with hydrogen being the most abundant [75%] component. The effect of slight contamination, however, was observed in the changes of some CEL spectra with time.

Measurements from the CEL spectra of the five metals revealed losses extending to over 100 eV from the zero loss peak. It appears that several of the losses recorded here have not been

observed previously, but in general the positions of the losses are in reasonable agreement with the results of previous workers. However, whilst various workers have found rather different CEL, the present spectra show evidence of nearly all previously reported losses. These observations are in accord with the results of THOMAS[22] who carried out his measurements [using an RPSA] in a similar vacuum environment.

The CEL spectra have been correlated with the theories of single electron interaction [atomic and band transitions] and plasmon interaction. In three of the metals a loss attributed to the excitation of surface plasmons was very close to the predicted $1/\sqrt{2}$ of the volume plasmon energy. This indicates the minimum of contamination on the surface. Identification of the plasmon losses has been based upon the best fit with theory and previous experimental attributions, although in the case of tungsten the change of spectrum with scattering angle indicated the choice made.

6.2 *Conclusions*

The present results show that to obtain true CEL spectra it is of great importance to work under ultra high vacuum conditions with the minimum of carbonaceous contamination. The spectra recorded here have considerable complexity and it appears that many previous experimenters, by using conventional diffusion pumped systems, have lost parts of the CEL spectrum. The following mechanism is suggested to account for this effect: the surface layer, providing it is thick enough [say about 10 to 20 Å], will provide CEL of its own. These may not be very intense since the layer will be an amorphous mixture of compounds and adsorbed gas. However they may raise the background level in critical parts of the spectrum to such an extent that weak losses are obscured. Conceivably different types of contamination would blot out different parts of the CEL spectrum and thus account for the many disagreements in published work.

The results suggest the validity of both the plasma and interband excitation theories, and in general the qualitative predictions of PINES appear to be borne out. Tantalum, tungsten and platinum give losses very close to the plasmon energy calculated on the basis of free valence electrons.

Most of their other losses may be considered as multiple volume and surface plasmon losses. Tantalum gave a broad peaked spectrum in agreement with PINES' suggestions, and this may well account for the fewer and less distinct losses observed in this case.

The results for nickel were obtained using the first 127° analyser and consequently the losses were not quite so well resolved. The spectra seem, however, to confirm the general finding of a plasmon energy corresponding to four free electrons per atom.

The silver CEL spectrum was found to be very complex and most of the losses can be explained on the basis of band transitions. The lower pair of energy losses fit very well with optical measurements, and two plasmon energies have been deduced. This assignment is questionable, however, since no CEL peaks were observed at twice these fundamental losses.

The theory of atomic transitions, or the ionisation of subshells, also seems a likely source of CEL and several losses have been ascribed to this process.

6.3 *Suggestions for further work*

This work could be most profitably continued and extended with an analyser of higher resolution. This would require a 127^{o} analyser with larger mean radius, perhaps situated in a vacuum tube coaxial with the electron beam.

However, in order to take advantage of a better resolving power, further modifications might have to be made: it would be desirable to provide a narrower primary energy spread, either by using a more sophisticated electron gun or by using a monochromating analyser. For the same reason the method of focusing the secondaries down into the analyser might have to be avoided, and the weak currents at the collector amplified as suggested in 5.5.

In order to expand the investigation two new facilities should be incorporated in the apparatus: firstly the target and electron gun should be mounted so they rotate about an axis passing through the centre of the target. This would make possible the observation of energy spectra as functions of angle of incidence and scattering angle. Admittedly this is a very difficult thing to achieve in conjunction with the requirements of UHV and target heating.

Secondly it would be useful to be able to evaporate target films onto a substrate and obtain CEL spectra without the surface having been exposed to the atmosphere. Again this is rather difficult if the system is to be kept at a reasonably low pressure [say less than 10^{-7} torr] during the evaporation. To this end a greater pumping speed would be desirable, so perhaps a titanium sublimation pump, orbitron or turbo-molecular pump could be employed.

Many of these suggestions require extensive structural changes to be made, but the possibility of using the present unmodified apparatus to repeat work on other metals should not be overlooked. On the basis of the present discoveries it is likely that the employment of UHV techniques in the field of secondary electron emission will reveal many new features.

APPENDIX A

THE 127° ELECTROSTATIC ANALYSER

A.1 Various electrostatic analysers

In recent years electrostatic analysers have become well established as a means of finding the energy spectra of charged particles. They have occasionally been used to determine ionic spectra[173,196-198], but more commonly the particles have been electrons. For the present purpose the particles are generally referred to as electrons.

The electrostatic analyser has several advantages over the magnetic type of analyser: they have often been used in scientific satellites [174] where their small weight and modest power requirements are invaluable. Their lack of magnetic field is also useful, in that they do not interfere with neighbouring apparatus. From the laboratory point of view, and this investigation in particular, it is undesirable to have stray magnetic fields in the region of low energy electrons. As far as their relative resolutions are concerned, several electrostatic analysers are equivalent to the magnetic analyser [175].

Several kinds of electrostatic analyser have been described and diagrams of some of them are given in figure A.1. The first was that of HUGHES & ROJANSKY[28],

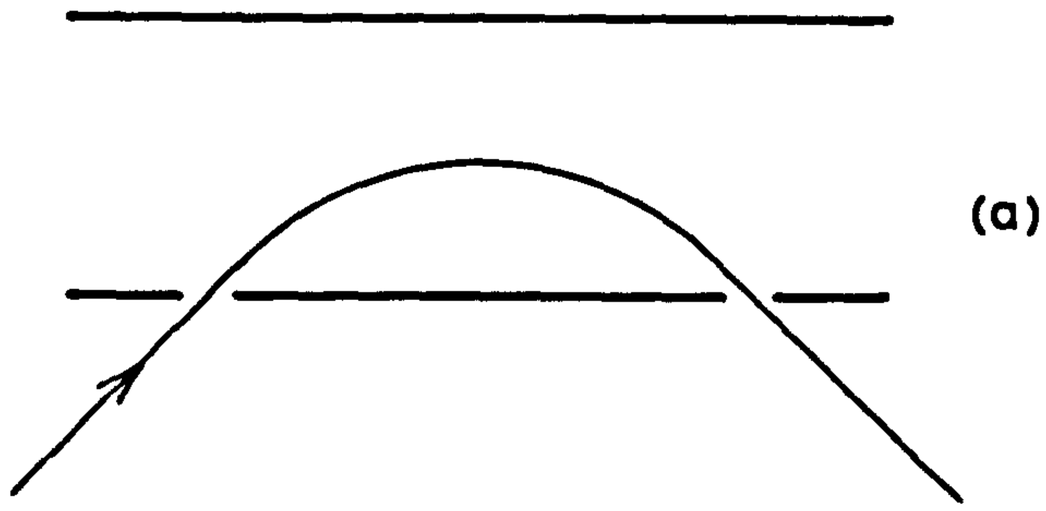

(a)

SECTIONS THROUGH

(a) PARALLEL PLATE ANALYSER.

(b) CYLINDRICAL MIRROR ANALYSER

(c) CONCENTRIC SPHERICAL ANALYSER

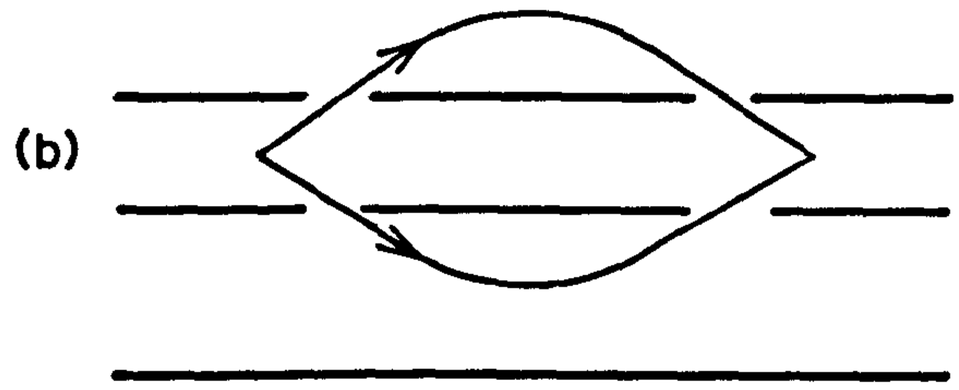

(b)

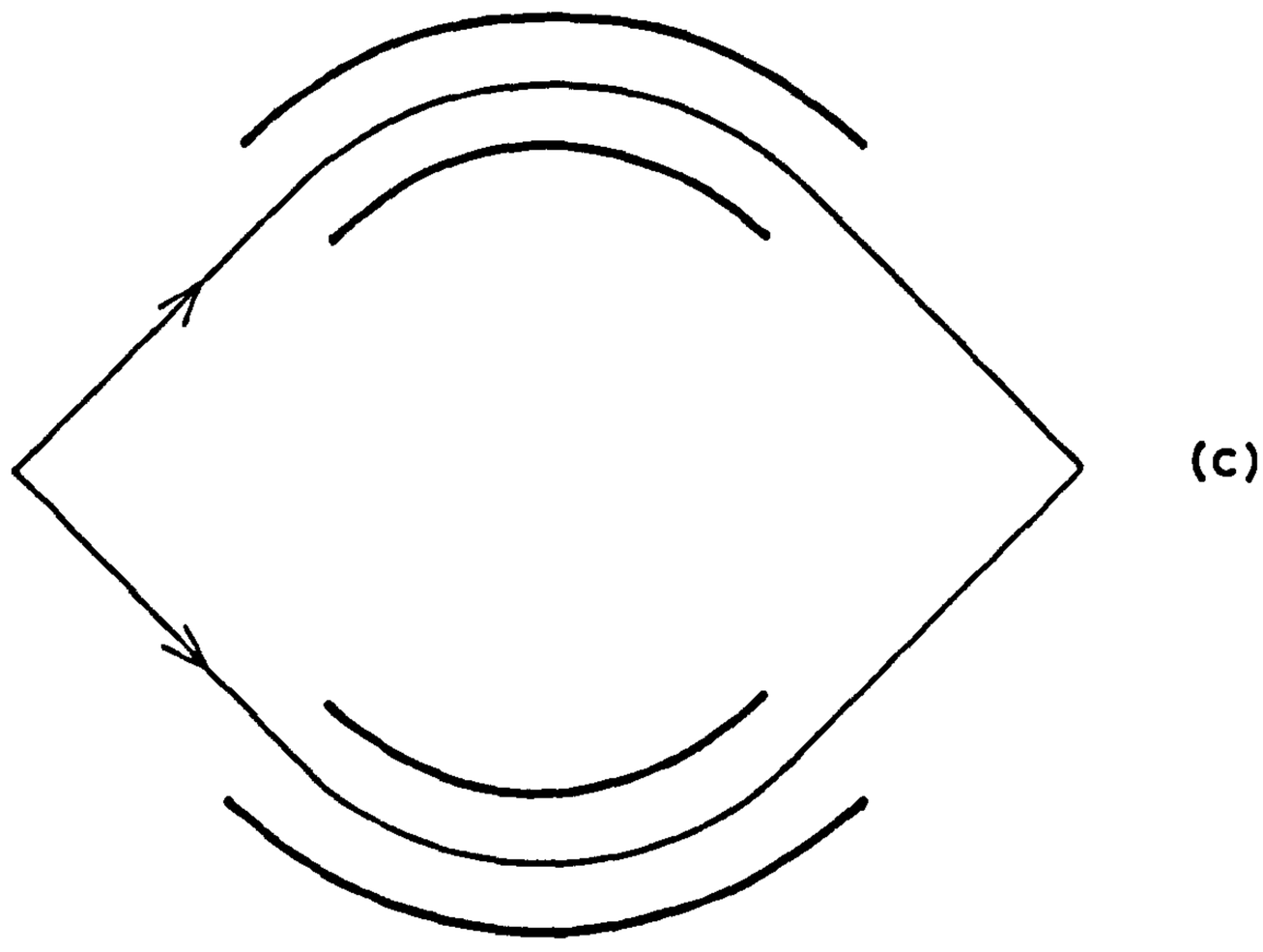

(c)

FIGURE A.1

this being the 127° analyser as used in this work. Then, following a suggestion of ASTON[176], PURCELL[175] gave details of the concentric spherical analyser. HARROWER[177] has given a treatment of the parallel plate analyser which acts as an electron mirror. BLAUTH, ZASHKVARA et al., SAR-EL, and HAFNER et al.[178-181] have done work on cylindrical mirror analysers. The RPSA has already been described in chapter 1.

The parallel plate analyser is undoubtedly the simplest to construct, but it suffers from the formation of electron lenses at the entry and exit slits. This limits the FWHM resolution to about 1%[177]. In operation an electron beam enters through a slit in one of the parallel plates at an angle θ, and is bent along a parabolic path. It is simple to show that the condition for best resolution is given by $\theta = 45^{\circ}$. Electrons of energy determined by the plate voltages are then focused at the exit slit, which lies in the same plane as the entry slit.

The cylindrical mirror analyser uses the same reflecting principle as the parallel plate analyser, but under certain conditions [$\theta = 42{\cdot}3^{\circ}$ etc.], it has the advantage of second order focusing. This means that a beam of circular cross-section is not distorted after analysis, and entry beams of fairly large angular spread

[say $\pm 5^{\circ}$] can be accepted without degrading the resolution beyond 1% .

This is significantly better than the concentric spherical analyser which acts, like the 127° cylindrical analyser, by deflecting the electron beams along paths about the local earth potential. It too has the advantage of double focusing. Under certain conditions it conforms with BARBER's rule[182] and can be directly compared with the sector magnetic analyser[175]. It is, however, the most difficult to construct of all these analysers, although its three dimensional geometry lend it to some elegant arrangements for the study of CEL.

The cylindrical electrostatic analyser is not necessarily restricted to $\pi/\sqrt{2}$. The angle chosen depends on the focusing conditions of the electron beam. In general the electrostatic field acts as a lens, a purely parallel input beam becoming focussed after going through only $\pi/2\sqrt{2}$ radians, and a beam which is focussed at the entry slit first becoming refocussed after $\pi/\sqrt{2}$. The dispersion at the exit slit in the second case, however, is twice that of the first. But this is not the only difference, because other considerations produce different aberrations in the two cases. Section A.3 is devoted to the derivation of formulae for the resolution in each case , but the section which follows immediately is valid for both.

A.2 *The cylindrical electrostatic field*

If two infinite coaxial cylinders of radii A and B bear a quantity of charge, λ/unit length, then the field between them as a function of radial distance r is

$$E = \frac{1}{2\pi\epsilon_o} \cdot \frac{\lambda}{r} = - \frac{dV}{dr}$$

If the cylinders have potentials V_A and V_B where $A < r < B$, then

$$\int_{V_A}^{V_B} - dV = \frac{\lambda}{2\pi\epsilon_o} \int_A^B \frac{1}{r}\, dr$$

$$\therefore \quad - V_{an} = \frac{\lambda}{2\pi\epsilon_o} \ln \frac{B}{A} \qquad \text{where} \quad V_{an} = V_B - V_A$$

$$\therefore \qquad E = - \frac{1}{r} \cdot V_{an} \,/\, \ln \frac{B}{A} \qquad \ldots\ldots\ldots\ldots\ldots\ldots [1]$$

Therefore the potential at radius r is

$$V_r = - V_{an} \cdot \ln \frac{r}{a} \,/\, \ln \frac{B}{A} \qquad \ldots\ldots\ldots [2]$$

where r = a is the radius of zero potential. If an electron is travelling along this radius then its velocity v is given by:

$$\frac{mv^2}{a} = \frac{e}{a} \cdot [-V_{an}] \,/\, \ln \frac{B}{A}$$

But $\frac{1}{2}mv^2 = eV$ so:

$$2\,eV = e.V_{an} \,/\, \ln \frac{B}{A}$$

$$\text{i.e.} \qquad V = V_{an} \,/\, 2 \ln \frac{B}{A} = F \cdot V_{an} \qquad \ldots\ldots\ldots [3]$$

The quantity F is fixed for a given analyser, and is called the analyser factor.

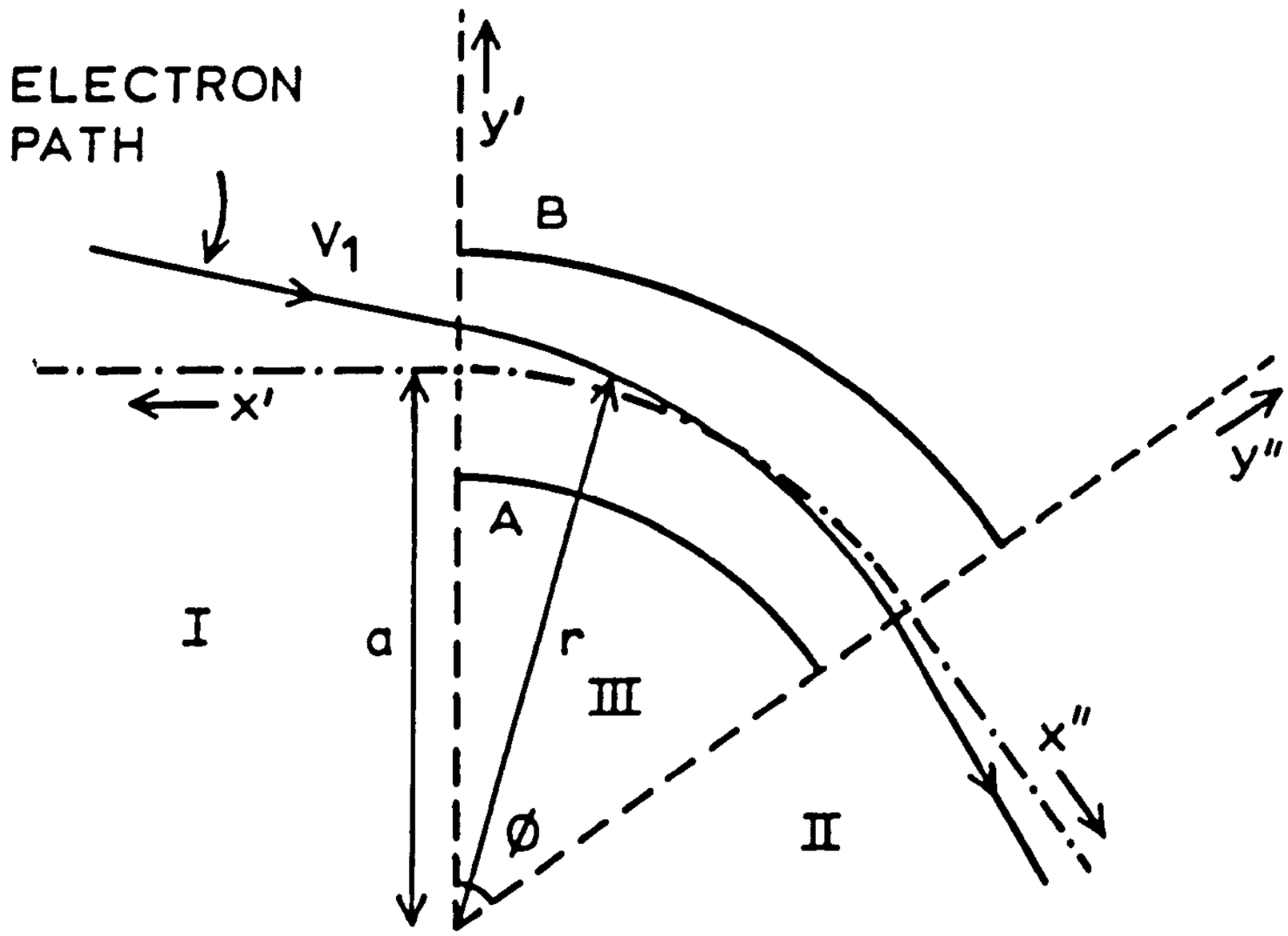

REGION	EQUATION OF ELECTRON PATH
I	$y' = y_1 + \tan \alpha_1 . x'$
III	$r = a . (1 + \delta)$
II	$y'' = y_2 + \tan \alpha_2 . x''$

FIGURE A.2 Coordinate systems used in HERZOG'S [183,196] analysis.

A.3 *Theory of the cylindrical electrostatic analyser.*

[a] Equation of motion

An approximate equation of motion can be deduced for electrons whose paths are close to circular. Using the coordinate systems shown in figure A.2 and putting the equations

$$m.\frac{d^2r}{dt^2} = mr.\dot{\phi}^2 - \frac{mv^2}{r}$$

$$\frac{m}{r}.\frac{d}{dt}[r\dot{\phi}] = 0$$

into an approximate form, HERZOG[183] found a simple differential equation with solution

$$\delta = \frac{y_1}{a}.\cos\sqrt{2}\,\phi + \beta[1-\cos\sqrt{2}\phi] - \frac{\tan\alpha}{\sqrt{2}}.\sin\sqrt{2}\phi \quad ...[4]$$

where $\beta = \frac{v_1 - v}{v}$ and all the other symbols are as explained in the figure. The separation of two components in the electron beam as a function of ϕ is given by their respective a.δ provided $|\delta| \ll 1$.

[b] Image aberrations

For a monoenergetic beam $\beta = 0$ and one finds first order focusing by putting $\delta = 0$ in equation 4. Two ideal cases can be considered:

parallel input beam In this case $\alpha = 0$ so the focusing occurs at $\cos\sqrt{2}\phi = 0$, or $\sqrt{2}\phi = [1+2n].\pi/2$ for n = 0, 1,...

i.e. the first position of focus is at

$$\phi_1 = \frac{\pi}{2\sqrt{2}} = 63^\circ 39'$$

fine focussed input beam In this case $y_1 = 0$ so the focusing occurs at $\sin\sqrt{2}\phi = 0$, or $\sqrt{2}\phi = n.\pi$ for n = 0, 1,.....

i.e. the first position of focus is at

$$\phi_2 = \frac{\pi}{\sqrt{2}} = 127^{\circ}17'$$

Neither of these ideal cases can be realised in practice since there is inevitably some non-normal component in a parallel beam of finite diameter, and no entrance slit can be infinitesimally narrow. Thus even a monoenergetic beam is not focussed into a perfectly thin image. If it contains rays diverging $\pm\alpha$ from the normal and is incident on a slit of width $s_1 = 2y_1$, then the image has a width $\sqrt{2}a.\tan\alpha$ at ϕ_1 and s_1 at ϕ_2.

The image width of a monoenergetic beam is called the aberration of the analyser. Equation 4 gives the aberrations which have just been quoted, but these are only accurate to the first order of approximation. HUGHES & ROJANSKY found the accurate equation of motion and various approximate solutions of it. By this means one can obtain improved accuracy, and to the second order the aberrations are increased by $\frac{2}{3}\, a.\tan^2\alpha.[1 - \cos\sqrt{2}\phi]$

Thus at ϕ_1 $\qquad A_1 = \sqrt{2}\, a.\tan\alpha + \frac{2}{3}\, a.\tan^2\alpha$ ..... [5i]

and at ϕ_2 $\qquad A_2 = s_1 + \frac{4}{3}\, a.\tan^2\alpha$ ..... [5ii]

The measured aberration, however, is increased by the width of the exit slit s_2. Thus equations 5 should be modified to read:

$$A_1 = s_2 + \sqrt{2}a.\tan\alpha + \frac{2}{3}a.\tan^2\alpha \quad \text{.....[6i]}$$

$$A_2 = s_1 + s_2 + \frac{4}{3}a.\tan^2\alpha \quad \text{.....[6ii]}$$

Although equation 6ii does not explicitly contain the entry slit width s_1, the relation is only valid provided s_1 is sufficiently small. This is because HERZOG assumes that the logarithmic potential is linear near r=a, and because $|\delta| << 1$ everywhere. Practically this means that s_1 must be smaller than, say, both [B-A]/10 and a/10.

[c] Image dispersion

Now if one puts $\beta \neq 0$ in equation 4, then one finds the separation between two monoenergetic beams [the dispersion] to be approximately:

at ϕ_1 $\quad D_1 = \beta.a \quad$ ..... [7i]

and at ϕ_2 $\quad D_2 = 2\beta.a \quad$ ..... [7ii]

in practical terms the dispersion is the distance [at the moment in velocity units] between the midpoints of the images.

When one takes into account second order terms one finds that equation 7ii should be modified to read:

$$D_2 = [2\beta + 2\beta^2].a$$

HUGHES & ROJANSKY appear to have overestimated this correction factor. The working is as follows:

$$\frac{a}{a[1+\delta]} = 2\frac{v}{v_1} - 1 \qquad \text{[their equation 6]}$$

$$= \frac{2}{\beta+1} - 1$$

i.e. $$1+\delta = \frac{1+\beta}{1-\beta}$$

$$\therefore \quad \delta = \frac{2\beta}{1-\beta} = 2\beta.[\,1 + \beta + \beta^2 + \ldots.\,]$$

$$\therefore \quad \delta.a = D_2 = [2\beta + 2\beta^2].a$$

If $\beta>0$ this correction shows that D_2 is increased. However, if $\beta<0$ the dispersion is in the other direction and reduced in magnitude to $D_2 = [2\beta - 2\beta^2].a$. This is to be compared with HUGHES & ROJANSKY's $D_2 = [2\beta - 4\beta^2].a$ [their equation 7] which they use to draw their figure 4.

On the average, therefore, the second order terms can be ignored and equation 7ii taken as sufficiently accurate.

If one expresses β as a function of electron voltage rather than velocity one finds:

$$\beta' = \tfrac{1}{2}\beta$$

where $\beta' = [V_1 - V]/V$, the fractional voltage difference.

Thus $$D_1 = \tfrac{1}{2}\beta' a \qquad \ldots\ldots\ldots \text{[8i]}$$

and $$D_2 = \beta' a \qquad \ldots\ldots\ldots \text{[8ii]}$$

[d] Resolution

The quality of the image may be expressed as $Q = D/A$

so, taking equations 6 and 8 together, one finds

for ϕ_1 $$1/Q_1 = \frac{s_2 + \sqrt{2}a.\tan\alpha + \frac{2}{3}a.\tan^2\alpha}{\frac{1}{2}\beta' a}$$

and ϕ_2 $$1/Q_2 = \frac{s_1 + s_2 + \frac{4}{3}a.\tan^2\alpha}{\beta' a}$$

For $Q > 1$ the images are perfectly distinguished, and when $Q = 1$ the images just touch at background level. Taking $Q = 1$ as the criterion one can find the β' for which this occurs:

for ϕ_1 $$\beta' = \frac{2}{a}\left[s_2 + \sqrt{2}a.\tan\alpha + \frac{2}{3}a.\tan^2\alpha\right]$$

and ϕ_2 $$\beta' = \frac{1}{a}\left[s_1 + s_2 + \frac{4}{3}a.\tan^2\alpha\right]$$

Practically, however, one finds it more convenient to measure the FWHM rather than the full energy width of the peak. Thus, assuming a peak shape such that $R = \frac{FWHM}{V} = \frac{1}{2}\beta'$, one obtains expressions for the resolution R:

at ϕ_1 $$R_1 = \frac{1}{a}\left[s_2 + \sqrt{2}a.\tan\alpha + \frac{2}{3}a.\tan^2\alpha\right] \quad \ldots\ldots [9i]$$

at ϕ_2 $$R_2 = \frac{1}{2a}\left[s_1 + s_2 + \frac{4}{3}a.\tan^2\alpha\right] \quad \ldots\ldots [9ii]$$

The relation 9ii has been quoted by SCHULTZ[184] from an unpublished work.

An immediate result of these equations is that the electron voltage width passed by the analyser depends linearly on the voltage.

i.e. $$\Delta V = K.V$$

Thus an energy spectrum which contains a constant number of electrons, n, per unit energy interval, is analysed as

$$n.\Delta V = n.K.V$$

Therefore, if a spectrum is scanned linearly with time, the collector current should be divided by the electron voltage at all points to obtain the true shape of the energy spectrum.

However the correction is only serious for very low energy electrons, when the division may raise the spectrum considerably. But, because spectral shape has not been the subject of this investigation and because in general $V>>0$, this correction has been ignored.

Using equation 9, one can compare the resolutions of the two analysers:

$$R_1 = R_2 + \sqrt{2}.\tan\alpha + \left[\frac{s_2 - s_1}{2a}\right]$$

Since s_1 is very similar to s_2 in normal circumstances, R_1 is worse than R_2 by about $\sqrt{2}.\tan\alpha$. For $\alpha = \pm 2^\circ$ this means that R_1 is worse by about 5%. Theoretically, if $s_1 = 0{\cdot}010''$ and $a = 2''$, then even if $s_2 = 0$ the resolutions are only comparable if $\alpha = 0{\cdot}1^\circ$. Thus for the same radius the 127° analyser has a superior resolution for less stringent input parameters.

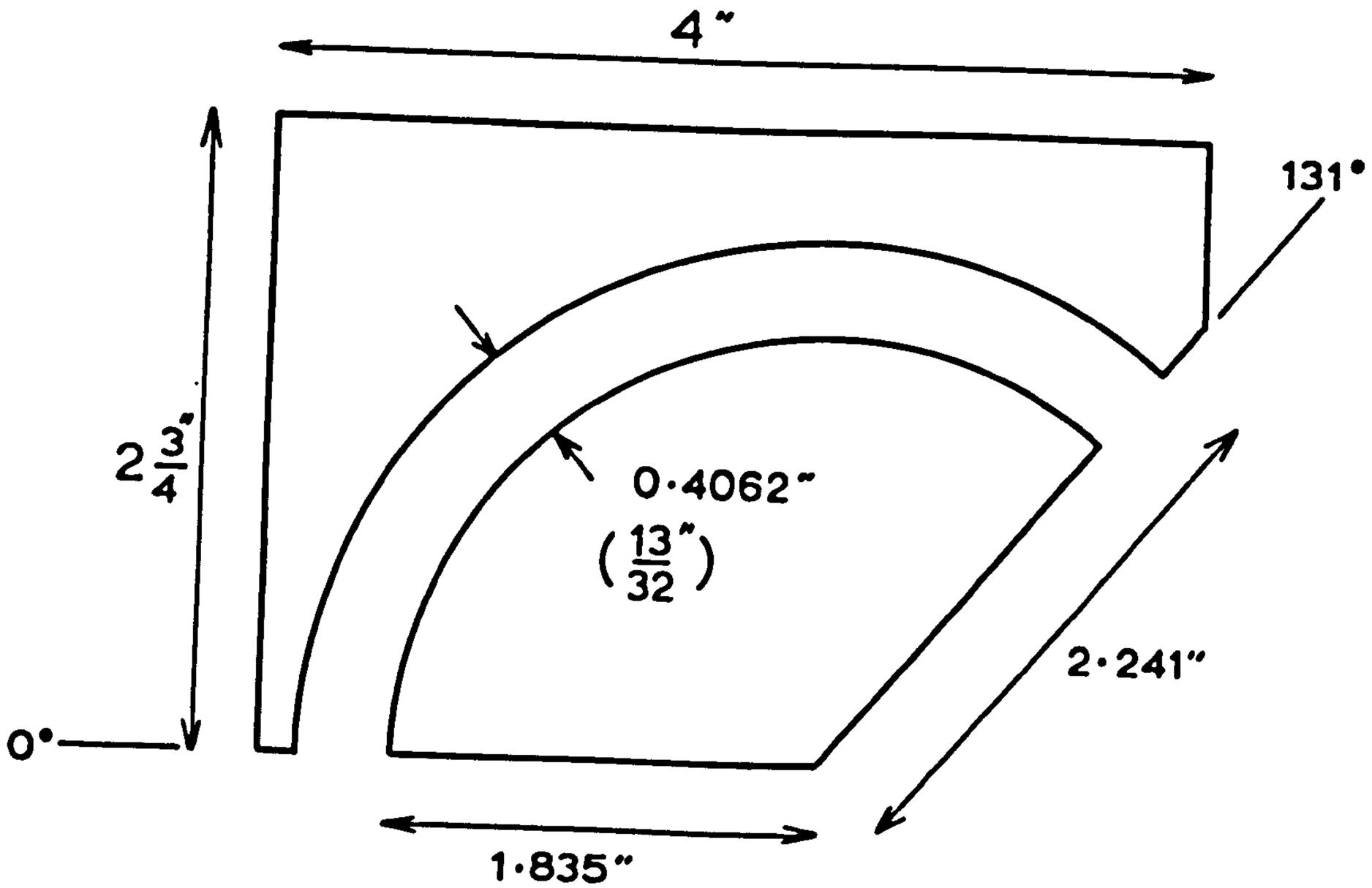

FIGURE A.3(i) Analyser plan

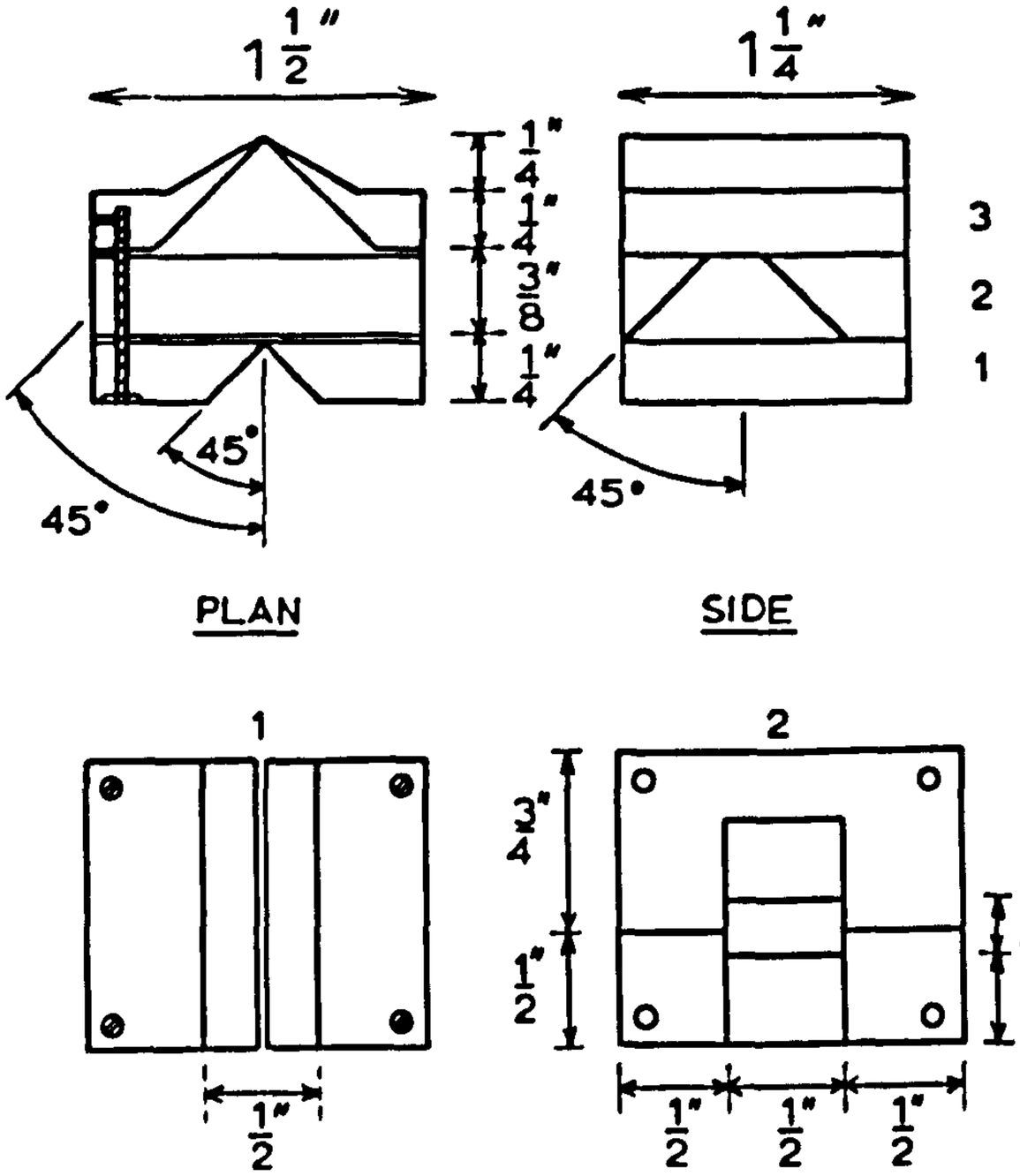

FRONT OF EACH SECTION

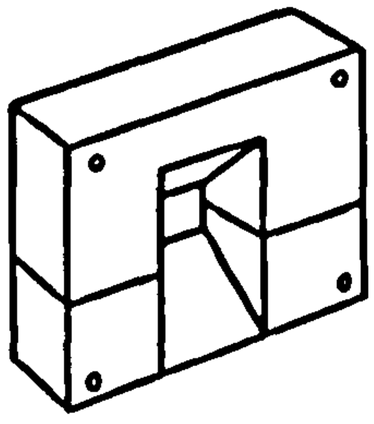

SLIT 1	VERTICAL AND CENTRAL OF WIDTH 0·020"
SLIT 2	HORIZONTAL AND OFF-CENTRE AS DRAWING, OF WIDTH 1/4"
SLIT 3	VERTICAL AND CENTRAL OF WIDTH 0·010"

SECTION 2

FIGURE A.3 (ii) Analyser entrance apertures

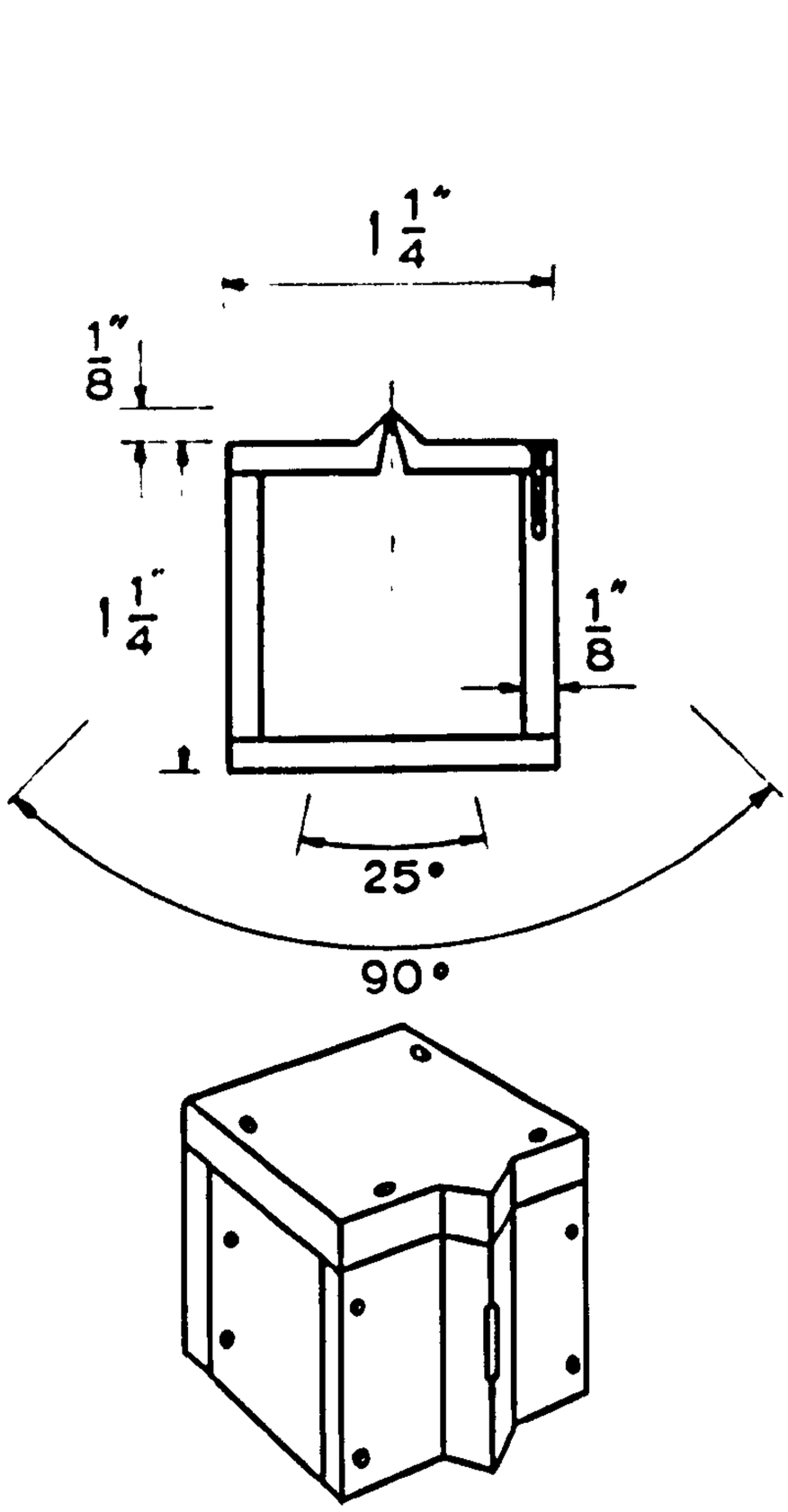

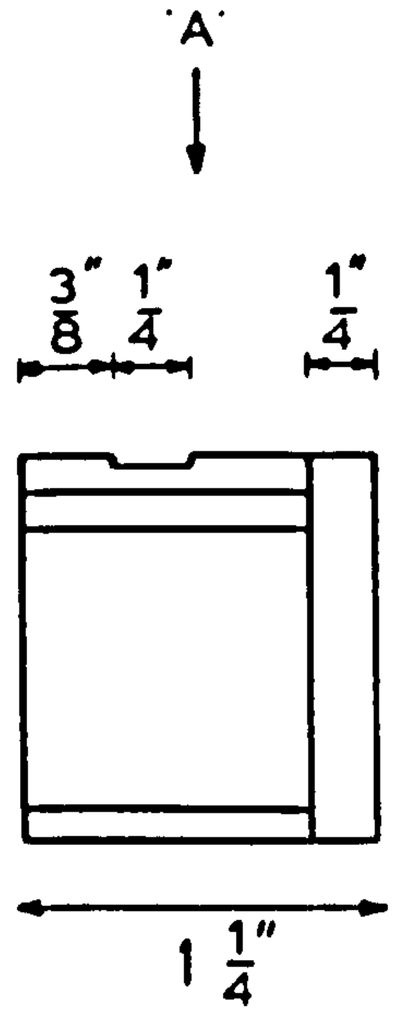

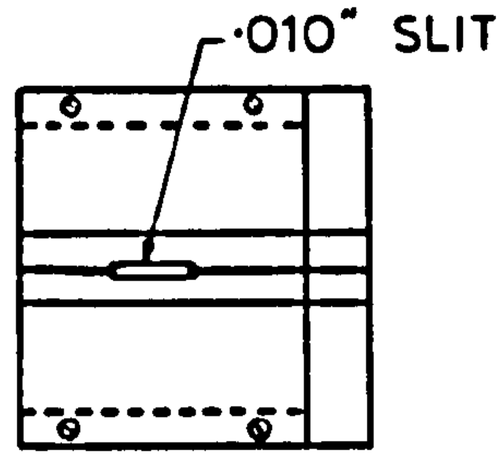

VIEW ON ARROW 'A'

FIGURE A3 (iii) Analyser exit aperture and collector shield.

A.4 *The third 127° analyser*

Drawings of this analyser are given in figures A.3.

The critical dimensions were:

$$B = 2{\cdot}241"$$

$$A = 1{\cdot}835"$$

$$s_1 = s_2 = 0{\cdot}010"$$

$$\alpha = \pm 2^{\circ}$$

Using these figures one can calculate the following parameters:

[a] Substituting into equation A.3 one finds the analyser factor:

$$F = \left[2.\ln\frac{2{\cdot}241}{1{\cdot}835}\right]^{-1} = 2{\cdot}5$$

i.e. $$V = 2{\cdot}5 \times V_{an}$$

[b] As a result of the logarithmic potential given by equation A.2, the radius of zero potential, a, is given by

$$V_A + V_B = -\frac{V_{an}.\ln[A/a] + V_{an}.\ln[B/a]}{\ln[B/A]} = 0$$

i.e. $$\ln[A/a] = -\ln[B/a]$$

$$a = \sqrt{A.B}$$

Thus in the case of the third analyser one finds

$$a = 2{\cdot}028"$$

This is 0·010" less than the mid-radius, so the slits were displaced towards the inner arc by this quantity.

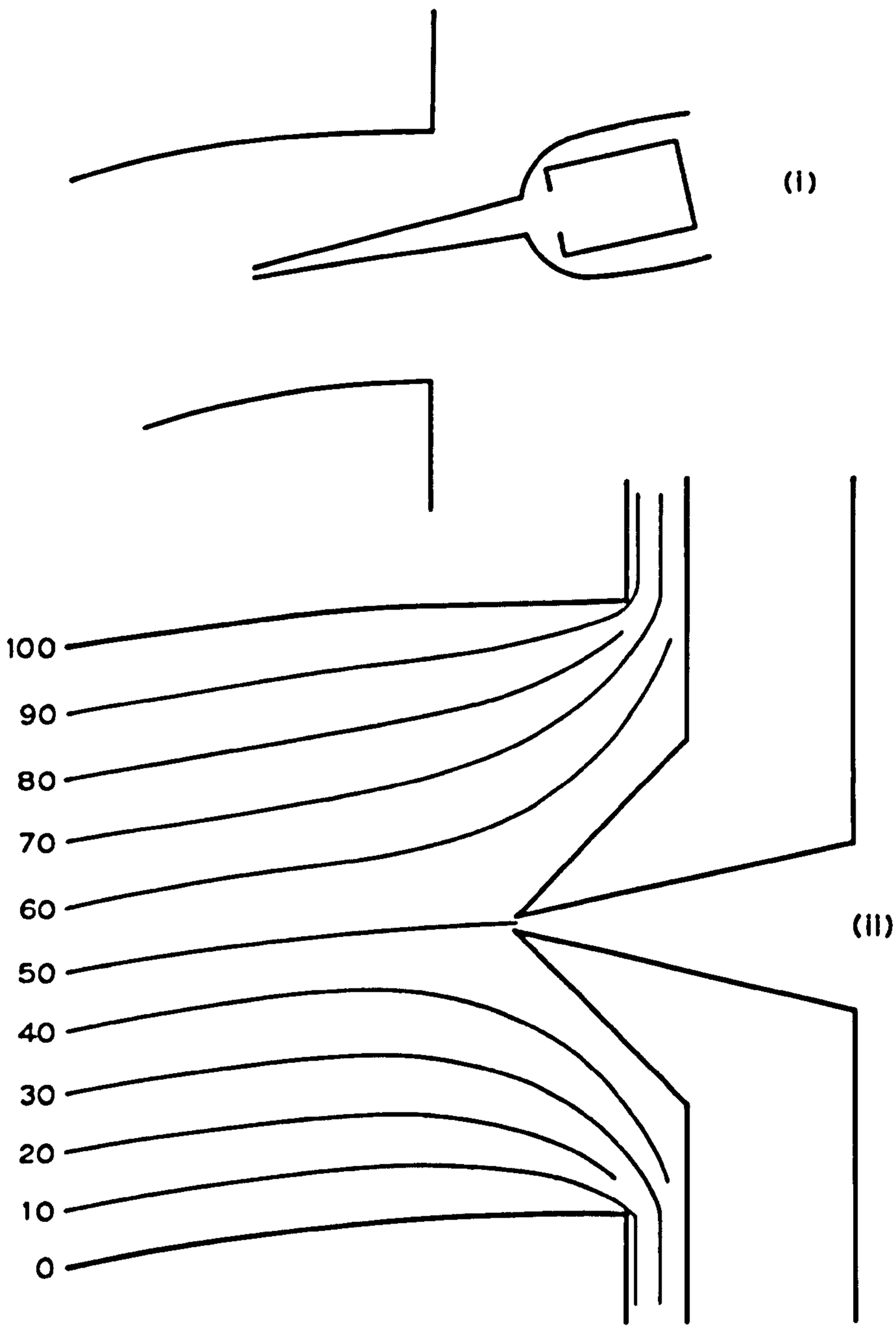

FIGURE A.4 Fringing fields at the analyser apertures.

[c] The resolution of the analyser [FWHM of peak] is given by equation 9ii :

$$R = \frac{1}{4.056}\left[0{\cdot}02 + \frac{4}{3} \times 2{\cdot}028 \times 0{\cdot}00122\right]$$

$$= 0{\cdot}0057$$

i.e. $$\underline{R = 0{\cdot}6\%}$$

[d] No account was taken of the stray fields between the analyser arcs and the entry and exit apertures. HERZOG[185] has analysed this problem for the case of the plane condenser, and his results can be applied to the cylindrical analyser.

An alternative scheme is that shown in figure A.4i. The exit slit is defined by the lips of two thin plates inserted between the analyser arcs along the zero potential. Being closely spaced the plates do not seriously disturb the logarithmic potential, but they introduce problems of electron transmission through the narrow gap. It seems that the continuous dynode electron multiplier might have some application here. A practical compromise was to use the geometry as described in chapter 3, with nose shaped slits penetrating a field larger than 127°. The results of a resistive paper plot given in figure A.4ii show that the potentials do not appear to be too badly affected.

However, since the potential field is different from the ideal in the neighbourhood of the entry and exit slits, one expects the aberration to be increased. Thus the resolution would also be slightly degraded.

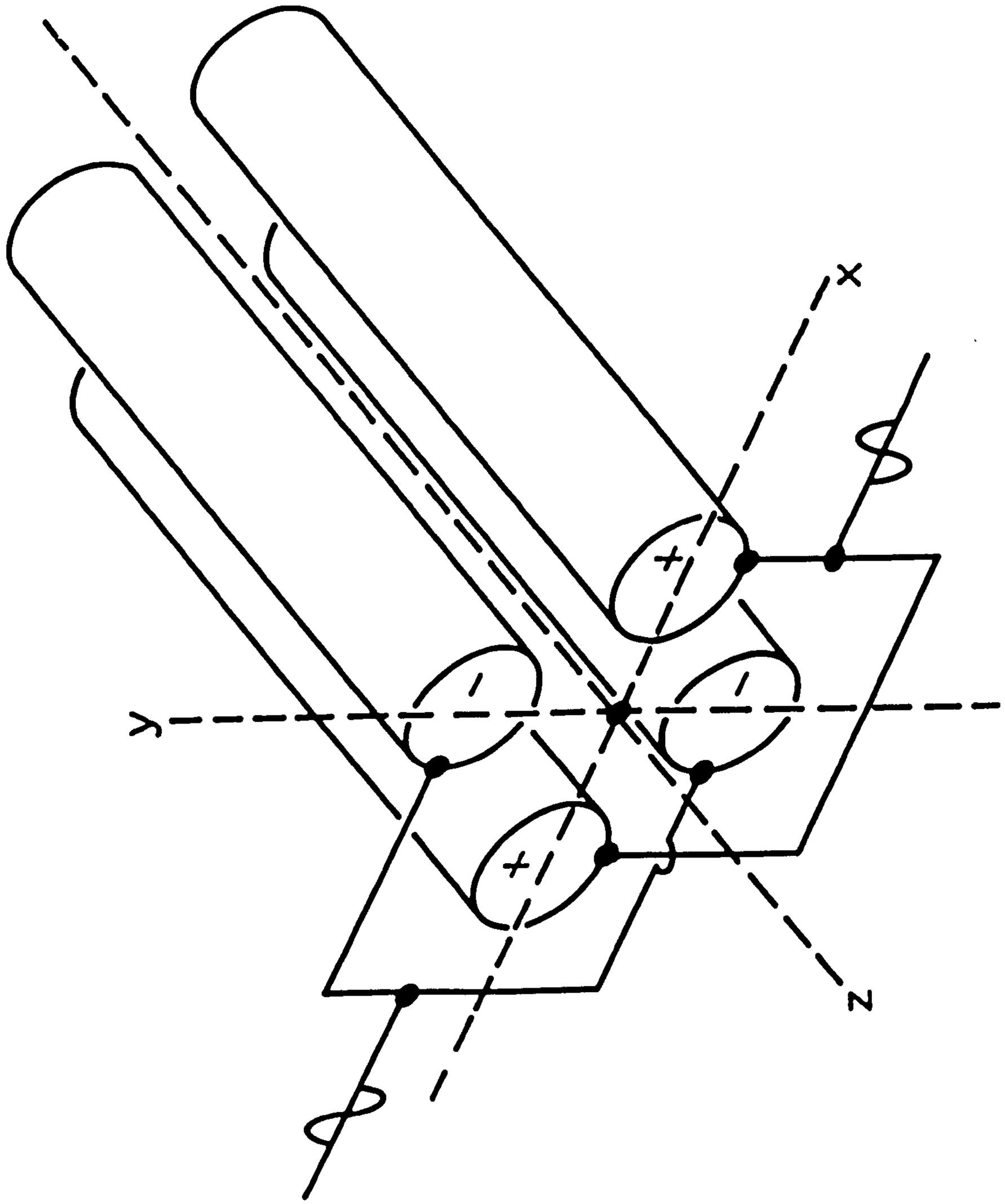

FIGURE B1. Geometry of the quadrupole mass filter.

APPENDIX B

THE QUADRUPOLE RESIDUAL GAS ANALYSER

B.1 Description

The quadrupole analyser, first described by PAUL & STEINWEDEL in 1953[186-188], is a purely electrostatic mass analyser. It was recognised that this device operated as a mass filter whose mass pass band is electrically adjustable and which is sensitive primarily to M/e rather than ion velocity. This makes a fairly crude ion source perfectly adequate. The analysis of the Mathieu equations, which describe the motion of ions through the filter, is well documented[189] and is only briefly presented here.

Ideally the quadrupole analyser is composed of four long hyperbolic cylinders in a square array, with the inside radius of the array equal to the smallest radius of curvature of the hyperbolae. The hyperbolic array can be well approximated, however, by using circular cylinders as shown in figure B.1. Opposite pairs of rods are connected electrically. The potentials applied to the two pairs of rods are equal in magnitude, but the DC potentials, U, are opposite in sign and the AC potentials, V, are shifted in phase by 180^{o}. This gives a set of negative U rods lying in the y-z plane, and a set of positive U rods lying in the y-z plane.

In practice the ion source is placed at one end of the quadrupole array on the z-axis, the ions are analysed as they pass through the array and the resulting signal collected at the other end, again on the z-axis.

B.2 The quadrupole field

The potential at any point in the quadrupole array is given by the following equation:

$$\phi = [\, U + V.\cos\omega t \,] . \frac{x^2 - y^2}{r_o^2}$$

where $2r_o$ is the spacing of opposite electrodes. It can be seen that the potential is zero along the z-axis, and in the two planes given by $x = y$.

Thus the electric fields are:

$$E_x = -\frac{\partial \phi}{\partial x} = -2\,[\, U + V.\cos\omega t \,] . \frac{x}{r_o^2}$$

$$E_y = -\frac{\partial \phi}{\partial y} = 2\,[\, U + V.\cos\omega t \,] . \frac{y}{r_o^2}$$

$$E_z = 0$$

B.3 *Equation of motion*

If a positively charged particle is injected into the quadrupole field it experiences the following forces:

$$F_x = M.\ddot{x} = e.E_x = -\frac{2ex}{r_o^2}[U + V.\cos\omega t]$$

$$F_y = M.\ddot{y} = e.E_y = \frac{2ey}{r_o^2}[U + V.\cos\omega t]$$

$$F_z = 0$$

These equations can be simplified by making the substitutions:

$$t = 2S, \qquad a = \frac{8eU}{Mr_o^2\omega^2}, \qquad q = \frac{4eV}{Mr_o^2\omega^2}$$

and the result is:

$$\frac{d^2x}{dS^2} - [a + 2q.\cos 2S].x = 0$$

and

$$\frac{d^2y}{dS^2} + [a + 2q.\cos 2S].y = 0.$$

These equations are known as Mathieu equations and generally can be solved only approximately. Moreover the solutions exist only for certain ranges of the parameters a and q. This condition is discussed in the next section, since it crucially affects the resolution of the mass spectrum.

The approximate solutions give ion trajectories which are close to modulated high frequency sinusoids. They are shown in figure B.2 for the two basic cases, the x-z and y-z planes. The qualitative explanation of the trajectories which follows, assumes that U = 200 volts and V = 1000 volts.

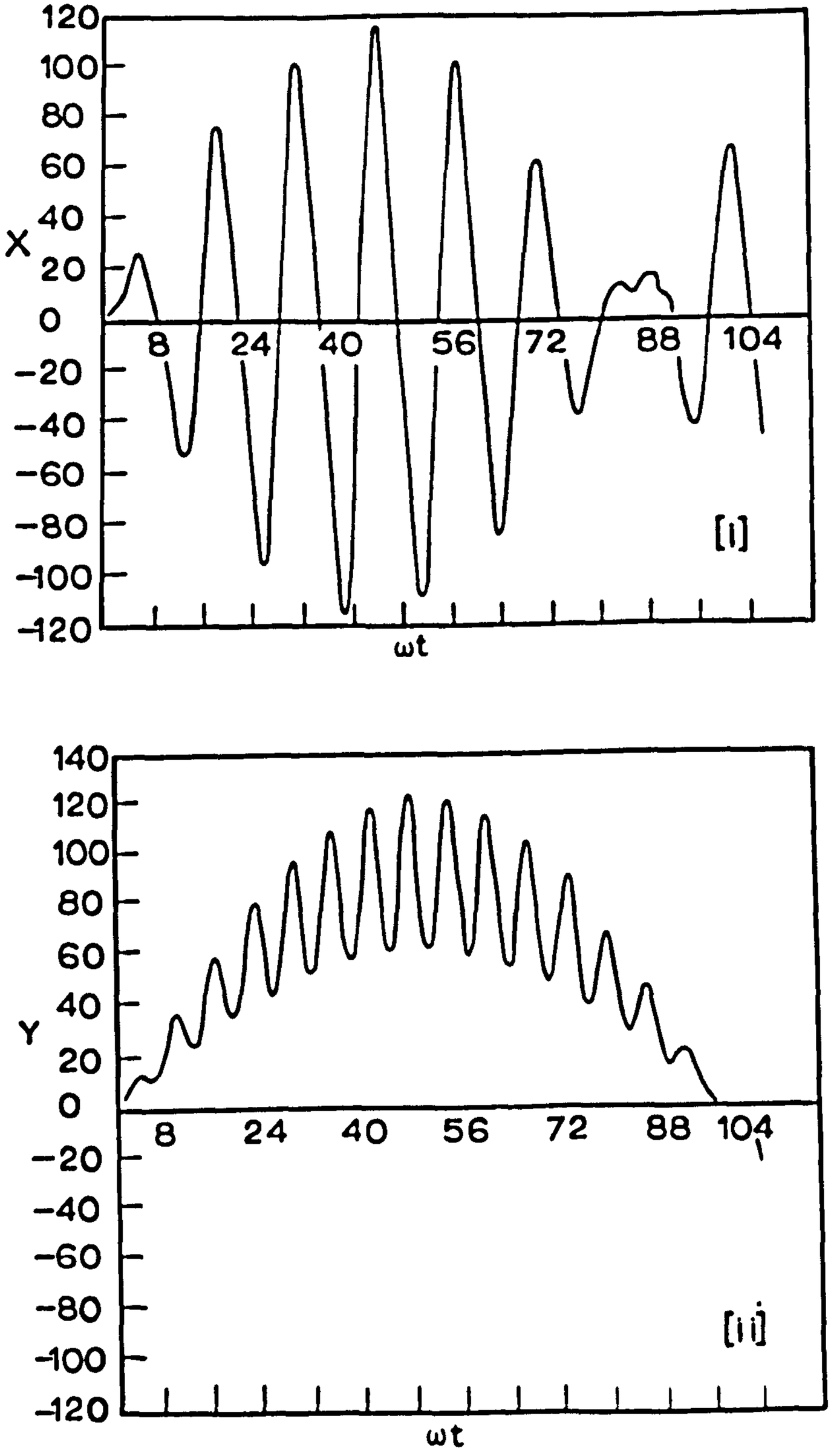

FIGURE B.2 Ion trajectories in
[i] the x-z plane
[ii] the y-z plane
for a = 0·231 and q = 0·7038

In the x-z plane positive ions are strongly focussed by the DC potential alone. The RF field produces oscillations in the ion trajectory which are at half the RF frequency: at each excursion from the z-axis the ion is reflected by the positive going cycle of RF. It returns through the z-axis during the negative cycle, and is reflected from the opposite rod by the next positive cycle.

In the y-z plane the ions are defocussed by the DC voltage, but the far greater RF voltage acts to produce a net focusing. The ion is attracted out from the z-axis by the DC voltage, but as it nears the rod it is reflected by the stronger RF during a positive cycle. This reverses the ion velocity, but as the ion moves back towards the z-axis it is retarded by the DC potential and when the RF swings negative it resumes its motion away from the z-axis. As it nears the rod again the RF swings positive and the ion is reflected. Thus the frequency of oscillation of the ion is equal to the RF frequency. The net focusing effect arises because at each turning point the acceleration towards the z-axis is always greater than that away from it. This is because the ion is closer to the rod when it is positive, than when it is negative.

It can be appreciated that if the ion is to follow the RF oscillations in this way and never stray too far from the z-axis in any direction, then the critical voltages and ion mass must be well balanced. If the ion has a mass such that the RF fails to counteract the DC potential in the y-z plane, or if the RF produces too large oscillations in the x-z plane, then the ion is collected on one of the rods.

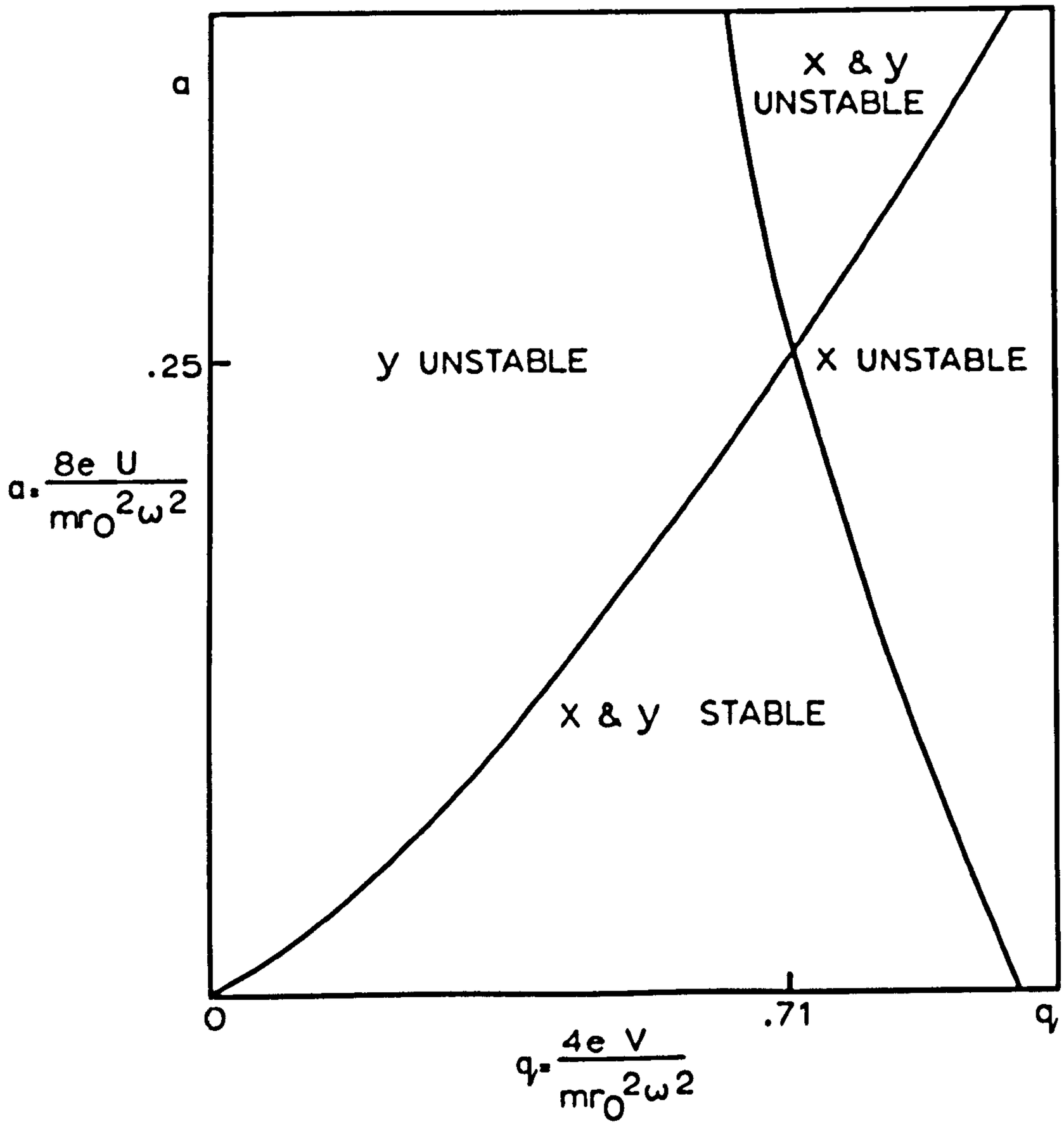

FIGURE B.3 Stability diagram showing the values of a and q for which stable ion trajectories are possible.

B.4 *The Spectrum*

It was pointed out in the last section that solutions of the Mathieu equations exist only for certain ranges of p and q. Figure B.3 shows a stability diagram in which the triangular shaped region corresponds to the area defined by the lowest range of p and q. There are other regions of stability at higher values of p and q[190-192] but these will not be considered further. If any ion passes through the filter with its [p,q] coordinate lying in the region of stability then it moves in a stable trajectory to the collector. Otherwise its trajectory is unstable in at least one plane and, given a long enough filter, the ion is collected on a rod.

To scan through a region of varying M/e, some of the parameters contained in a and q must be varied. As an example consider the case where the values of r_o, e, and ω are kept fixed and the variation in mass range is accomplished by varying the potentials. The resulting stability diagrams for four masses are shown in figure B.4. It is apparent that the mass varies linearly with applied V, and that the size of the stability diagram varies linearly with mass. Thus, if one keeps the ratio U/V constant whilst the individual values are swept linearly with time, the collector receives a linearly varying mass spectrum.

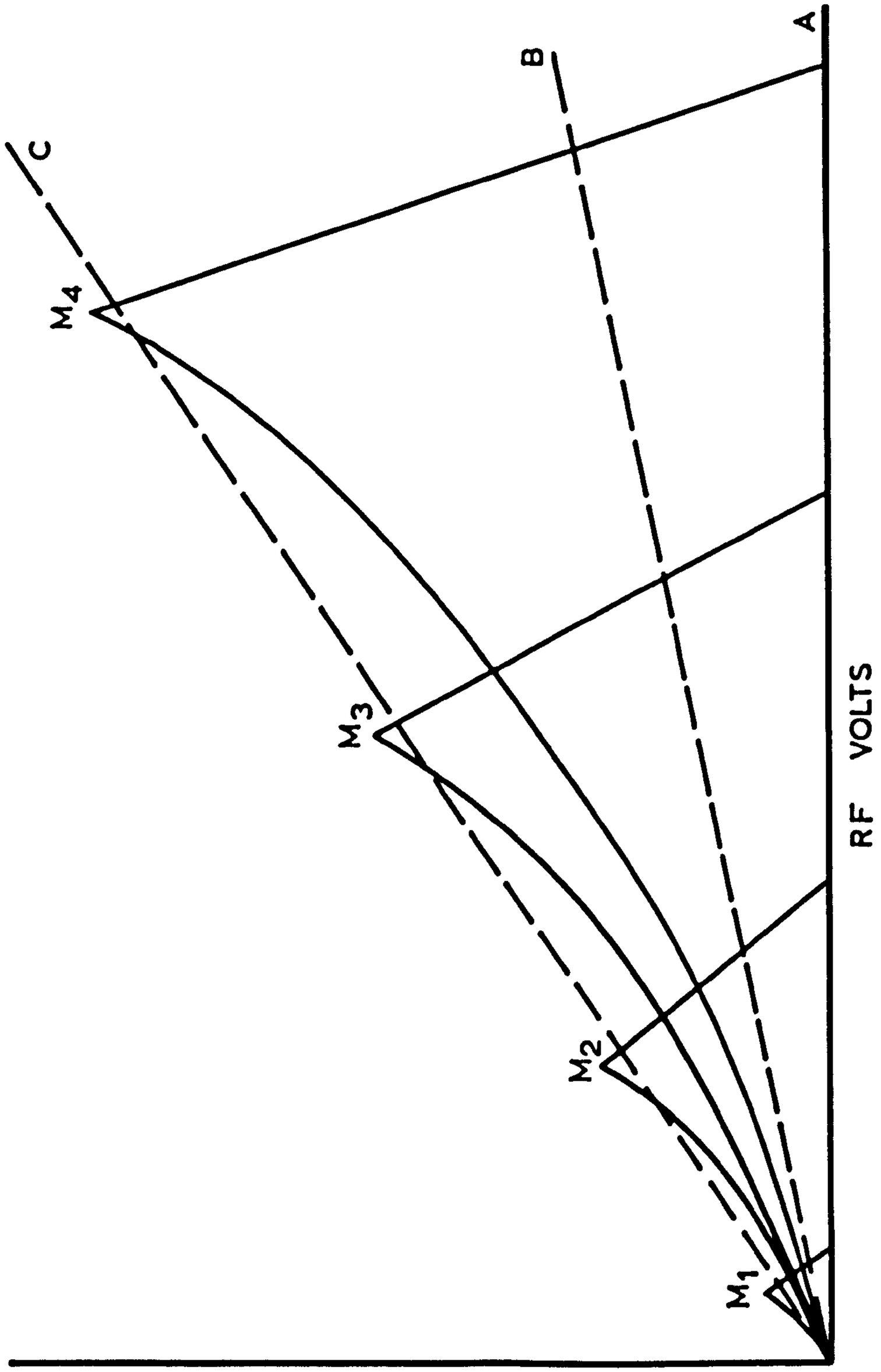

FIGURE B 4 Stability diagrams for four masses $M_1 < M_2 < M_3 < M_4$

The width of the mass peaks and their separation depends on the ratio U/V. If U/V = 0 then the peaks are never resolved: this corresponds to the line A drawn in figure B.4. This means that for low RF voltage [and U = 0] the filter passes all ions on stable trajectories, and this can be used for total pressure measurement. If the U/V ratio is too low, as in line B on the figure, some mass separation is achieved but the peak width is rather large. Operating along line C, however, where the ratio U/V is approximately 0·16, optimum mass separation is achieved.

So far the discussion has assumed several ideal conditions. Practically, one has to consider the effect of the analyser length, the radial and axial velocity of the ions, and the fringing fields at the entry and exit apertures etc., etc. The net result of those non-ideal conditions is that the stability diagram only has a core of 100% stability, and towards its edges and top the probability of stability decreases.

Thus if the ratio U/V is chosen high enough to give optimum resolution, the scan line never passes through a region of 100% transmission. Thus increasing resolution decreases the sensitivity and vice-versa.

H_2	He	CH_4	H_2O	Ne	N_2	CO	C_2H_6	O_2	Ar	CO_2	AMU
.086											1
12	.45										2
	20										4
		1				1.7				1.5	12
		2									13
		4.5			3.9	.45					14
		33									15
		41	.82			1.05		5.1		3.9	16
			9								17
			35								18
				80					14		20
				8						.85	22
							.3				24
							1.4				25
							8.5				26
							13				27
					120	120	44			11	28
						1.2	9.8				29
							12	66	120	90	30
											32
											40
											44

TABLE B.1 Sensitivity of quadrupole RGA to various gases in μA/torr

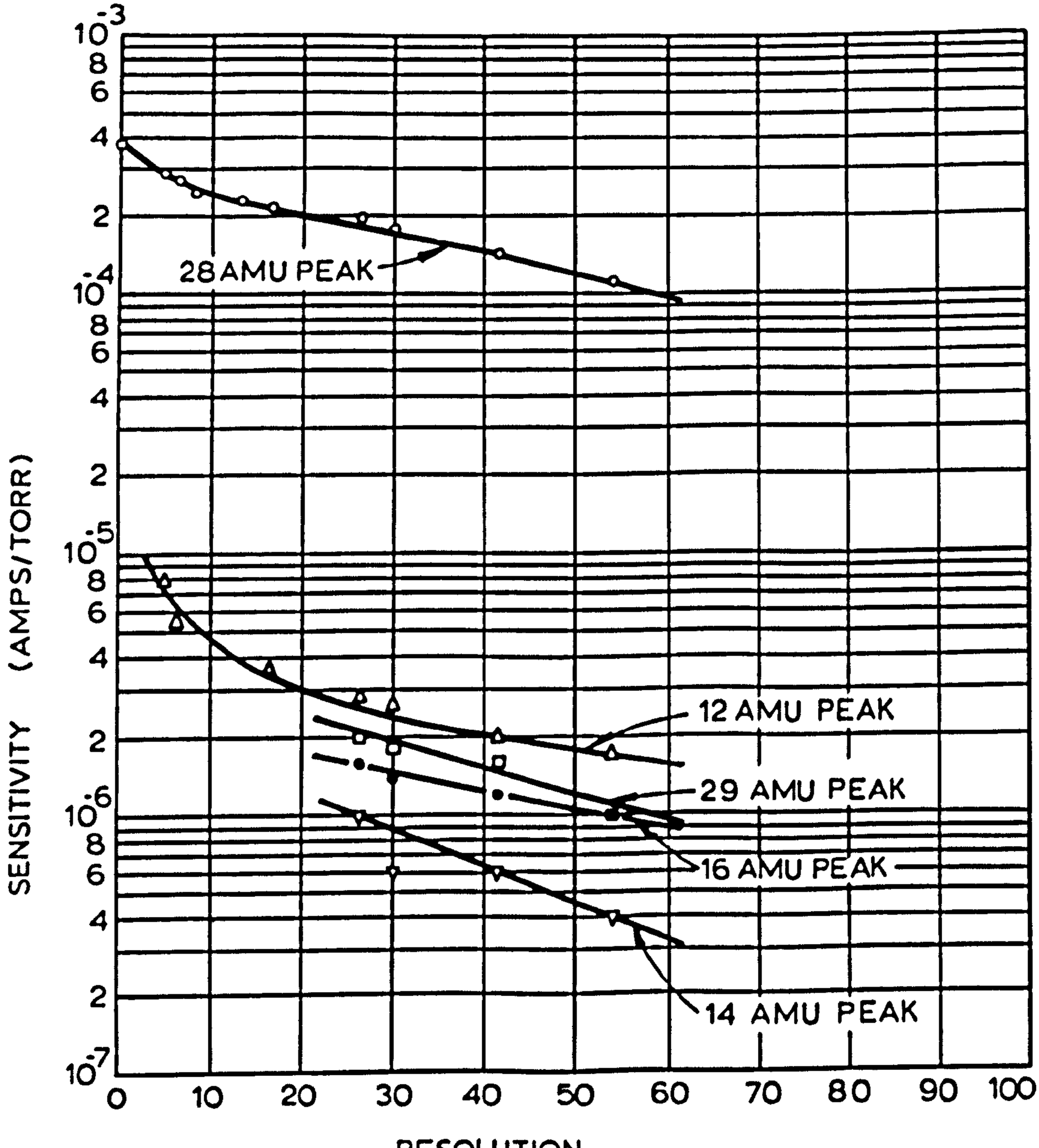

FIGURE B5. Sensitivity as a function of the resolution of the quadrupole RGA. The gas is carbon monoxide at a pressure of 1×10^{-6} torr.

B.5 *Analysis of quadrupole spectra*

Once a spectrum has been obtained from the quadrupole further work has to be done to determine the absolute partial pressures. This arises because of:

[a] the variation of ionisation efficiency in the source

[b] variation of sensitivity/resolution with ion species.

These functions have been investigated by VARIAN and the calculations made in this part of the investigation have been based on a set of graphs which they provided. These graphs plot the product of the two factors [a] and [b]. The graph applying to carbon monoxide is shown in figure B.5. It can be seen that the major peak at 28 amu is accompanied by several minor peaks. This is due to the cracking of the parent molecule in the ion source.

Table B.1 has been drawn from all the graphs provided, and it shows the sensitivity in μA/torr at a FWHM resolution of 2% [their 50]. In the range 0-50 amu this is the normal operating resolution.

Compilation of the table tacitly assumes that the sensitivity does not change with pressure. However, since the data was originally obtained under a vacuum of 10^{-6} torr, it is reasonable to assume it continues to be valid for pressures less than 10^{-6} torr: the change in mean free path length is unlikely to affect

the degree of recombination very seriously.

Accepting this table, however, there is still more work to be done before the individual partial pressures can be deduced. One has to find the best fit solution whereby the weighted contributions at each mass peak from all the overlapping cracking patterns, combine to produce the spectrum obtained. The method adopted here was to choose a given mass peak which could be ascribed to only one charged particle and measure its amplitude. Using the table one can then go through the whole cracking pattern associated with that particle and assign a partial pressure to the parent molecule.

In this manner it is easy to find the partial pressures of H_2, He, H_2O, Ne, O_2, Ar, and CO_2. The other gases usually required the solution of a number of simultaneous equations. At the limit of sensitivity of the quadrupole, however, it was impossible to distinguish between the contributions of N_2 and CO to the peak at 28 amu since the remainder of their cracking patterns was undetectable. The column marked "others" in table 5.1 was the sum of the fractions of each peak which were left unaccounted for by this analysis. The sensitivity of nitrogen was taken to calculate the partial pressure due to this error.

SYMBOLS AND ABBREVIATIONS

All the symbols used in this thesis are explained in the text where they first appear. Those which are used freely throughout are:

A	atomic transition
B	band transition
e	electron charge
E_F	electron energy at the Fermi level
L	lowered, or surface, plasmon loss
m	electron mass
M	ion mass
N[E]	density of states
P	volume plasmon loss
v	electron velocity
V	voltage
X	transition revealed by x-ray data
δ	yield
ε_o	permittivity of empty space
ω_p	plasmon frequency
CEL	characteristic energy loss[es]
FWHM	full width at half maximum
LEED	low energy electron diffraction
PSD	phase sensitive detector
RGA	residual gas analys[er/is]
RPSA	retarding potential spherical analyser
UHV	ultra-high vacuum

REFERENCES

1	L.AUSTIN, H. STARKE	Ann. Physik	9, 271, [1902]
2	H.E.FARNSWORTH	Phys. Rev.	20, 358, [1922]
3	H.E.FARNSWORTH	Phys. Rev.	25, 41, [1925]
4	H.E.FARNSWORTH	J. Opt. Soc. America	15, 290, [1927]
5	H.E.FARNSWORTH	Phys. Rev.	31, 405, [1928]
6	H.E.FARNSWORTH	Phys. Rev.	31, 414, [1928]
7	H.E.FARNSWORTH	Phys. Rev.	31, 419, [1928]
8	N.R.CAMPBELL	Phil. Mag.	29, 369, [1915]
9	A.W.HULL	Phys. Rev.	7, 1, [1916]
10	O.W.RICHARDSON	Proc. Roy. Soc.	A128, 63, [1930]
11	S.R.RAO	Proc. Roy. Soc.	A128, 41, [1930]
12	S.R.RAO	Proc. Roy. Soc.	A128, 57, [1930]
13	J.A.BECKER	Phys. Rev.	23, 664, [1924]
14	E.RUDBERG	Sven.Vet.Akad.Handl.	7, 1, [1929]
15	E.RUDBERG	Proc. Roy. Soc.	A130, 182, [1930]
16	E.RUDBERG	Phys. Rev.	50, 138, [1936]
17	G.RUTHEMANN	Ann. Phys. Lpz.	2, 113, [1948]
18	O.KLEMPERER & J.P.G.SHEPHERD	Brit. J. Appl. Phys.	14, 85, [1963]
19	O.KLEMPERER	Rep. Prog. Phys.	28, 77, [1965]
20	J.A.SIMPSON	Rev. Sci. Instr.	32,1283, [1961]
21	L.B.LEDER, J.A.SIMPSON	Rev. Sci. Instr.	29, 571, [1958]
22	S.THOMAS	Ph.D. Thesis, Keele,	[1967]
23	H.BOERSCH	Z. Phys.	139, 118, [1954]
24	G.HABERSTROH	Z. Phys.	145, 20, [1956]

25	J.A.SIMPSON	Rev. Sci. Instr.	32,1283, [1961]
26	J.A.SIMPSON, L.MARTON	Rev. Sci. Instr.	32, 802, [1961]
27	A.LL.HUGHES, J.H.McMILLEN	Phys. Rev.	34, 291, [1929]
28	A.LL.HUGHES, V.ROJANSKY	Phys. Rev.	34, 284, [1929]
29	P.P.REICHERTZ, H.E.FARNSWORTH	Phys. Rev.	75,1902, [1949]
30	G.A.HARROWER	Phys. Rev.	102, 340, [1956]
31	G.A.HARROWER	Phys. Rev.	102,1288, [1956]
32	C.J.POWELL, J.L.ROBINS	Phys. Rev.	110, 657, [1958]
33	C.J.POWELL, J.B.SWAN	Phys. Rev.	115, 869, [1959]
34	C.J.POWELL, J.B.SWAN	Phys. Rev.	116, 81, [1959]
35	C.J.POWELL, J.B.SWAN	Phys. Rev.	118, 640, [1960]
36	C.J.POWELL	Proc. Phys. Soc.	76, 593, [1960]
37	J.L.ROBINS, J.B.SWAN	Proc. Phys. Soc.	76, 857, [1960]
38	J.L.ROBINS, P.E.BEST	Proc. Phys. Soc.	79, 110, [1962]
39	J.L.ROBINS	Proc. Phys. Soc.	79, 119, [1962]
40	E.J.SCHEIBNER et al.	Rev. Sci. Instr.	31, 112, [1960]
41	R.L.PARK, H.E.FARNSWORTH	J. Chem. Phys.	43,2351, [1965]
42	C.C.CHANG, L.H.GERMER	Surface Sci.	8, 115, [1967]
43	E.E.HUBER	Appl. Phys. Lett.	8, 169, [1966]
44	J.C.RIVIERE	Appl. Phys. Lett.	8, 172, [1966]
45	SATCHLER	Surface Sci.	5, 221, [1966]
46	HOLSCHER	Surface Sci.	4, 89, [1966]
47	O.KLEMPERER & J.P.G.SHEPHERD	Adv. in Phys.	12, 355, [1963]

48	KANINSKY	Atomic & ionic phenomena, Springer,	1965
49	H.D.EGSTRUM, C.D'AMICO	J. Appl. Phys.	31, 715, [1960]
50	G.EHRLICH	Brit. J. Appl. Phys	15, 349, [1964]
51	R.J.ZOLLWEG	Surface Sci.	2, 409, [1964]
52	Yu.G.PTUSHINSKII, B.A.CHUIKOV	Surface Sci.	6, 42, [1967]
53	J.L.ROBINS et al.	J. Chem. Phys.	46, 665, [1967]
54	L.J.HAWORTH	Phys. Rev.	50, 216, [1936]
55	H.E.FARNSWORTH, J.TUUL	Phys. J. Chem. Solids	9, 48, [1958]
56	H.E.FARNSWORTH et al.	J. Appl. Phys.	29,1150, [1958]
57	S.HAGSTROM et al.	Phys. Rev. Lett.	15, 491, [1965]
58	J.C.TURNBULL & H.E.FARNSWORTH	Phys. Rev.	54, 509, [1938]
59	W.LANG	Optik	3, 233, [1948]
60	L.MARTON, L.B.LEDER	Phys. Rev.	94, 203, [1954]
61	L.MARTON	Rev. Mod. Phys.	28, 172, [1956]
62	L.B.LEDER	Phys. Rev.	103,1721, [1956]
63	L.B.LEDER	Phys. Rev.	107,1569, [1957]
64	L.MARTON	Phys. Rev.	110,1057, [1958]
65	L.B.LEDER, L.MARTON	Phys. Rev.	112, 341, [1958]
66	L.MARTON et al.	Phys. Rev.	126, 182, [1962]
67	L.MARTON et al.	Adv.in El.& Electron Phys.	7, 183, [1955]
68	W.KLEINN	Optik	11, 226, [1954]
69	H.WATANABE	J. Phys. Soc. Japan	9,1035, [1954]
70	H.WATANABE	Phys. Rev.	95,1684, [1954]

71	H.WATANABE	J. Phys. Soc. Japan	11, 112, [1956]
72	H.WATANABE	J. Phys. Soc. Japan	16, 912, [1961]
73	B.GAUTHE	Ann. Phys	3, 915, [1958]
74	B.GAUTHE	Phys. Rev.	114,1265, [1959]
75	H.BOERSCH, H.MEISSNER	Z. Phys.	168, 298, [1962]
76	H.BOERSCH et al.	Z. Phys.	169, 252, [1962]
77	H.BOERSCH et al.	Z. Phys.	212, 130, [1968]
78	O.KLEMPERER & J.P.G.SHEPHERD	Brit. J. Appl. Phys.	14, 89, [1963]
79	E.J.SCHEIBNER, L.N.THARP	Surface Sci.	8, 247, [1967]
80	L.N.THARP & E.J.SCHEIBNER	J. Appl. Phys.	38,3320, [1967]
81	B.GAUTHE	Comptes Rendues	239, 399, [1954]
82	A.W.BLACKSTOCK et al.	Phys. Rev.	100,1078, [1955]
83	G.JULL	Proc. Phys. Soc.	B69,1237, [1956]
84	C.FERT, F.PRADAL	Comptes Rendues	246, 252, [1958]
85	L.B.LEDER, J.A.SIMPSON	Rev. Sci. Instr.	29, 567, [1958]
86	J.M.ZIMAN	Electrons in metals, Taylor & Francis Ltd.,	[1963]
87	S.RAIMES	The wave mechanics of electrons in metals, North Holland,	[1961]
88	D.BOHM, E.P.GROSS	Phys. Rev.	75,1851,[1949]
89	D.BOHM, E.P.GROSS	Phys. Rev.	75,1864, [1949]
90	D.PINES	Rev. Mod. Phys.	28, 184, [1956]
91	F.M.PENNING	Nature	118, 301, [1926]
92	L.TONKS, I.LANGMUIR	Phys. Rev.	33, 195, [1929]

93	L.TONKS, I.LANGMUIR	Phys. Rev.	33, 990, [1929]
94	J.J. & G.P.THOMPSON	Conduction of electrons through gases, 2, Cambridge	[1933]
95	D.BOHM, D.PINES	Phys. Rev.	82, 625, [1951]
96	D.PINES, D.BOHM	Phys. Rev.	85, 338, [1952]
97	D.BOHM, D.PINES	Phys. Rev.	92, 609, [1953]
98	D.PINES	Phys. Rev.	92, 626, [1953]
99	P.NOZIERES, D.PINES	Phys. Rev.	109, 741, [1958]
100	P.NOZIERES, D.PINES	Phys. Rev.	109, 762, [1958]
101	P.NOZIERES, D.PINES	Phys. Rev.	109,1062, [1958]
102	P.NOZIERES, D.PINES	Phys. Rev.	111, 442, [1958]
103	P.NOZIERES, D.PINES	Phys. Rev.	113,1254, [1959]
104	J.HUBBARD	Proc. Phys. Soc.	A68, 441, [1955]
105	H.FROHLICH, H.PELZER	Proc. Phys. Soc.	A68, 525, [1955]
106	C.B.WILSON	Proc. Phys. Soc.	76, 481, [1960]
107	R.A.FERRELL	Phys. Rev,	107, 450, [1957]
108	R.A.FERRELL	Phys. Rev.	101, 554, [1956]
109	J.J.QUINN	Phys. Rev.	126,1453, [1962]
110	F.BLOCH	Helv. Phys. Acta	1, 385, [1934]
111	R.H.RITCHIE	Phys. Rev.	106, 874, [1957]
112	R.H.RITCHIE	Surface Sci.	4, 234, [1965]
113	E.A.STERN, R.A.FERRELL	Phys. Rev.	120, 130, [1960]
114	H.JENSEN	Z.Phys.	106, 620, [1937]
115	P.A.WOLFF	Phys. Rev.	92, 18, [1953]
116	R.A.FERRELL	Phys. Rev.	111,1214, [1958]

117	R.H.RITCHIE, H.B.ELDRIDGE	Phys. Rev.	126,1935,[1962]
118	A.L.FRANK et al.	Phys. Rev.	126,1947, [1962]
119	W.STEINMANN	Phys. Rev. Lett.	5, 470, [1960]
120	R.W.BROWN et al.	Phys. Rev. Lett.	5, 472, [1960]
121	E.T.ARAKAWA et al.	Phys. Rev. Lett.	12, 319, [1964]
122	R.J.HERICKHOFF et al.	Phys. Rev.	137,A1433,[1965]
123	J.BRAMBRING,H.RAETHER	Phys. Rev. Lett.	15, 882, [1965]
124	W.STEINMANN et al.	Phys. Rev. Lett.	16, 989, [1966]
125	H.MENDLOWITZ	Proc. Phys. Soc.	75, 664, [1960]
126	H.EHRENREICH, H.R.PHILIPP	Phys. Rev.	128,1622, [1962]
127	E.A.TAFT,H.R.PHILIPP	Phys. Rev.	121,1100, [1961]
128	B.R.COOPER et al.	Phys. Rev.	138,A494, [1965]
129	J.G.FLETCHER, D.C.LAPSON	Phys. Rev.	111, 455, [1958]
130	H.MENDLOWITZ	J. Opt. Soc. America	50, 739, [1960]
131	F.BERZ	Surface Sci.	2, 75, [1964]
132	R.H.RITCHIE	Surface Sci.	4, 497, [1965]
133	H.W.WILLIAMS et al.	Surface Sci.	6, 127, [1967]
134	C.J.POWELL	Phys. Rev. Lett.	15, 852, [1965]
135	C.KUNZ	Phys. Stat. Sol.	1, 441, [1961]
136	D.GABOR,G.W.JULL	Nature	175, 718, [1955]
137	N.R.WIETTEN	Appl. Phys. Lett.	8, 135, [1966]
138	E.RUDBERG, J.C.SLATER	Phys. Rev.	50, 150, [1936]

139	J.M.ZIMAN	Electrons and phonons,	Oxford,	[1960]
140	G.F.COSTER	Phys. Rev.	98, 901,	[1955]
141	G.C.FLETCHER	Proc. Phys. Soc.	A65, 192,	[1952]
142	E.P.WOHLFARTH	Proc.Leeds Phil. Soc.	5, 89,	[1949]
143	A.Ia.VIATSKIN	Sov. Phys., Tech. Phys.	3,2038,	[1958]
144	A.Ia.VIATSKIN	Sov. Phys., Tech. Phys.	3,2252,	[1958]
145	L.B.LEDER et al.	Phys. Rev.	101,1460,	[1956]
146	J.THIRLWELL	Proc. Phys. Soc.	91, 552,	[1967]
147	A.E.SANDSTROM	Encycl. Phys. 30, Springer,		[1957]
148	E.J.STERNGLASS	Nature	178,1387,	[1956]
149	N.BOHR	K.Danske Vidensk. Selsk.Mat.Phys.Medd.	18, 3	[1948]
150	E.M.HORL, J.A.SUDDETH	J. Appl. Phys.	32,2521,	[1961]
151	C.J.POWELL	Advances in Phys.	16, 203,	[1967]
152	L.J.HAWORTH	Phys. Rev.	48, 88,	[1935]
153	J.J.LANDER	Phys. Rev.	91,1382,	[1953]
154	O.H.ZINKE	Phys. Rev.	106,1163,	[1957]
155	L.A.HARRIS	J. Appl. Phys.	39,1419,	[1968]
156	L.A.HARRIS	J. Appl. Phys.	39,1428,	[1968]
157	Y.TAKEISHI,H.D.HAGSTRUM	Phys. Rev.	137,A641,	[1965]
158	D.W.FISCHER, W.L.BAUN	J. Appl. Phys.	37, 768,	[1966]
159	E.J.CALLAN	Phys. Rev.	124, 793,	[1961]
160	P.WEINHOLD	Z.Phys.	208, 313,	[1968]
161	J.C.RIVIERE, J.D.ALLINSON	Nuovo Cimento Suppl.	1, 520,	[1963]

162	W.D.DAVIES	G.E.Report, 63-RL-3301 G		[1963]
163	S.L.RUTHERFORD et al.	Trans.7th AVS Vac.Symp., Pergamon		[1961]
164	S.L.RUTHERFORD R.L.JEPSEN	Rev. Sci. Instr.	32,1144 ,	[1961]
165	R.L.JEPSEN	On the physics of sputter-ion pumps, 4th international vac.cong., Manchester		[1968]
166	B.J.HOPKINS, K.R.PENDER	Surface Sci.	5, 316,	[1966]
167	R.E.SCHLIER	J. Appl. Phys.	29,1162,	[1958]
168	J.ANDERSON, P.J.ESTRUP	J. Chem. Phys.	46, 563,	[1967]
169	P.A.REDHEAD	Nuovo Cimento Suppl.	5, 586,	[1967]
170	O.KLEMPERER, J.THIRLWELL	Solid State Comm.	4, 15,	[1966]
171	A.OTTO, J.B.SWAN	Z. Phys,	206, 277,	[1967]
172	H.BOERSCH et al.	Phys, Rev. lett.	7, 52,	[1961]
173	H.P.EUBANK, T.WILKERSON	Rev. Sci. Instr.	34, 12,	[1962]
174	F.R.PAOLINI, G.C.THEODORIS	Rev. Sci. Instr.	38, 579,	[1967]
175	E.M.PURCELL	Phys. Rev.	54, 818,	[1938]
176	F.W.ASTON	Phil. Mag.	38, 710,	[1919]
177	G.A.HARROWER	Rev. Sci. Instr.	26, 850,	[1955]
178	E.BLAUTH	Z. Phys.	147, 228,	[1951]
179	V.V.ZASHKVARA et al.	Sov. Phys., Tech. Phys.	11, 96,	[1966]
180	M.Z.SAR-EL	Rev. Sci. Instr.	38,1210,	[1967]
181	M.HAFNER	Rov. Sci. Instr.	39, 33,	[1968]
182	M.F.BARBER	Proc. Leeds Phil. Soc.	2, 427,	[1933]
183	R.HERZOG	Z. Phys.	89, 447,	[1934]

184	G.J.SCHULZ	Phys. Rev.	125, 229,	[1962]
185	R.HERZOG	Z. Phys.	97, 596,	[1935]
186	W.PAUL, H.STEINWEDEL	Z. Naturforsch.	8a, 448,	[1953]
187	W.PAUL, H.RAETHER	Z.Phys.	140, 262,	[1955]
188	W.PAUL et al.	Z. Phys.	152, 143,	[1958]
189	N.W.McLACHLAN	Theory & application of Mathieu functions,	Oxford,	[1951]
190	S.L.RUTHERFORD	Varian report	VPR-15	[1965]
191	W.M.BRUBAKER, J.TUUL	Rev. Sci. Instr.	35,1007,	[1964]
192	W.M.BRUBAKER	Instruments & Measurements Conference proceedings,	Stockholm	[1960]
193	J.L.ROBINS	Proc. Phys. Soc.	78,1177,	[1961]
194	E.RUDBERG	Proc. Roy. Soc.	A127, 111,	[1930]
195	G.MOLLENSTEDT	Optik	5, 499,	[1949]
196	H.WOLLNIK	Focussing of charged particles [ed. Septier], Academic Press,		[1967]
197	R.E.WARREN et al.	Rev. Sci. Instr.	18, 559,	[1947]
198	W.A.FOWLER et al.	Rev. Sci. Instr.	18, 818,	[1947]
199	E.RUDBERG	Proc. Roy. Soc.	A127, 111,	[1930]
200	O.KLEMPERER	Electron Physics,	Butterworths,	[1961]